arXiv:0705.3764v1 [gr-qc] 24 May 2007

Università degli Studi di Bologna

FACOLTÀ DI SCIENZE MATEMATICHE, FISICHE E NATURALI

Dottorato di Ricerca in Fisica

Semiclassical Approximations to Cosmological Perturbations

Tesi di Dottorato di:
Mattia Luzzi

Relatore: **Chiar.mo**
Prof. Giovanni Venturi
Corelatori:
Dott. Roberto Casadio
Dott. Fabio Finelli
Dott. Alexander Kamenshchik

Sigla del Settore Scientifico Disciplinare: FIS/02

Visto del Coordinatore di Dottorato, Prof. Fabio Ortolani

XIX Ciclo

Anno Accademico 2005-2006

“Would you tell me, please, which way I ought go from here?”
“That depends a good deal on where you want to get to”, said the Cat.
“I don’t much care where -” said Alice.
“Then it doesn’t matter which way you go,” said the Cat.
“- so long as I get somewhere,” Alice added as an explanation.
“Oh, you’re sure to do that,” said the Cat, “if you only walk long enough.”

from “Alice’s Adventures in Wonderland” by Lewis Carroll

I would like to thank my supervisor Prof. Giovanni Venturi for his support and encouragement. I would also like to thank the whole INFN Bologna group BO11. I warmly thank Dr. Roberto Casadio for being always so kind and ready–to–help me in any respect. For the many interactions I had and specially for the fact that working with them was lots of fun, I want to express my acknowledgement to Dr. Fabio Finelli and Dr. Alexander Kamenshchik. Our fruitful collaboration forms the basis of much of the work presented here.

SEMICLASSICAL APPROXIMATIONS TO COSMOLOGICAL PERTURBATIONS

Mattia Luzzi

Index

Index 9

Introduction 13

Units and Conventions 15

1 What's the matter? 17
- 1.1 A short (incomplete) introduction to a long history 19
- 1.2 CMB experiments 20

2 FRW Universes and their inhomogeneities 23
- 2.1 FRW Universes 23
- 2.2 Fluctuations of the geometry in flat FRW Universes 24
- 2.3 Gauge fixing and gauge-invariant variables 26
  - 2.3.1 Vector modes 26
  - 2.3.2 Scalar modes 26

3 Evolution of metric fluctuations 29
- 3.1 Evolution of the tensor modes 29
  - 3.1.1 Hamiltonians for the tensor problem 30
- 3.2 Evolution of the vector modes 32
- 3.3 Evolution of the scalar modes 33
  - 3.3.1 Physical interpretation of curvature perturbations 34
  - 3.3.2 Curvature perturbations induced by scalar fields 35
  - 3.3.3 Horizon flow functions 37
  - 3.3.4 Hamiltonians for the scalar problem 38
- 3.4 Quantum amplification of metric fluctuations 40
  - 3.4.1 Large-scale power spectra of tensor fluctuations 40
  - 3.4.2 Large-scale power spectra of scalar fluctuations 42

4 WKB-type approximations 45
- 4.1 Standard WKB approximation 45
- 4.2 The "Turning Point" problem 46
- 4.3 Improved WKB approximation 48

4.3.1 Perturbative expansion 51
4.3.2 Adiabatic expansion 52
4.4 Method of Comparison Equation 54
4.4.1 MCE vs Ermakov&Pinney 55

5 Analysis of Cosmological Perturbations 67
5.1 Standard WKB approximation 67
5.2 Improved WKB approximation 70
5.2.1 Perturbative expansion 70
5.2.2 Adiabatic expansion 74
5.3 Method of Comparison Equation 76

6 Applications 81
6.1 Power-law Inflation 81
6.1.1 Improved WKB leading order results 83
6.1.2 Improved WKB next-to-leading order results 83
6.1.3 MCE results 85
6.2 Slow-Roll Inflation 86
6.2.1 Improved WKB leading and second slow-roll order 86
6.2.2 Improved WKB next-to-leading and first slow-roll order 92
6.2.3 Improved WKB next-to-leading and second slow-roll order 94
6.2.4 MCE and second slow-roll order 97
6.2.5 Second slow-roll order MCE and WKB versus GFM 98
6.2.6 GFM and slow-roll approximation 100
6.2.7 Beyond slow-roll 104

Conclusions 107

A First Order Fluctuations 111
A.1 Scalar modes 112
A.2 Vector modes 113
A.3 Tensor modes 114
A.4 Energy-Momentum Tensor 114
A.5 Gauge invariant scalar perturbations 117

B Slow-Roll *vs* Horizon Flow 119

C An application of MCE 121
C.0.1 Linear comparison function 121
C.0.2 A more complicated comparison function 123

D Other results in the literature 127

E Undetermined parameters in the WKB* 129

F Perturbative approximations **131**

G MCE and Black Holes **135**

G.1 Scalar field on Schwarzschild background 136
G.2 MCE solutions 137
    G.2.1 Turning Points 141
    G.2.2 Evaluation of ξ 142
    G.2.3 Cubic interpolation 143

Bibliography **145**

Introduction

One of the main ideas of modern cosmology is that there was an epoch in the history of the Universe when vacuum energy dominated other forms of energy density such as radiation or matter. During this vacuum-dominated (or potential-dominated) era, the scale factor grew exponentially (or almost exponentially) in time and, for this reason, it is known as *inflation*. During inflation, a small and smooth spatial region of size less than the Hubble radius at that time could have grown so large to easily encompass the comoving volume of the entire Universe presently observable. If the early Universe underwent a period of so rapid expansion, one can then understand why the observed Universe is homogeneous and isotropic to such a high accuracy. All these virtues of inflation were already noted when it was first proposed in a seminal paper by Guth in 1981 [1]. Other, and more dramatic consequences of the inflationary paradigm were discovered soon after. Starting with a Universe which is absolutely homogeneous and isotropic at the classical level, the inflationary expansion will "freeze in" the vacuum fluctuations of the "inflaton" (the field responsible for the rapid expansion) which then becomes a classical quantity. On each comoving scale, this happens soon after the fluctuation exits the Hubble horizon. A primordial energy density, which survives after the end of inflation, is associated with these vacuum fluctuations and may be responsible for both the anisotropies in the Cosmic Microwave Background (CMB) and for the large-scale structures of the Universe, like galaxies, clusters of galaxies, and dark matter. Inflation also generates primordial gravitational waves, which may contribute to the low multipoles of the CMB anisotropy. The amazing prediction of inflation is therefore that all of the structures we see in the present Universe are the result of quantum-mechanical fluctuations during the inflationary epoch.

Units and Conventions

The so–called natural units, namely $\hbar = c = 1$, will be employed, so that

$$[\text{Energy}] = [\text{Mass}] = [\text{Length}]^{-1} = [\text{Time}]^{-1}\ .$$

$m_{\rm Pl} = 1/\sqrt{G}$ is the Planck mass, whereas $M_{\rm Pl} = 1/\sqrt{8\,\pi\,G}$ stands for the reduced Planck mass, and $\ell_{\rm Pl} = \sqrt{8\,\pi}\,M_{\rm Pl}^{-1}$ is the Planck length. The present Hubble expansion rate is customarily parameterised as $H_0 = 100\,h\,{\rm km\,sec^{-1}\,Mpc^{-1}}$ where h parameterises the uncertainty in the present value of the Hubble parameter.

We shall also adopt the Einstein sum rule for repeated indices and the following conventions: The metric signature is $(+, -, -, -)$, Greek letters denote space-time indices which run from 0 to 3 and Latin letters denote spatial indices which run from 1 to 3.

Some abbreviations used in this thesis are the following:

CMB = Cosmic Microwave Background
EW = electroweak
BBN = Big Bang Nucleosintesis
GR = General Relativity
COBE = COsmic Background Explorer satellite
DMR = Differential Microwave Radiometer
WMAP = Wilkinson Microwave Anisotropy Probe
ACBAR = Arcminute Cosmology Bolometer Array Receiver
VSA = Very Small Array
CBI = Cosmic Background Imager
Λ CDM = ΛCold Dark Matter
FRW= Friedmann-Robertson-Walker
WKB = Wentzel-Kramers-Brillouin
MCE = Method of Comparison Equation
PS = Power Spectrum
HFF = Horizon Flow Functions
SR = Slow Roll
HSR = Hubble Slow Roll
PSR = Hubble Slow Roll
GFM = Green Function Method

Chapter 1

What's the matter?

What is the origin of the inhomogeneities we observe in the sky? What is their typical wavelength? How come that we are able to observe these inhomogeneities? The term inhomogeneity is rather generic and indicates fluctuations both in the background geometry and in the energy content of the Universe. These inhomogeneities can be represented by plane waves characterized by a comoving wave-number k. Since the evolution of the Universe is characterized by a scale factor $a(t)$ which is a function of the cosmic time t, the physical wave-number is given by $k_{\mathrm{ph}} = k/a$. The comoving wave-number is a constant and does not feel the expansion of the Universe, while the physical momentum is different at different epochs. Conversely the value of a given physical frequency is fully specified only by stating the time at which the physical frequency is "measured".

For example, if a given fluctuation has a momentum comparable with the present value of the Hubble parameter, $k_{\mathrm{ph},0} \simeq H_0 \simeq 5.6{\times}10^{-61}\, M_{\mathrm{Pl}}$, we will have that $k_{\mathrm{ph},0} \simeq 2.3{\times}10^{-18}$ Hz. Fluctuations with momentum smaller that H_0 have a wave-length larger than the present value of the Hubble radius and are therefore impossible to detect directly since the distance between two of their maxima (or minima) is larger than our observable Universe.

At the decoupling epoch, when the radiation became free to propagate, the temperature of the Universe was of the order of a fraction of eV and the Hubble rate was $H_{\mathrm{dec}} \simeq 6.7 \times 10^{-56}\, M_{\mathrm{Pl}}$. The corresponding decoupling frequency was then red-shifted to the present value $k_{\mathrm{ph,dec}} \simeq 3 \times 10^{-16}\,\mathrm{Hz}$. Fluctuations of this typical frequency appear as temperature inhomogeneities of the CMB induced by the primordial fluctuations in the background geometry and in the matter density. The latter fluctuations have already collapsed due to gravitational instability and formed galaxies and clusters of galaxies. At the epoch of the formation of light nuclei, the Universe was hotter, with a temperature of a fraction of MeV and the corresponding value of the Hubble expansion rate was about $8 \times 10^{-44}\, M_{\mathrm{Pl}}$. When the electroweak (EW) phase transition took place, the temperature of the Universe was of the order of $100\,\mathrm{GeV}$ leading, approximately, to $H_{\mathrm{EW}} \sim 10^{-32}\, M_{\mathrm{Pl}}$. Comoving wave-numbers of the order of the Hubble rate at the EW phase transition or at the epoch of the Big Bang Nucleosintesis (BBN) correspond, today, to physical frequencies of the order of $k_{\mathrm{ph,EW}} \sim 2 \times 10^{-5}\,\mathrm{Hz}$ or $k_{\mathrm{ph,BBN}} \simeq 9 \times 10^{-11}\,\mathrm{Hz}$. Finally, in the context of the inflationary paradigm the value of the Hubble rate during inflation was

$H_{\rm inf} \sim 10^{-6}\, M_{\rm Pl}$. Under the assumption that the Universe was dominated by radiation right after inflation, the corresponding physical frequency today is of the order of 10^8 Hz.

The detectors developed to measure anisotropies in the CMB are sensitive to frequency scales only slightly higher than 10^{-16} Hz. Therefore, they cannot be used to "observe" fluctuations originated at earlier epochs and whose physical frequencies presently lie in the range $10^{-3}\,\mathrm{Hz} < k_{\rm ph} < 1\,\mathrm{MHz}$. For frequencies in this interval, one can only hope to detect the stochastic background of gravitational radiation which is therefore the only means we have to obtain direct information about the EW phase transition, the BBN and inflation itself.

The cosmological inhomogeneities are usually characterized by their correlation functions. The simplest correlation function encoding informations on the nature of the fluctuations is the two-point function which is computed by taking averages of the fluctuation amplitude at two spatially separated points but at the same time. Its Fourier transform is usually called the *power spectrum.* On considering the physical scales discussed above, one is led to conclude that the power spectrum of cosmological inhomogeneities is defined over a huge interval of frequencies. For instance, the tensor fluctuations of the geometry, which only couple to the curvature and not to the matter sources, have a spectrum ranging, in some specific models, from 10^{-18} Hz up to about 1 GHz.

From the history of the Universe sketched so far, some questions may be naturally raised. For our purposes, we just quote two of them:

- Given that the precise thermodynamical history of the Universe above 10 MeV is unknown, how it is possible to have a reliable framework describing the evolution of the cosmological fluctuations?
- Does it make sense to apply General Relativity (GR) to curvatures which can reach up to almost the Planck scale?

As recalled above, we do not have any direct evidence for the thermodynamical state of the Universe for temperatures above the MeV, although some indirect predictions can be made. For example, the four lighter isotopes (D, ^{3}He, ^{4}He and ^{7}Li) should have been mainly produced at the BBN below a typical temperature of 0.8 MeV when neutrinos decouple from the plasma and the neutron abundance evolves via free neutron decay. The abundances calculated in the homogeneous and isotropic BBN model agree fairly well with the astronomical observations. This is the last indirect test of the thermodynamical state of the Universe. For temperatures larger than 10 MeV, collider physics and the success of the standard model of particle physics offer a precious handle up to the epoch of the EW phase transition occurring for temperatures of the order of 100 GeV. There is then hope that our knowledge of particle physics could help us to fill the gap between the epoch of nucleosynthesis and that of the EW phase transition.

The evolution of inhomogeneities over cosmological distances may well be unaffected by our ignorance of the specific history of the expansion rate. The key concept is that of conservation laws and, in the framework of metric theories of gravity (and of GR in particular), one can show that there exist conservation laws for the evolution of the fluctuations which become exact in the limit of vanishing comoving frequency $k \to 0$. This conclusion holds under the assumption that GR is a valid description throughout the whole evolution of the Universe and similar properties also hold, with some modifications, in scalar-tensor theories of gravity (of the Brans-Dicke type) like those suggested by the low-energy limit of superstring theory. The conservation laws of cosmological perturbations apply strictly in the case of the tensor modes of the geometry whereas, for scalar fluctuations which couple directly to the (scalar) matter sources, the precise form of the conservation laws depends upon the matter content of the early Universe. Experiments aimed at the direct detection of stochastic backgrounds of relic gravitons which regard the high-frequency behaviour of cosmological fluctuations should therefore yield valuable clues on the early evolution of the Hubble rate.

1.1 A short (incomplete) introduction to a long history

The history of the studies about the CMB anisotropies and cosmological fluctuations is closely related with the history of the standard cosmological model (see, for instance, the textbooks by Weinberg [2] and Kolb and Turner [3]).

During the development of the standard model of cosmology, one of the recurrent issues has been the explanation of the structures we observe in the present Universe, which goes under the name of the structure formation. The reviews of Kodama and Sasaki [4] and of Mukhanov, Feldman and Brandenberger [5] contain some historical surveys that are a valuable introduction to this subject.

A seminal contribution to the understanding of cosmological perturbations is the paper of Sachs and Wolfe [6] on the possible generation of anisotropies in the CMB, where the basic general relativistic effects were estimated assuming that the CMB itself was of cosmological origin. The authors argued that galaxy formation would imply $\Delta T/T \sim 10^{-2}$. Subsequent calculations [7, 8, 9, 10, 11] brought the estimate down to 10^{-4}, closer to what is experimentally observed. A second foundamental paper is the contribution of Sakharov [12] where the concept of acoustic oscillations was introduced. This paper contained two ideas whose legacy, somehow unexpectedly, survived until the present. The first idea is summarized in the abstract

> *A hypothesis of the creation of astronomical bodies as a result of gravitational instability of the expanding Universe is investigated. It is assumed that the initial inhomogeneities arise as a result of* quantum fluctuations*...*

The model indeed assumed that the initial state of the baryon-lepton fluid was cold. So the premise was wrong, but, still, it is amusing to notice that a variety of models today assume quantum fluctuations as initial conditions for the fluctuations of the geometry at a totally different curvature (or energy).

To summarise, Refs. [6] and [12] highlight three important problems regarding the fluctuations of the gravitational inhomogeneities:

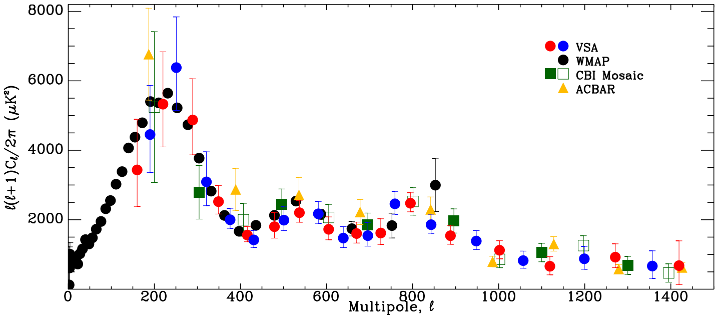

Figure 1.1: Some of the most recent CMB anisotropy data from [20]: WMAP (filled circles); VSA (shaded circles) [20]; CBI (squares) [21, 22] and ACBAR (triangles) [23].

- their initial conditions;
- their evolution;
- their imprint on the CMB temperature fluctuations.

1.2 CMB experiments

Although we shall just study a particular aspect of the theory of cosmological perturbations, it is appropriate to give a swift account of our recent experimental knowledge of CMB anisotropies. A new twist in the study of CMB anisotropies came from the observations of the COsmic Background Explorer satellite (COBE) and, more precisely, from the Differential Microwave Radiometer (DMR). The DMR was able to probe the angular power spectrum C_ℓ [1] up to $\ell \simeq 25$ (see, for instance, [13, 14] and references therein). DMR was a differential instrument measuring temperature differences in the microwave sky. The angular separation ϑ of the two horns of the antenna is related to the largest multipole according to the approximate relation $\vartheta \simeq \pi/\ell$.

COBE explored angular separations $\vartheta \gtrsim 7^0$ and, after the COBE mission, various experiments have probed smaller angular separation, i.e., larger multipoles. A finally convincing evidence of the existence and location of the first peak in C_ℓ came from Boomerang [15, 16], Maxima [17] and Dasi [18]. These last three experiments explored multipoles up to $\ell = 1000$, determining the first acoustic oscillation for $\ell \simeq 220$. Another important experiment was Archeops [19] providing interesting data for the region characterizing the first rise of the angular spectrum.

The angular spectrum, as measured by different recent experiments is reported in Fig. 1.1. The data from the Wilkinson Microwave Anisotropy Probe (WMAP) are displayed as filled circles in Fig. 1.1 and provide, among other important evidences, a precise determination of the position of the first peak (i.e., $\ell = 220.1 \pm 0.8$ [24]) and a clear evidence of the second peak. Further, once all the four-years data are collected, the spectrum will be obtained with good resolution up to $\ell \sim 1000$, i.e., around the third peak. In Fig. 1.1, we also display the results of the Arcminute Cosmology Bolometer Array Receiver (ACBAR) as well as the data points of the Very Small Array (VSA) and of the Cosmic Background Imager (CBI).

---

[1] We just recall here that $\ell(\ell+1)\,C_\ell/(2\,\pi)$ measures the degree of inhomogeneity in the temperature distribution per logarithmic interval of ℓ. Consequently, a given multipole ℓ can be related to a given spatial structure in the microwave sky: small ℓ will correspond to smaller and high ℓ to larger wave-numbers around a present physical frequency of the order of 10^{-16} Hz.

In recent years, thanks to the combined observations of CMB anisotropies [25], Large scale structure [26, 27], supernovae of type Ia, BBN [28], some kind of paradigm for the evolution of the late time (or even present) Universe has emerged. This is normally called ΛCold Dark Matter (Λ CDM) model or, sometimes, "concordance model". The term ΛCDM refers to the fact that, in this model, the dominant (present) component of the energy density of the Universe is given by a cosmological constant Λ and a fluid of cold dark matter particles interacting only gravitationally with the other (known) particle species such as baryons, leptons, photons. According to this paradigm, our understanding of the Universe can be summarized in two sets of cosmological parameters, one referring to the homogeneous background and one to the inhomogeneities. As far as the homogeneous background is concerned, the most important parameter is the indetermination on the (present) Hubble expansion rate which is customarily parameterised as $H_0 = h \times 100\mathrm{km}/[\mathrm{sec} \times \mathrm{Mpc}]$ ($h \simeq 0.72$ in the concordance model). There are various other parameters, such as the dark and CDM energy densities in critical units, $\Omega_{\mathrm{cdm}} \simeq 0.224$ and $\Omega_{\Lambda} \simeq 0.73$, respectively; the radiation and baryon energy densities in critical units, $\Omega_{\mathrm{r}} \simeq 8 \times 10^{-5}$ and $\Omega_{\mathrm{b}} \simeq 0.046$; the number of neutrino species and their masses; the possible contribution of the spatial curvature ($\Omega_{\kappa} = 0$ in the concordance model) the optical depth of the plasma at recombination (of the order of 0.16 in the concordance model).

The second set of parameters refers to the inhomogeneities. In the ΛCDM model the initial conditions for the inhomogeneities belong to a specific class of scalar fluctuations of the geometry which are called adiabatic and are characterized by the Fourier transform of their two-point function. This is the power spectrum which is usually parametrized in terms of an amplitude and a spectral slope. Besides these two parameters, one usually considers the ratio between the amplitudes of the scalar and tensor modes of the geometry.

The purpose of this thesis is to report the development of a method for the resolution of the differential equation that drives the modes of scalar and tensorial perturbations of the cosmological inhomogeneities. This work is organized as follows: in Chapter 2 we review the Friedmann-Robertson-Walker (FRW) space-time and remark some aspects about gauge choices. Chapter 3 deals with the process of generation of cosmological perturbations by quantum fluctuations of a scalar field and a second-order differential equation for the quantities of interest is obtained. Such a kind of equations will be treated with semiclassical approximations in Chapter 4. In Chapter 5 we give new general results for the power spectra of cosmological perturbations, while in Chapter 6 we use those results to find, in detail, explicit expressions for the power spectra in several inflationary models. The thesis ends with our Conclusions and several Appendicies.

Chapter 2

FRW Universes and their inhomogeneities

2.1 FRW Universes

A Friedmann-Robertson-Walker (FRW) metric can be written in terms of the cosmic time t as

$$^{(0)}g_{\mu\nu}\,\mathrm{d}x^{\mu}\,\mathrm{d}x^{\nu}=\mathrm{d}t^2-a^2(t)\,\left[\frac{\mathrm{d}r^2}{1-\kappa\,r^2}+r^2\,\left(\mathrm{d}\theta^2+\sin^2\theta\mathrm{d}\varphi^2\right)\right]\ , \tag{2.1}$$

where κ can be 1, 0 and -1 for spherical, eucledian or hyperbolic spatial sections, respectively; a is the scale factor, while r,θ,φ are the spherical coordinates. We can also write the metric in terms of the conformal time η, defined by $\mathrm{d}\eta\equiv\mathrm{d}t/a(t)$, as

$$^{(0)}g_{\mu\nu}\,\mathrm{d}x^{\mu}\,\mathrm{d}x^{\nu}=a^2(\eta)\,\left\{\mathrm{d}\eta^2-\left[\frac{\mathrm{d}r^2}{1-\kappa\,r^2}+r^2\,\left(\mathrm{d}\theta^2+\sin^2\theta\mathrm{d}\varphi^2\right)\right]\right\}\ . \tag{2.2}$$

The evolution of the geometry is driven by the matter sources according to the Einstein equations

$$G_{\mu\nu}\equiv R_{\mu\nu}-\frac{1}{2}\,\delta_{\mu\nu}\,R=8\,\pi\,G\,T_{\mu\nu}\ , \tag{2.3}$$

where $G_{\mu\nu}$ is the Einstein tensor, $R_{\mu\nu}$ and R are the Ricci tensor and Ricci scalar, respectively; $T_{\mu\nu}$ is the energy-momentum tensor of the sources. Under the hypothesis of homogeneity and isotropy, we can always write the energy-momentum tensor in the form $T_{\mu\nu}=\mathrm{diag}\,(\rho,p,p,p,p)$ where ρ is the energy density of the system and p its pressure and are functions of the time. Using Eq. (2.3) we obtain the Friedmann equations which, in conformal time, read

$$\mathcal{H}^2=\frac{8\,\pi\,G\,\rho\,a^2}{3}-\kappa\ ,\quad \mathcal{H}'=-\frac{4\,\pi\,G}{3}\,\left(\rho+3\,p\right)\,a^2 \tag{2.4}$$

along with the continuity equation

$$\rho' + 3\mathcal{H}\,(\rho + p) = 0 \; . \tag{2.5}$$

In the above formulae $\mathcal{H} \equiv a'/a$ and a prime denotes a derivation with respect to the conformal time. In cosmic time, the same equations become

$$H^2 = \frac{8\,\pi\,G\,\rho}{3} - \frac{\kappa}{a^2} \; , \quad \dot{H} = -\,4\,\pi\,G\;(\rho + p) + \frac{\kappa}{a^2} \tag{2.6}$$

and the continuity equation is given by

$$\dot{\rho} + 3\,H\,(\rho + p) = 0 \; , \tag{2.7}$$

where $H \equiv \dot{a}/a$ is the Hubble expansion rate and dot denotes a derivation with respect to t. The relation between the Hubble factors in the two time parametrizations is $\mathcal{H} = a\,H$.

2.2 Fluctuations of the geometry in flat FRW Universes

Let us now consider a conformally flat (i.e., $\kappa = 0$) background metric of FRW type,

$$g_{\mu\nu}(\eta) = a^2(\eta)\,\eta_{\mu\nu} \; , \tag{2.8}$$

where $\eta_{\mu\nu}$ is the flat Minkowski metric. Its first-order fluctuations can be written as

$$\delta\,g_{\mu\nu}(\eta,\vec{x}) = \delta_{\rm s}\,g_{\mu\nu}(\eta,\vec{x}) + \delta_{\rm v}\,g_{\mu\nu}(\eta,\vec{x}) + \delta_{\rm t}\,g_{\mu\nu}(\eta,\vec{x}) \; , \tag{2.9}$$

where the subscripts define, respectively, the scalar, vector and tensor perturbations. The perturbed metric $\delta\,g_{\mu\nu}$ has ten independent components whose explicit form can be parametrized as

$$\begin{aligned} \delta\,g_{00} &= 2\,a^2\,\phi \\ \delta\,g_{ij} &= 2\,a^2\;(\psi\,\delta_{ij} - \partial_i\,\partial_j\,E) - a^2\,h_{ij} - a^2\;(\partial_i\,F_j + \partial_j\,F_i) \\ \delta\,g_{0i} &= -a^2\,\partial_i\,B + a^2\,S_i \; , \end{aligned} \tag{2.10}$$

with the conditions

$$\partial_i\,S^i = \partial_i\,F^i = 0 \; , \quad h^i_i = \partial_i\,h^i_j = 0 \; . \tag{2.11}$$

The decomposition given in Eqs. (2.10) is that normally employed in the Bardeen formalism [29] (see Ref. [5]).

The scalar fluctuations are parametrized by the scalar functions ϕ, ψ, B and E. The vector fluctuations are described by two divergenceless (see Eqs. (2.11)) vectors in three (spatial) dimensions F_i and S_i (i.e., by four independent degrees of freedom). Finally the tensor modes are described by h_{ij}, leading to two independent components (see Eqs. (2.11)).

Under general infinitesimal coordinate transformations

$$\eta \to \tilde{\eta} = \eta + \epsilon_0 \ , \quad x^i \to \tilde{x}^i = x^i + \epsilon^i \tag{2.12}$$

the fluctuations of the geometry defined in Eqs. (2.10) transform as

$$\delta\, g_{\mu\nu} \to \delta\, \tilde{g}_{\mu\nu} = \delta\, g_{\mu\nu} - \nabla_\mu\, \epsilon_\nu - \nabla_\nu\, \epsilon_\mu \ , \tag{2.13}$$

where ∇_μ is the covariant derivative with respect to the background goemetry and $\epsilon_\mu = a^2(\eta)\,(\epsilon_0, -\epsilon_i)$. These infinitesimal coordinate transformations form a group and the functions ϵ_0 and ϵ_i are the gauge parameters. The gauge-fixing procedure amounts to fixing the four gauge parameters. Further, the spatial components ϵ_i can be separated into divergenceless and divergencefull parts

$$\epsilon_i = \partial_i\, \epsilon + \zeta_i \ , \tag{2.14}$$

where $\partial_i\, \zeta^i = 0$. The gauge transformations involving ϵ_0 and ϵ preserve the scalar nature of the fluctuations while those parametrized by ζ_i preserve the vector nature of the fluctuation.

The background covariant derivatives in Eq. (2.13) are given by $\nabla_\mu\, \epsilon_\nu = \partial_\mu\, \epsilon_\nu - {}^{(0)}\Gamma^\sigma_{\mu\nu}\, \epsilon_\sigma$ and, in terms of the unperturbed connections (see Eqs. (A.7)), the fluctuations for the scalar modes can be written in the tilded coordinate system as

$$\phi \to \tilde{\phi} = \phi - \mathcal{H}\, \epsilon_0 - \epsilon_0' \tag{2.15}$$
$$\psi \to \tilde{\psi} = \psi + \mathcal{H}\, \epsilon_0 \tag{2.16}$$
$$B \to \tilde{B} = B + \epsilon_0 - \epsilon' \tag{2.17}$$
$$E \to \tilde{E} = E - \epsilon \ . \tag{2.18}$$

Under a coordinate transformation preserving the vector nature of the fluctuation, $x^i \to \tilde{x}^i = x^i + \zeta^i$ (with $\partial_i\, \zeta^i = 0$), the rotational modes of the geometry transform as

$$S_i \to \tilde{S}_i = S_i + \zeta_i' \tag{2.19}$$
$$F_i \to \tilde{F}_i = F_i - \zeta_i \ . \tag{2.20}$$

Finally, the tensor fluctuations in the parametrization of Eqs. (2.10) are automatically gauge invariant.

The perturbed components of the energy-momentum tensor can be written as

$$\delta\, T_0^0 = \delta\, \rho \ , \quad \delta\, T_i^j = -\delta\, p\, \delta_i^j \ , \quad \delta\, T_0^i = (p + \rho)\ \partial^i\, v \ , \tag{2.21}$$

where v is the velocity field and $\delta u_i = \partial_i\, v$. Under the infinitesimal coordinate transformations (2.12), the fluctuations given in Eq. (2.21) transform as

$$\delta\, \rho \to \delta\, \tilde{\rho} = \delta\, \rho - \rho'\, \epsilon_0 \tag{2.22}$$
$$\delta\, p \to \delta\, \tilde{p} = \delta\, p - w\, \rho'\, \epsilon_0 \tag{2.23}$$
$$v \to \tilde{v} = v + \epsilon' \ . \tag{2.24}$$

Using the covariant conservation equation (2.5) for the background fluid density, the gauge transformation for the density perturbation $\delta \equiv \delta\,\rho/\rho$ follows from Eq. (2.22) and reads

$$\tilde{\delta} = \delta - 3\,\mathcal{H}\left(1 + \frac{P}{\rho}\right)\epsilon_0 \ . \tag{2.25}$$

We now have two possible ways of proceeding:

- fix, completely or partially, the coordinate system (i.e., the gauge);
- use a gauge-invariant approach.

We shall briefly review both.

2.3 Gauge fixing and gauge-invariant variables

As we recalled above, the tensor modes are already gauge-invariant, whereas the vector and scalar modes change for infinitesimal coordinate transformations. Since the gauge fixing of the vector fluctuations is analogous, but simpler, to the one of the scalar modes, vectors will be discussed before scalars.

2.3.1 Vector modes

We have two different gauge choices for the vector modes. The first is to set $\tilde{S}_i = 0$ so that, from Eq. (2.19), we have

$$\zeta_i(\eta, \vec{x}) = -\int^{\eta} S_i(\eta', \vec{x})\,\mathrm{d}\eta' + C_i(\vec{x}) \ . \tag{2.26}$$

Since the gauge function is determined up to arbitrary (space-dependent) constants C_i, the coordinate system is not completely fixed by this choice. The second choice is $\tilde{F}_i = 0$ and, from Eq. (2.20), $\zeta_i = F_i$. The gauge freedom is therefore completely fixed in this manner.

Instead of fixing a gauge, we could work directly with gauge-invariant quantities. We note that, from Eqs. (2.19) and (2.20), the combination $F_i' + S_i$ is invariant under infinitesimal coordinate transformations preserving the vector nature of the fluctuations. This is the vector counterpart of the Bardeen potentials [29].

2.3.2 Scalar modes

More options are available in the literature for scalar modes and we briefly review the more common ones (see Ref. [5] for more details).

Conformally Newtonian (or Longitudinal) gauge

In this gauge we eliminate all the off-diagonal entries $\tilde{E}$ and $\tilde{B}$ of the perturbed metric in Eq. (2.13), i.e. $\tilde{E}_{\rm L} = \tilde{B}_{\rm L} = 0$. From Eqs. (2.17) and (2.18) the gauge functions are then determined as $\epsilon = E$ and $\epsilon_0 = E' - B$ and the only non-vanishing entries of the perturbed metric are $\tilde{\phi}$ and $\tilde{\psi}$.

Off-diagonal (or Uniform Curvature) gauge

This gauge is characterized by the conditions $\tilde{E}_{\rm od} = 0$ and $\tilde{\psi}_{\rm od} = 0$. From Eqs. (2.16) and (2.18) we find $\epsilon_0 = -\psi/\mathcal{H}$ and $\epsilon = E$. The two non-vanishing metric fluctuations are then $\tilde{B}$ and $\tilde{\phi}$. Since $\tilde{\psi}_{\rm od} = 0$, the fluctuation of the spatial curvature also vanishes.

Synchronous gauge

This coordinate system is defined by $\tilde{\phi}_{\rm S} = \tilde{B}_{\rm S} = 0$, which however does not fix the gauge completely. In fact, Eqs. (2.15) and (2.17) imply that the gauge functions are determined by

$$(\epsilon_0\, a)' = a\, \phi\ , \quad \epsilon' = (B + \epsilon_0)\ , \tag{2.27}$$

leaving, after integration over η, two undetermined space-dependent functions. This gauge freedom is closely related with unphysical gauge modes.

Comoving Orthogonal gauge

In this gauge the quantity $\tilde{v}_{\rm C} + \tilde{B}_{\rm C}$ is set to zero and the expression of the curvature fluctuations coincides with a relevant gauge-invariant expression whose evolution obeys a conservation law.

Uniform Density gauge

With this choice the total matter density is unperturbed, $\delta\, \tilde{\rho}_{\rm D} = 0$. From Eq. (2.22) the gauge function is then fixed as $\epsilon_0 = (\delta\, \rho)/\rho'$. The curvature fluctuations on constant density hypersurfaces also obey a simple conservation law. If the total energy-momentum tensor of the sources is represented by a single scalar field one can also define the *Uniform Field Gauge*, i.e. the gauge in which the scalar field fluctuation vanishes

Gauge-Invariant approach

The set of gauge-invariant fluctuations can be written as [29, 5]

$$\Phi = \phi + (B - E')' + \mathcal{H}\,(B - E') \tag{2.28}$$

$$\Psi = \psi - \mathcal{H}\,(B - E')\ , \tag{2.29}$$

for the metric perturbations and

$$\delta\,\rho_{\rm g} = \delta\,\rho + \rho'\,(B - E') \tag{2.30}$$

$$\delta\,p_{\rm g} = \delta\,p + p'\,(B - E') \tag{2.31}$$

$$V^i_{\rm g} = v^i + \partial^i\,E'\ , \tag{2.32}$$

for the fluid inhomogeneities. Using Eqs. (2.15)–(2.18) and (2.22)–(2.24), it can be verified that the quantities defined in the above equations are gauge-invariant. Eq. (2.32) can also be written as $V_{\rm g} = v + E'$ since $V^i_{\rm g} = \partial^i\,V_{\rm g}$ and $v^i = \partial^i\,v$. Sometimes it is also convenient to introduce the divergence of the peculiar velocity $\theta = \partial_i\,v^i$, whose associated gauge-invariant quantity is $\Theta = \partial_i\,V^i_{\rm g}$.

Chapter 3

Evolution of metric fluctuations

We have seen in the previous Chapter that the tensor modes of the geometry are gauge-invariant. The vector modes are not invariant under gauge transformation, however, their description is rather simple if the Universe expands and in the absence of vector sources. The scalar modes are the most difficult ones: they are not gauge-invariant and couple directly to the sources of the background geometry. The analysis will be given for the case of a spatially flat background geometry.

3.1 Evolution of the tensor modes

For the tensor modes the perturbed Einstein equations imply that [1] $\delta_{\rm t} R_i^j = 0$. Hence, according to Eq. (A.23), we have in Fourier space

$$h_i^{i\,\prime\prime} + 2\,\mathcal{H}\,h_i^{j\,\prime} + k^2\,h_i^j = 0\ , \tag{3.1}$$

which is satisfied by the two tensor polarizations. In fact, since $\partial_i h_j^i = h_k^k = 0$, the direction of propagation can be chosen along the third axis and, in this case, the two physical polarizations of the graviton will be

$$h_1^1 = -h_2^2 \equiv h_\oplus\ , \quad h_1^2 = h_2^1 \equiv h_\otimes \tag{3.2}$$

where $h_\oplus$ and $h_\otimes$ obey the same evolution Eq. (3.1) and will be denoted by h. Eq. (3.1) can be written in two slightly different, but mathematically equivalent forms

$$\left(a^2\,h_k'\right)' = -k^2\,h_k \tag{3.3}$$

$$\mu_k'' + \left[k^2 - \frac{a''}{a}\right]\,\mu_k = 0\ , \tag{3.4}$$

where $\mu_k = a\,h_k$. For $k^2 \gg |a''/a|$ the solutions of Eq. (3.4) are oscillatory, and the amplitudes of the tensor modes decrease as $1/a$, if the background expands. For $k^2 \ll$

---

[1] We recall that $\delta_{\rm t}$, $\delta_{\rm v}$ and $\delta_{\rm s}$ denote the first-order fluctuation with respect to tensor, vector and scalar modes respectively.

$|a''/a|$ the solution is non-oscillatory and is given by

$$\mu_k(\eta) \simeq A_k\, a(\eta) + B_k\, a(\eta) \int^{\eta} \frac{d\eta'}{a^2(\eta')} \,, \tag{3.5}$$

where A_k and B_k are numerical coefficients.

3.1.1 Hamiltonians for the tensor problem

The variable $\mu_k = a\, h_k$ introduced above plays a special role in the theory of primordial fluctuations, since it is the canonical variable that diagonalises the action for the tensor fluctuations. Such a quadratic action for the tensor modes of the geometry can be obtained by perturbing the Einstein-Hilbert action to second-order in the amplitude of the tensor fluctuations of the metric.

To this end, it is convenient to start from a form of the gravitational action which excludes, from the beginning, the known total derivative. In the case of tensor modes this calculation is rather straightforward and the result can be written as

$$S_{\rm gw} = \frac{1}{64\,\pi\, G} \int \mathrm{d}^4x\, a^2\, \eta^{\alpha\beta}\, \partial_\alpha h_i^j\, \partial_\beta h_j^i \,, \tag{3.6}$$

where $\eta_{\alpha\beta}$ is the Minkowski metric. After a redefinition of the tensor amplitude through the reduced Planck mass [2],

$$h = \frac{h_{\oplus}\, M_{\rm Pl}}{\sqrt{2}} \quad \text{or} \quad h = \frac{h_{\otimes}\, M_{\rm Pl}}{\sqrt{2}} \,, \tag{3.7}$$

the action (3.6) for a single tensor polarization becomes

$$S^{(1)}_{\rm gw} = \frac{1}{2} \int \mathrm{d}^4x\, a^2\, \eta^{\alpha\beta}\, \partial_\alpha h\, \partial_\beta h \,, \tag{3.8}$$

and its canonical momentum is simply given by $\Pi = a^2\, h'$. The classical Hamiltonian associated with Eq. (3.8) is

$$H^{(1)}_{\rm gw}(\eta) = \frac{1}{2} \int \mathrm{d}^3x \left[\frac{\Pi^2}{a^2} + a^2\, (\partial_i h)^2\right] \,, \tag{3.9}$$

which is time-dependent. It is therefore possible to perform a time-dependent canonical transformation, leading to a different Hamiltonian that will be classically equivalent to (3.9). Defining the rescaled field $\mu = a\, h$, the action (3.8) becomes

$$S^{(2)}_{\rm gw} = \frac{1}{2} \int \mathrm{d}^4x \left[\mu'^2 - 2\,\mathcal{H}\,\mu\,\mu' + \mathcal{H}^2\,\mu^2 - (\partial_i \mu)^2\right] \,, \tag{3.10}$$

---

[2] In our notation, $M_{\rm Pl}^{-1} = \sqrt{8\,\pi\, G}$.

which yields the Hamiltonian

$$H^{(2)}_{\rm gw}(\eta) = \frac{1}{2}\int {\rm d}^3x \,\left[\pi^2 + 2\,\mathcal{H}\,\mu\,\pi + (\partial_i\mu)^2\right]\,, \tag{3.11}$$

for μ and of its canonically conjugate momentum $\pi = \mu' - \mathcal{H}\,\mu$. A further canonical transformation can be performed starting from (3.11) which is defined by the generating functional

$$\mathcal{G}_{2\to 3}(\mu, \tilde{\pi}, \eta) = \int {\rm d}^3x\,\left(\mu\,\tilde{\pi} - \frac{\mathcal{H}}{2}\,\mu^2\right)\,, \tag{3.12}$$

where $\tilde{\pi} = \mu'$ is the new momentum conjugated to μ. The new Hamiltonian can now be obtained by taking the partial time derivative of (3.12) and reads

$$H^{(3)}_{\rm gw}(\eta) = \frac{1}{2}\int {\rm d}^3x\,\left[\tilde{\pi}^2 + (\partial_i\,\mu)^2 - \left(\mathcal{H}^2 + \mathcal{H}'\right)\,\mu^2\right]\,. \tag{3.13}$$

The possibility of defining different Hamiltonians is connected with the possibility of dropping total (non covariant) derivatives from the action. To illustrate this point, let us consider the action given in Eq. (3.8) for a single polarization which can be rewritten as

$$S_{\rm gw} = \frac{1}{2}\int {\rm d}^3x\,{\rm d}\eta\,a^2\,\left[h'^2 - (\partial_i h)^2\right]\,. \tag{3.14}$$

Recalling that, from the natural definition of the canonical field $\mu = a\,h$, we also have $a\,h' = \mu' - \mathcal{H}\,\mu$, Eq. (3.14) becomes

$$S_{\rm gw} = \frac{1}{2}\int {\rm d}^3x\,{\rm d}\eta\,\left[\mu'^2 + \mathcal{H}^2\,\mu^2 - 2\,\mathcal{H}\,\mu\,\mu' - (\partial_i\mu)^2\right]\,. \tag{3.15}$$

In Eq. (3.15), the canonically conjugate momentum is obtained by functionally differentiating the associated Lagrangian density $\mathcal{L}\,(\eta, \vec{x})$, where

$$S_{\rm gw} = \int {\rm d}\eta\,L(\eta)\,, \quad L(\eta) = \int {\rm d}^3x\,\mathcal{L}\,(\eta, \vec{x})\,, \tag{3.16}$$

with respect to μ' and the result is $\pi = \mu' - \mathcal{H}\,\mu$. Hence, the Hamiltonian will be

$$H_{\rm gw}(\eta) = \int {\rm d}^3x\,\left[\pi\,\mu' - \mathcal{L}_{\rm gw}\,(\eta, \vec{x})\right]\,. \tag{3.17}$$

Consequently, from Eqs. (3.15) and recalling the expression of $\tilde{\pi}$, one exactly obtains the result given in Eq. (3.11). We now note that one can write

$$\mathcal{H}\,\mu\,\mu' = -\frac{\mathcal{H}'}{2}\,\mu^2 + \frac{\rm d}{{\rm d}\eta}\left[\frac{\mathcal{H}\,\mu^2}{2}\right]\,, \tag{3.18}$$

which can be replaced in Eq. (3.15) and leads to

$$\tilde{S}_{\rm gw} = \frac{1}{2}\int {\rm d}^4x \left[\mu'^2 + \left(\mathcal{H}^2 + \mathcal{H}'\right)\, \mu^2 - (\partial_i\mu)^2\right] \, . \tag{3.19}$$

The latter will be classically equivalent to the action (3.15) for μ and its conjugate momentum $\tilde{\pi} = \mu'$. Hence, the Hamiltonian for μ and $\tilde{\pi}$ can be easily obtained from Eq. (3.17) with π replaced by $\tilde{\pi}$ and will exactly be the one given in Eq. (3.13).

The same conclusion also applies to the scalar fluctuations. In the Lagrangian approach, this aspect reflects in the possibility of defining classical actions that differ by the addition of a total time derivative. While at the classical level the equivalence among the different actions is complete, at the quantum level this equivalence is somehow broken since the minimization of an action may lead to computable differences with respect to another.

3.2 Evolution of the vector modes

This paragraph is inserted for completeness, but in the following we only focus on the vector and scalar perturbations.

The evolution of the vector modes of the geometry can be obtained by perturbing the Einstein equations and the covariant conservation equation with respect to the vector modes of the geometry

$$\delta_{\rm v}\, \mathcal{G}_\mu^\nu = 8\,\pi\, G\, \delta_{\rm v}\, T_\mu^\nu \tag{3.20}$$

$$\nabla_\mu\, \delta_{\rm v}\, T^{\mu\nu} = 0 \, . \tag{3.21}$$

Using Eqs. (A.18) and (A.19) of Appendix A, the explicit form of the above equations can be obtained as

$$\nabla^2\, S_i = 16\,\pi\, G\, (p+\rho)\; a^2\, \mathcal{V}_i \tag{3.22}$$

$$S_i' + 2\,\mathcal{H}\, S_i = 0 \tag{3.23}$$

$$\mathcal{V}_i' + (1-3\,w)\; \mathcal{H}\, \mathcal{V}_i = 0 \, , \tag{3.24}$$

where $\mathcal{V}_i$ is the divergenceless part of the velocity field and, as discussed in Chapter 2, the gauge has been completely fixed by requiring $\tilde{F}_i = 0$, implying, according to Eqs. (2.19) and (2.20), that $\zeta_i = F_i$. Note also that, according to our conventions for the velocity field (see Eq. (A.31)), $\delta_{\rm v}\, T_0^i = (p+\rho)\; \mathcal{V}^i$. Eqs. (3.22)–(3.24) follow, respectively, from the $0-i$ and $i-j$ components of the Einstein equations and from the spatial component of the covariant conservation equation.

Eqs. (3.22) and (3.23) are not independent. In fact, it is easy to check, using Eq. (3.22), that S_i can be eliminated from Eq. (3.23) and Eq. (3.24) is then obtained. By Fourier transforming Eqs. (3.22) and (3.23), we find the solution

$$S_i(\eta) = \frac{C_i(k)}{a^2} \tag{3.25}$$

$$\mathcal{V}_i\,(\eta) = \frac{k^2\, C_i(k)}{16\,\pi\, G\, a^4\, (p+\rho)} \, , \tag{3.26}$$

where $C_i(k)$ is an integration constant. Two distinct situations are possible. If the Universe is expanding, S_i is always decreasing. However, $\mathcal{V}_i$ may also increase. Consider, for example, the case of a single barotropic fluid $p = w\,\rho$. Since, according to Eqs. (2.4) and (2.5) we have $\rho \simeq a^{-3\,(w+1)}$, then

$$\mathcal{V}_i \propto a^{3\,w-1}\ . \tag{3.27}$$

If $w = 1$, $\mathcal{V}_i$ increases like η (since $a(\eta) \sim \sqrt{\eta}$), while $S_i(\eta) \simeq \eta^{-1}$ decays for large conformal times and is negligible for our purposes of describing the CMB. This observation was indeed raised in the past, in connection with the idea that the early Universe could be dominated by vorticity. If the Universe contracts in the future, the evolution of the vector modes will be reversed and S_i may increase again.

Finally, the situation may change even more radically if the theory is not of Einstein-Hilbert type or if it is higher-dimensional. Note that, if the energy-momentum tensor of the fluid sources possesses a non-vanishing torque, rotational perturbations can be copiously produced.

3.3 Evolution of the scalar modes

In analogy with the case of the tensor modes, large-scale scalar fluctuations follow a set of conservation laws that hold approximately for $k\,\eta \ll 1$ and become exact only in the limit $k\,\eta \to 0$.

The evolution equations for the fluctuations of the geometry and of the sources can be written without fixing a specific coordinate system. Then, by using the definitions of the Bardeen potentials the wanted gauge-invariant form of the equations can be obtained. Inserting the definitions (2.28)–(2.32) into Eqs. (A.51) and (A.52), the gauge-invariant Hamiltonian and momentum constraint become

$$\nabla^2\Psi - 3\,\mathcal{H}\ (\Psi' + \mathcal{H}\,\Phi) = 4\,\pi\,a^2\,G\,\delta\,\rho_{\rm g} \tag{3.28}$$

$$\nabla^2\ (\Psi' + \mathcal{H}\,\Phi) = -4\,\pi\,G\,a^2\ (p+\rho)\ \Theta\ , \tag{3.29}$$

where $\Theta = \partial_i V^i_{\rm g}$ is the divergence of the gauge-invariant (scalar) peculiar velocity field. Inserting the expressions of the gauge-invariant fluctuations given in Eqs. (2.28)–(2.32) into Eqs. (A.54) we can derive

$$\Psi'' + \mathcal{H}\ (\Phi' + 2\,\Psi') + \left(\mathcal{H}^2 + 2\,\mathcal{H}'\right)\ \Phi + \frac{1}{3}\,\nabla^2\,(\Phi - \Psi) = 4\,\pi\,G\,a^2\,\delta\,p_{\rm g} \tag{3.30}$$

$$\nabla^2\,(\Phi - \Psi) = 12\,\pi\,G\,a^2\ (p+\rho)\ \sigma\ . \tag{3.31}$$

Finally, the gauge-invariant form of the perturbed covariant conservation equations become

$$\delta\,\rho_{\rm g}' - 3\ (p+\rho)\,\Psi' + (p+\rho)\ \Theta + 3\,\mathcal{H}\ (\delta\,\rho_{\rm g} + \delta\,p_{\rm g}) = 0 \tag{3.32}$$

$$(p+\rho)\ \Theta' + [(p'+\rho') + 4\,\mathcal{H}\ (p+\rho)]\ \Theta + \nabla^2\delta\,p_{\rm g} + (p+\rho)\ \nabla^2\Phi = 0\ , \tag{3.33}$$

as follows from inserting Eqs. (2.28)–(2.32) into Eqs. (A.57) and (A.58) without imposing any gauge condition. Eqs. (3.28) and (3.29) and Eqs. (3.30) and (3.31) have the same form of the evolution equations in the longitudinal gauge. We also define the quantity

$$\mathcal{R} \equiv -\left(\Psi - \mathcal{H}\, V_{\rm g}\right) = -\Psi - \frac{\mathcal{H}\,(\Psi' + \mathcal{H}\,\Phi)}{\mathcal{H}^2 - \mathcal{H}'}\ , \tag{3.34}$$

which is gauge-invariant and will be used extensively later.

3.3.1 Physical interpretation of curvature perturbations

In the comoving gauge, the three-velocity of the fluid vanishes, i.e. $v_{\rm C} = 0$. Since hypersurfaces of constant (conformal) time should be orthogonal to the four-velocity, we will also have that $B_{\rm C} = 0$. In this gauge the curvature perturbation can be computed directly from the expressions of the perturbed Christoffel connections bearing in mind that we want to compute the fluctuations in the spatial curvature,

$$\delta\, R^{(3)}_{\rm C} = \delta_{\rm s}\, \gamma^{ij}\, \overline{R}^{(3)}_{ij} + \overline{\gamma}^{ij}\, \delta_{\rm s}\, R^{(3)}_{ij} \equiv \frac{4}{a^2}\, \nabla^2 \psi_{\rm C}\ , \tag{3.35}$$

where the subscript C is to remind that the expression holds on comoving hypersurfaces. The curvature fluctuations in the comoving gauge can be connected to the fluctuations in a different gauge characterized by a different value of the time coordinate, i.e. $\eta_{\rm C} \to \eta = \eta_{\rm C} + \epsilon_0$. Under this shift

$$\psi_{\rm C} \to \psi = \psi_{\rm C} + \mathcal{H}\,\epsilon_0 \tag{3.36}$$

$$(v_{\rm C} + B_{C}) \to v + B = (v_{\rm C} + B_{\rm C}) + \epsilon_0\ . \tag{3.37}$$

Since in the comoving orthogonal gauge $v_{\rm C} + B_{\rm C} = 0$, Eqs. (3.36) and (3.37) imply, in the new coordinate system, that

$$\psi_{\rm C} = \psi - \mathcal{H}\,(v + B) = (\Psi - \mathcal{H}\, V_{\rm g})\ , \tag{3.38}$$

where the second equality follows from the definitions of gauge-invariant fluctuations given in Eqs (2.28)–(2.32). From Eq. (3.38), one can conclude that $\mathcal{R}$ in Eq. (3.34) corresponds to the curvature fluctuations of the spatial curvature on comoving orthogonal hypersurfaces.

Other quantities, defined in specific gauges, turn out to have a gauge-invariant interpretation. Take, for instance, the curvature fluctuations on constant density hypersurfaces $\psi_{\rm D}$. Under infinitesimal gauge transformations we have

$$\begin{aligned} &\psi_{\rm D} \to \psi = \psi_{\rm D} + \mathcal{H}\,\epsilon_0 \\ &\delta\,\rho_{\rm D} \to \delta\,\rho = \delta\,\rho_{\rm D} - \rho'\,\epsilon_0\ , \end{aligned} \tag{3.39}$$

where, on constant density hypersurfaces, $\delta\,\rho_{\rm D} = 0$ by definition of the uniform density gauge. Hence, from Eq. (3.39), we obtain

$$\psi_{\rm D} = \psi + \mathcal{H}\,\frac{\delta\,\rho}{\rho'} = \Psi + \mathcal{H}\,\frac{\delta\,\rho_{\rm g}}{\rho'}\ , \tag{3.40}$$

where the second equality follows from Eqs. (2.28)–(2.32). Hence, the (gauge-invariant) curvature fluctuations on constant density hypersurfaces can be defined as

$$\zeta \equiv -\left(\Psi + \mathcal{H}\,\frac{\delta\,\rho_{\rm g}}{\rho'}\right) \,, \tag{3.41}$$

which coincides with the curvature fluctuations in the uniform density gauge.

The values of ζ and $\mathcal{R}$ are equal up to terms proportional to the Laplacian of Ψ. This can be shown by using the definitions of $\mathcal{R}$ and ζ, whose difference gives

$$\zeta - \mathcal{R} = -\mathcal{H}\left(V_{\rm g} + \frac{\delta\,\rho_{\rm g}}{\rho'}\right) \,. \tag{3.42}$$

From the Hamiltonian and momentum constraints and from the conservation of the energy density of the background

$$\begin{aligned} V_{\rm g} &= -\frac{1}{4\,\pi\,G\,a^2\,(p+\rho)}\,\left(\mathcal{H}\,\Phi + \Psi'\right) \\ \frac{\delta\,\rho_{\rm g}}{\rho'} &= \frac{1}{4\,\pi\,G\,a^2\,(p+\rho)}\,\left[\nabla^2\Psi - 3\,\mathcal{H}\,\left(\mathcal{H}\,\Phi + \Psi'\right)\right] \,, \end{aligned} \tag{3.43}$$

we in fact obtain

$$\zeta - \mathcal{R} = \frac{\nabla^2\Psi}{12\,\pi\,G\,a^2\,(p+\rho)} \,. \tag{3.44}$$

The density fluctuation on comoving orthogonal hypersurfaces can be also defined as [29]

$$\epsilon_{\rm m} \equiv \frac{\delta\,\rho_{\rm C}}{\rho} = \frac{\delta\,\rho + \rho'\,(v+B)}{\rho} = \frac{\delta\,\rho_{\rm g} - 3\,\mathcal{H}\,(p+\rho)\,V_{\rm g}}{\rho} \,, \tag{3.45}$$

where the second equality follows from the first one by using the definitions of gauge-invariant fluctuations. Again, using the Hamiltonian and momentum constraints, one obtains

$$\epsilon_{\rm m} = \frac{1}{4\,\pi\,G\,a^2\,\rho}\,\nabla^2\Psi \,, \tag{3.46}$$

which means that $(\zeta - \mathcal{R}) \propto \epsilon_{\rm m}$.

3.3.2 Curvature perturbations induced by scalar fields

Some of the general considerations developed earlier in this section will now be specialized to the case of scalar field sources characterized by a potential $V(\varphi)$. For a single scalar field, the background Einstein equations In a spatially flat FRW geometry read

$$\mathcal{H}^2 = \frac{8\,\pi\,G}{3}\left(\frac{\varphi'^2}{2} + V\,a^2\right) \tag{3.47}$$

$$\left(\mathcal{H}^2 - \mathcal{H}'\right) = 4\,\pi\,G\,\varphi'^2 \tag{3.48}$$

$$\varphi'' + 2\,\mathcal{H}\,\varphi' + \frac{\partial V}{\partial\varphi}\,a^2 = 0 \,. \tag{3.49}$$

The fluctuation of φ defined in Appendix A under a coordinate transformation (2.12) changes as

$$\chi \to \tilde{\chi} = \chi - \varphi' \, \epsilon_0 \; . \tag{3.50}$$

Consequently, the associated gauge-invariant scalar field fluctuation is given by

$$X = \chi + \varphi' \, (B - E') \; . \tag{3.51}$$

The two Bardeen potentials and the gauge-invariant scalar field fluctuation X define the coupled system of scalar fluctuations of the geometry,

$$\nabla^2 \Psi - 3\,\mathcal{H}\,(\mathcal{H}\,\Phi + \Psi') = 4\,\pi\,G \left[-\varphi'^2\,\Phi + \varphi'\,X' + \frac{\partial V}{\partial \varphi}\,a^2\,X \right] \tag{3.52}$$

$$\mathcal{H}\,\Phi + \Psi' = 4\,\pi\,G\,\varphi'\,X \tag{3.53}$$

$$\Psi'' + \mathcal{H}\,(\Phi' + 2\,\Psi') + \left(\mathcal{H}^2 + 2\,\mathcal{H}'\right)\,\Phi = 4\,\pi\,G \left[-\varphi'^2\,\Phi + \varphi'\,X' - \frac{\partial V}{\partial \varphi}\,a^2\,X \right] \; , \tag{3.54}$$

where Eqs. (3.52), (3.53) and (3.54) are, respectively, the perturbed $0-0$, $0-i$ and $i-j$ components of the Einstein equations. Although these equations are sufficient to determine the evolution of the system, it is also appropriate to recall the gauge-invariant form of the perturbed Klein-Gordon equation

$$X'' + 2\,\mathcal{H}\,X' - \nabla^2 X + \frac{\partial^2 V}{\partial \varphi^2}\,a^2\,X + 2\,\Phi\,\frac{\partial V}{\partial \varphi}\,a^2 - \varphi'\,(\Phi' + 3\,\Psi') = 0 \; . \tag{3.55}$$

The above equation can be obtained from the perturbed Klein-Gordon equation without gauge fixing, reported in Eq. (A.50) of Appendix A, by inserting the gauge-invariant fluctuations of the metric given in Eqs. (2.28)–(2.29) into Eq. (A.50) together with Eq. (3.51).

If the perturbed energy-momentum tensor has vansihing anisotropic stress, the $(i \neq j)$ component of the perturbed Einstein equations leads to $\Phi = \Psi$. The gauge-invariant curvature fluctuations on comoving orthogonal hypersurfaces are, for a scalar field source,

$$\mathcal{R} = -\Psi - \mathcal{H}\,\frac{X}{\varphi'} = -\Psi - \frac{\mathcal{H}\,(\mathcal{H}\,\Phi + \Psi')}{\mathcal{H}^2 - \mathcal{H}'} \; . \tag{3.56}$$

Eq. (3.56) and a linear combination of Eqs. (3.52)–(3.54) lead to

$$\mathcal{R}' = -\frac{\mathcal{H}}{4\,\pi\,G\,\varphi'^2}\,\nabla^2 \Psi \; , \tag{3.57}$$

which implies that $\mathcal{R}$ is constant for the modes k such that $k\,\eta \ll 1$ [29]. The power spectrum of the scalar modes amplified during the inflationary phase is customarily expressed in terms of $\mathcal{R}$, which is conserved on super-horizon scales.

Curvature perturbations on comoving spatial hypersurfaces can also be simply related to curvature perturbations on the constant density hypersurfaces,

$$\zeta = -\Psi - \mathcal{H}\,\frac{\delta\,\rho_\varphi}{\rho'_\varphi} = -\Psi + \frac{a^2\,\delta\,\rho_\varphi}{3\,\varphi'^2} \; . \tag{3.58}$$

Taking Eqs. (3.34) and (3.58), and using Eq. (3.52) we have

$$\zeta - \mathcal{R} = \mathcal{H}\,\frac{X}{\varphi'} + \frac{a^2\,\delta\,\rho_\varphi}{3\,\varphi'^2} = \frac{2\,m_{\mathrm{Pl}}^2}{3}\,\frac{\nabla^2\Psi}{\varphi'^2}\ , \tag{3.59}$$

which confirms that $\mathcal{R}$ and ζ differ by the Laplacian of a Bardeen potential. Taking the time derivative of Eq. (3.57) and using Eq. (3.56) and Eqs. (3.52)–(3.54), we obtain the second-order equation

$$\mathcal{R}'' + 2\,\frac{z'}{z}\,\mathcal{R}' - \nabla^2\mathcal{R} = 0\ , \tag{3.60}$$

where the function $z(\eta)$ is

$$z(\eta) = \frac{a\,\varphi'}{\mathcal{H}}\ . \tag{3.61}$$

Eq. (3.60) is formally similar to Eq. (3.1), i.e. the evolution equation of a single tensor polarization. We can eliminate the first time derivative appearing in Eq. (3.60) by introducing the gauge-invariant variable

$$q = -z\,\mathcal{R}\ , \tag{3.62}$$

which leads to

$$q'' - \frac{z''}{z}\,q - \nabla^2 q = 0\ . \tag{3.63}$$

After a Fourier transformation, we have

$$q_k'' + \left[k^2 - \frac{z''}{z}\right]\,q_k = 0\ , \tag{3.64}$$

i.e., the scalar analog of Eq. (3.4).

3.3.3 Horizon flow functions

The driving fields of the scalar and tensor modes are usually referred to as *pump fields*. They appear explicitly as the term a''/a in Eq. (3.4) and z''/z in Eq. (3.64). For general potentials leading to a quasi-de Sitter expansion of the geometry, they are conventionally described in terms of the hierarchy of horizon flow functions (HFF; see Appendix B for a comparison with different conventions), defined according to

$$\begin{aligned} \epsilon_0 &\equiv \frac{H(N_i)}{H(N)} \\ \epsilon_{j+1} &\equiv \frac{\mathrm{d}\ln|\epsilon_j|}{\mathrm{d}N}\ , \qquad j \geq 0 \end{aligned} \tag{3.65}$$

where N is the number of e-folds, $N \equiv \ln(a/a_i)$ [where $a_i = a(\eta_i)$] after the arbitrary initial time η_i. A general result is that inflation takes place for $\epsilon_1 < 1$.

To find the expressions of the pump fields in terms of the HFF it is useful to write the background equations as a first-order set of non-linear differential equations

$$\left(\frac{\partial H}{\partial \varphi}\right)^2 - \frac{3}{2\, m_{\rm Pl}^2}\, H^2\,(\varphi) = -\frac{V(\varphi)}{2\, m_{\rm Pl}^4} \tag{3.66}$$

$$\dot{\varphi} = -2\, m_{\rm Pl}^2\, \frac{\partial H}{\partial \varphi}\ . \tag{3.67}$$

Bearing in mind Eq. (3.65), the explicit relation determining the form of the pump field for tensor modes follows from

$$\frac{a''}{a} = \mathcal{H}^2 + \mathcal{H}' = 2\, a^2\, H^2\, + a^2\, \dot{H} = a^2\, H^2\, (2-\epsilon_1)\,, \tag{3.68}$$

where in the last equality, we use $\epsilon_1 = -\dot{H}/H^2$. In the same manner, for the scalar case we obtain

$$\frac{z''}{z} = a^2\, H^2\, \left(2 - \epsilon_1 + \frac{3}{2}\,\epsilon_2 - \frac{1}{2}\,\epsilon_1\,\epsilon_2 + \frac{1}{4}\,\epsilon_2^2 + \frac{1}{2}\,\epsilon_2\,\epsilon_3\right)\ . \tag{3.69}$$

We conclude this section with a useful expression that relates η, a, H and the HFF. Starting from the definition of the conformal time $\mathrm{d}\eta \equiv \mathrm{d}t/a(t)$, we can integrate by parts and find that

$$\eta = -\frac{1 + \epsilon_1\,\epsilon_2 + \mathcal{O}\left(\epsilon_j^3\right)}{a\,H\,(1-\epsilon_1)}\ . \tag{3.70}$$

3.3.4 Hamiltonians for the scalar problem

Different Hamiltonians for the evolution of the scalar fluctuations can be defined.

We begin by expressing the action of the scalar fluctuations of the geometry in terms of the curvature fluctuations

$$S^{(1)}_{\rm scal} = \frac{1}{2}\int \mathrm{d}^4x\, z^2\, \left[\mathcal{R}'^2 - (\partial_i \mathcal{R})^2\right]\ . \tag{3.71}$$

Using the canonical momentum $\pi_{\mathcal{R}} \equiv z^2\,\mathcal{R}'$, the Hamiltonian related to the above action becomes

$$H^{(1)}_{\rm scal}(\eta) = \frac{1}{2}\int \mathrm{d}^3x\, \left[\frac{\pi_{\mathcal{R}}^2}{z^2} + z^2\,(\partial_i\mathcal{R})^2\right]\ , \tag{3.72}$$

and the Hamilton equations

$$\pi_{\mathcal{R}}' = z^2\,\nabla^2\mathcal{R}\ , \quad \mathcal{R}' = \frac{\pi_{\mathcal{R}}}{z^2}\ . \tag{3.73}$$

Eqs. (3.73) can then be combined in the single second order equation (3.60).

The canonically conjugate momentum $\pi_{\mathcal{R}}$ is related to the density perturbation on comoving hypersurfaces. In particular, for a single scalar field source, one finds [29]

$$\epsilon_{\rm m} = \frac{\delta\,\rho_\varphi + 3\,\mathcal{H}\,(\rho_\varphi + p_\varphi)\,V}{\rho_\varphi} = \frac{a^2\,\delta\,\rho_\varphi + 3\,\mathcal{H}\,\varphi'\,X}{a^2\,\rho_\varphi}\ , \tag{3.74}$$

where the second equality can be obtained using $\rho_\varphi + p_\varphi = {\varphi'}^2/a^2$ and the fact that the effective "velocity" in the case of a scalar field is $V = X/\varphi'$. Inserting now Eq. (3.53) into Eq. (3.52), Eq. (3.74) can be expressed as

$$\epsilon_{\rm m} = \frac{2\,m_{\rm Pl}^2\,\nabla^2\Psi}{a^2\,\rho_\varphi} = \frac{2}{3}\,\frac{\nabla^2\Psi}{\mathcal{H}^2}\ , \tag{3.75}$$

where the last equality follows from the first equation in (2.4). From Eq. (3.75), it also follows that

$$\pi_{\mathcal{R}} = -6\,a^2\,\mathcal{H}\,\epsilon_{\rm m}\ , \tag{3.76}$$

in which we used Eq. (3.57) to express $\mathcal{R}'$. Hence, in this description, the canonical field is the curvature fluctuation on comoving spatial hypersurfaces and the canonical momentum is the density fluctuation on the same hypersurfaces.

To bring the second-order action in the simple form of Eq. (3.71), various (non-covariant) total derivatives have been dropped. Hence, there is always the freedom of redefining the canonical fields through time-dependent functions of the background geometry. In particular, the action (3.71) can be rewritten in terms of the variable q defined in Eq. (3.62). Then [30, 31]

$$S^{(2)}_{\rm scal} = \frac{1}{2}\int {\rm d}^4x\,\left[{q'}^2 - 2\,\frac{z'}{z}\,q\,q' - (\partial_i q)^2 + \left(\frac{z'}{z}\right)^2\,q^2\right]\ , \tag{3.77}$$

whose related Hamiltonian and canonical momentum are, respectively

$$H^{(2)}_{\rm scal}(\eta) = \frac{1}{2}\int {\rm d}^3x\,\left[\pi_q^2 + 2\,\pi_q\,q + (\partial_i q)^2\right]\ ,\quad \pi = q' - \frac{z'}{z}\,q\ . \tag{3.78}$$

In Eq. (3.77) another total derivative term can be dropped, leading to the action

$$S^{(3)}_{\rm scal} = \frac{1}{2}\int {\rm d}^4x\,\left[{q'}^2 - (\partial_i q)^2 + \frac{z''}{z}\,q^2\right]\ , \tag{3.79}$$

and Hamiltonian

$$H^{(3)}_{\rm scal}(\eta) = \frac{1}{2}\int {\rm d}^3x\,\left[\tilde{\pi}_q^2 + (\partial_i q)^2 - \frac{z''}{z}\,q^2\right]\ . \tag{3.80}$$

where $\tilde{\pi} = q'$. As in the case of the Hamiltonians for the tensor modes, Eqs. (3.72), (3.78) and (3.80) are all related by canonical transformations.

3.4 Quantum amplification of metric fluctuations

In the framework of quantum theory, the evolution of the metric fluctuations can be described either in the Schrödinger formalism or the Heisenberg picture.

In the Schrödinger description, the quantum evolution can be pictured as the spreading of a quantum mechanical wave-functional. The initial wave-functional is constructed as the direct product of states minimising the uncertainty relations for the harmonic oscillator modes forming the quantum field. This initial vacuum state has zero momentum and each Fourier mode of the field will evolve into a (two mode) squeezed quantum state. The uncertainty relations are still minimised on such states, but in such a way that one of the two canonically conjugate operators will have a variance much larger than the quantum limit, while the other canonically conjugate operator will have a variance much smaller than the quantum uncertainty limit. As a background pumping electromagnetic field (a laser) is able to produce, under some circumstances, squeezed states of photons, the classical gravitational field (for instance the curvature) is able to produce squeezed states of gravitons (for the tensor modes) or of phonons (in the case of the scalar modes).

In fully equivalent terms, the evolution of the fluctuations can be described in the Heisenberg representation. This is the description which will be adopted here. The expectation values of the Hamiltonians of the scalar and tensor modes of the geometry will then be minimized for $\eta \to -\infty$, which is physically identified with the beginning of inflation.

3.4.1 Large-scale power spectra of tensor fluctuations

Let us consider the Hamiltonian given in Eq. (3.13) and drop the tildes in the momenta,

$$H(\eta) = \frac{1}{2}\int d^3x \left[\pi^2 - \frac{a''}{a}\,\mu^2 + (\partial_i\,\mu)^2\right] , \tag{3.81}$$

where $\mu = a\,h_{\oplus}\,M_{\rm Pl}/\sqrt{2}$ (an identical expression holds for the other polarization). After imposing the commutation relations for the canonically conjugate quantum fields (in natural units with $\hbar = 1$)

$$[\hat{\mu}(\vec{x},\eta), \hat{\pi}(\vec{y},\eta)] = i\,\delta^{(3)}(\vec{x}-\vec{y}), \tag{3.82}$$

the operator corresponding to the Hamiltonian (3.81) becomes

$$\hat{H}(\eta) = \frac{1}{2}\int d^3x \left[\hat{\pi}^2 - \frac{a''}{a}\,\hat{\mu}^2 + (\partial_i\,\hat{\mu})^2\right] . \tag{3.83}$$

In Fourier space the quantum fields can be written as

$$\begin{aligned}
\hat{\mu}(\vec{x},\eta) &= \frac{1}{2\,(2\,\pi)^{3/2}}\int d^3k \left[\hat{\mu}_{\vec{k}}\,e^{-i\,\vec{k}\cdot\vec{x}} + \hat{\mu}^{\dagger}_{\vec{k}}\,e^{i\,\vec{k}\cdot\vec{x}}\right] \\
\hat{\pi}(\vec{x},\eta) &= \frac{1}{2\,(2\,\pi)^{3/2}}\int d^3k \left[\hat{\pi}_{\vec{k}}\,e^{-i\,\vec{k}\cdot\vec{x}} + \hat{\pi}^{\dagger}_{\vec{k}}\,e^{i\,\vec{k}\cdot\vec{x}}\right] ,
\end{aligned} \tag{3.84}$$

Inserting now Eqs. (3.84) into Eq. (3.82) and demanding the validity of the latter implies the following canonical commutation relations for the Fourier components of the quantum operators

$$\begin{aligned} \left[\hat{\mu}_{\vec{k}}(\eta), \hat{\pi}^{\dagger}_{\vec{p}}(\eta)\right] &= \left[\hat{\mu}^{\dagger}_{\vec{k}}(\eta), \hat{\pi}_{\vec{p}}(\eta)\right] = i\,\delta^{(3)}(\vec{k}-\vec{p}) \\ \left[\hat{\mu}_{\vec{k}}(\eta), \hat{\pi}_{\vec{p}}(\eta)\right] &= \left[\hat{\mu}^{\dagger}_{\vec{k}}(\eta), \hat{\pi}^{\dagger}_{\vec{p}}(\eta)\right] = i\,\delta^{(3)}(\vec{k}+\vec{p}) \ . \end{aligned} \tag{3.85}$$

Inserting now Eq. (3.84) into Eq. (3.83) we get the Fourier space representation of the quantum Hamiltonian [3]

$$\hat{H}(\eta) = \frac{1}{4}\int \mathrm{d}^3k \left[\left(\hat{\pi}_{\vec{k}}\,\hat{\pi}^{\dagger}_{\vec{k}} + \hat{\pi}^{\dagger}_{\vec{k}}\,\hat{\pi}_{\vec{k}}\right) + \left(k^2 - \frac{a''}{a}\right)\left(\hat{\mu}_{\vec{k}}\,\hat{\mu}^{\dagger}_{\vec{k}} + \hat{\mu}^{\dagger}_{\vec{k}}\,\hat{\mu}_{\vec{k}}\right)\right] \ . \tag{3.86}$$

In the Heisenberg representation the field operators obey

$$i\,\hat{\mu}' = \left[\hat{\mu}, \hat{H}\right] \quad \text{and} \quad i\,\hat{\pi}' = \left[\hat{\pi}, \hat{H}\right] \ . \tag{3.87}$$

Using now the mode expansion (3.84) and the Hamiltonian (3.86), the evolution for the Fourier components of the operators is determined by

$$\hat{\mu}'_{\vec{k}} = \hat{\pi}_{\vec{k}} \tag{3.88}$$

$$\hat{\pi}'_{\vec{k}} = -\left(k^2 - \frac{a''}{a}\right)\hat{\mu}_{\vec{k}} \ , \tag{3.89}$$

whose general solution is

$$\hat{\mu}_{\vec{k}}(\eta) = \hat{a}_{\vec{k}}(\eta_0)\, f_k(\eta) + \hat{a}^{\dagger}_{-\vec{k}}(\eta_0)\, f^*_k(\eta) \tag{3.90}$$

$$\hat{\pi}_k(\eta) = \hat{a}_{\vec{k}}(\eta_0)\, g_k(\eta) + \hat{a}^{\dagger}_{-\vec{k}}(\eta_0)\, g^*_k(\eta) \ , \tag{3.91}$$

where the mode function f_k obeys

$$f''_k + \left[k^2 - \frac{a''}{a}\right] f_k = 0, \tag{3.92}$$

and $g_k = f'_k$. In Eqs. (3.90) and (3.91) the operators $\hat{a}_{\vec{k}}(\eta_0)$ annihilate the vacuum,

$$\hat{a}_{\vec{k}}(\eta_0)|0_{-\infty}\rangle = 0 \quad \text{for } \eta_0 \to -\infty \ . \tag{3.93}$$

As anticipated, this is the state which minimises the Hamiltonian (3.83) close to the onset of inflation. We remark that the time η_0 is the same for all the modes k. The second remark is that the vacuum has zero total momentum during the entire evolution. This means that particles can only be produced in pairs from the vacuum triggered by the pumping action of the gravitational field. Inserting Eqs. (3.90) and (3.91) into Eq. (3.84), the following Fourier expansions can be simply obtained

---

[3] Note that, in order to derive the following equation, the relations $\hat{\mu}^{\dagger}_{-\vec{k}} \equiv \hat{\mu}_{\vec{k}}$ and $\hat{\pi}^{\dagger}_{-\vec{k}} \equiv \hat{\pi}_{\vec{k}}$ should be used.

$$\begin{aligned}\hat{\mu}(\vec{x},\eta) &= \frac{1}{(2\,\pi)^{3/2}}\int \mathrm{d}^3k\,\left[\hat{a}_{\vec{k}}(\eta_0)\,f_k(\eta)\,e^{-i\,\vec{k}\cdot\vec{x}}+\hat{a}^{\dagger}_{\vec{k}}(\eta_0)\,f^{*}_k(\eta)\,e^{i\,\vec{k}\cdot\vec{x}}\right] &(3.94)\\ \hat{\pi}(\vec{x},\eta) &= \frac{1}{(2\,\pi)^{3/2}}\int \mathrm{d}^3k\,\left[\hat{a}_{\vec{k}}(\eta_0)\,g_k(\eta)\,e^{-i\,\vec{k}\cdot\vec{x}}+\hat{a}^{\dagger}_{\vec{k}}(\eta_0)\,g^{*}_k(\eta)\,e^{i\,\vec{k}\cdot\vec{x}}\right]\;, &(3.95)\end{aligned}$$

since, upon integration by parts, one has $\hat{a}_{-\vec{k}}\,e^{i\,\vec{k}\cdot\vec{x}}=\hat{a}_{\vec{k}}e^{-i\,\vec{k}\cdot\vec{x}}$ and $\hat{a}^{\dagger}_{-\vec{k}}\,e^{-i\,\vec{k}\cdot\vec{x}}=\hat{a}^{\dagger}_{\vec{k}}e^{i\,\vec{k}\cdot\vec{x}}$. The two point function for the tensor fluctuations can then be obtained as

$$\left\langle 0_{-\infty}\left|\hat{h}(\vec{x},\eta)\,\hat{h}(\vec{y},\eta)\right|0_{-\infty}\right\rangle=\frac{2\,l^2_{\mathrm{Pl}}}{(2\,\pi)^3\,a^2(\eta)}\int \mathrm{d}^3k\,|f_k(\eta)|^2\,e^{-i\,\vec{k}\cdot\vec{r}} \tag{3.96}$$

where $\vec{r}=(\vec{x}-\vec{y})$. After angular integration, the previous expression becomes

$$\left\langle 0_{-\infty}\left|\hat{h}(\vec{x},\eta)\,\hat{h}(\vec{y},\eta)\right|0_{-\infty}\right\rangle=\int \mathrm{d}\ln k\,\mathcal{P}_h\,\frac{\sin k\,r}{k\,r} \tag{3.97}$$

where

$$\mathcal{P}_h=\frac{l^2_{\mathrm{Pl}}}{a^2(\eta)}\,\frac{k^3}{\pi^2}\,|f_k(\eta)|^2\,, \tag{3.98}$$

is the tensor power spectrum. In the study of inflation, the tensor spectral index is usually defined as

$$n_{\mathrm{T}}=\frac{\mathrm{d}\ln\mathcal{P}_h}{\mathrm{d}\ln k}\;, \tag{3.99}$$

and its α-running is

$$\alpha_{\mathrm{T}}=\frac{\mathrm{d}^2\ln\mathcal{P}_h}{(\mathrm{d}\ln k)^2}\;. \tag{3.100}$$

3.4.2 Large-scale power spectra of scalar fluctuations

The calculation of the scalar power spectrum follows exactly the same steps discussed in the case of the tensor modes.

In full analogy with the calculation of the tensor power spectrum, the Hamiltonian given in Eq. (3.80) can be chosen. Promoting the canonical mode q and its conjugate momentum to quantum operators which satisfy

$$[\hat{q}(\eta,\vec{x}),\hat{\pi}_q(\eta,\vec{y})]=i\,\delta^{(3)}(\vec{x}-\vec{y})\;, \tag{3.101}$$

one can also define a vacuum state $|0_{-\infty}\rangle$ for the scalar modes at $\eta \to -\infty$. Recalling the relation between the canonical modes and the gauge-invariant curvature fluctuations, obtained in Eq. (3.62), we can then write the scalar two-point function as

$$\left\langle 0_{-\infty} \left| \hat{\mathcal{R}}(\eta, \vec{x})\, \hat{\mathcal{R}}(\eta, \vec{y}) \right| 0_{-\infty} \right\rangle = \frac{1}{z^2} \int \frac{\mathrm{d}^3 k}{2\,\pi^3} \left| f_{\mathrm{s}\,k}(\eta) \right|^2 e^{-i\,\vec{k}\cdot\vec{r}} \ , \tag{3.102}$$

where $f^{q}_{\mathrm{s}\,k}(\eta)$ are the mode functions pertaining to the scalar problem and obeying the equation

$$f''_{\mathrm{s}\,k} + \left[k^2 - \frac{z''}{z} \right] f_{\mathrm{s}\,k} = 0 \ . \tag{3.103}$$

The scalar power spectrum, the scalar spectral index and its running will be defined, with a convenient redefinition of the tensor quantities, in the Chapter 5.

Chapter 4

WKB-type approximations

In this chapter we give a review of some Wentzel-Kramers-Brillouin (WKB)-type approaches used to solve second-order differential equations. We start in the first section by reviewing the standard WKB approximation and then proceed, in the second section, by presenting the problem that arises around the turning point(s) of the frequency and how it can be avoided in other WKB-type approximations. In particular, we give a first improved version of the WKB analysis in the third section and a generalized WKB method, also called Method of Comparison Equations, in the last section.

4.1 Standard WKB approximation

In this Section we begin by recalling the standard WKB method, as is introduced in almost all Quantum Mechanics textbooks (See, for example [32]).

The WKB approximation is defined by first introducing a "small" parameter $\delta > 0$ in order to perform the formal adiabatic (or semiclassical) expansion of the mode functions [33]. Let us briefly recall that such an expansion is called adiabatic when $\sqrt{\delta}$ is the inverse of a (typically very large) time over which the system evolves slowly, and semiclassical when $\sqrt{\delta} \sim \hbar$. Further, the limit $\delta \to 1$ must be taken at the end of the computation. Consequently, second-order differential equations such as Eqs. (3.4) and (3.64) [or equivalently Eqs. (3.92) and (3.103)] are formally replaced by

$$\left[\delta \frac{\mathrm{d}^2}{\mathrm{d}\eta^2} + \Omega^2(k,\eta)\right] \mu = 0 \ . \tag{4.1}$$

We then denote the leading order term in such an expansion of μ by

$$\mu_{\mathrm{WKB}}(k,\eta) = \frac{\mathrm{e}^{\pm \frac{i}{\sqrt{\delta}} \int^{\eta} \Omega(k,\tau)\mathrm{d}\tau}}{\sqrt{2\,\Omega(k,\eta)}} \ , \tag{4.2}$$

which satisfies the following differential equation

$$\left[\delta \frac{\mathrm{d}^2}{\mathrm{d}\eta^2} + \Omega^2(k,\eta) - \delta\, Q_{\Omega}(k,\eta)\right] \mu_{\mathrm{WKB}} = 0 \ , \tag{4.3}$$

where

$$Q_\Omega(k,\eta) \equiv \frac{3}{4}\,\frac{(\Omega')^2}{\Omega^2} - \frac{\Omega''}{2\,\Omega}\ . \tag{4.4}$$

We now observe that $\mu_{\rm WKB}$ is the exact solution of Eq. (4.1) in the "adiabatic limit" $\delta \to 0$, and is expected to be a good approximation to the exact μ (in the limit $\delta \to 1$) if

$$\Delta \equiv \left|\frac{Q_\Omega}{\Omega^2}\right| \ll 1\ . \tag{4.5}$$

Sometimes, to respect the above condition, we need to perform a suitable change of variables. This will indeed be the case for the cosmological perturbation and in Chapter 5 we shall give the correct transformation to improve all WKB-type approximations. After that change of variables we shall use the following form for the differential equation

$$\left[\frac{{\rm d}^2}{{\rm d}x^2} + \omega^2(x)\right]\,\chi = 0\ , \tag{4.6}$$

which is itroduced here to keep track of that transformation. Finally, we recall that Eq. (4.6), but also Eq. (4.1), in general suffer of some problems near the turning point of the frequency $\omega(x)$ which we now discuss.

4.2 The "Turning Point" problem

We describe here a kind of problem that can arise around the turning point of the frequency for the standard WKB approximation and how we can avoid it in other WKB-type approximations. First of all, a "Turning Point" is defined as that point where the frequency of a second-order differential equation like (4.1) or (4.6) vanishes (see Fig. 4.1). A solution of the type given in Eq. (4.2) (or the analogue for Eq. (4.6)) diverges in this point (as well as the error given by the term in Eq. (4.4)) and it is well known that one therefore needs a different branch of solution there.

Schematically, for the standard WKB approximation we have the situation shown in Fig. 4.2, where we see the solution for an ordinary second-order differential equation with only one turning point. The standard procedure to address this problem is to divide the domain of the independent variable into three regions: on the left and on the right of the turning point, where the standard WKB solution is valid, and the "turning point region", where we use a non-WKB solution. Usually, around the turning point, the true frequency is then replaced by a linear approximation and the approximate solution is then given by a linear combination of Airy functions.

The next step is to connect the three branches to obtain a "global" solution on the whole range of the independent variable. We usually match the WKB solutions (i.e., the oscillatory and exponential branches) to that around the turning point using two asymptotic expansions of the latter branch. The overlap regions, where this asymptotic match is performed, are not *a priori* defined but should be determined so as to minimise the error,

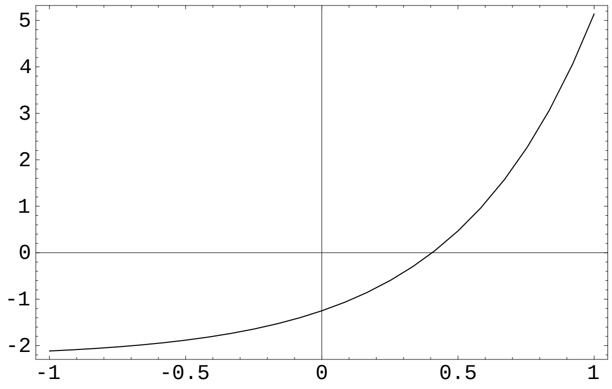

Figure 4.1: Sketch of a typical frequency with one turning point (as is the case for cosmological perturbations). The independent variable is irrelevant for the discussion developed here.

which is usually a very difficult task, although it does not normally affect the accuracy of the solution to leading order in δ (in Fig. 4.2 we use two grey bands to indicate their possible location). This subtlety has already been studied by the physicists and mathematicians who first used the WKB approximation and it is known that the method can give some problems, for example, if one needs a more accurate solution at next-to-leading order in the expansion in δ. In fact, if we used next-to-leading order expressions of the standard WKB expansion, we could find that the overlap regions, where the match is to be performed, become too narrow (or disappear at all!) and an accurate match of the different branches is no more possible [34, 35]. This could even lead to next-to-leading

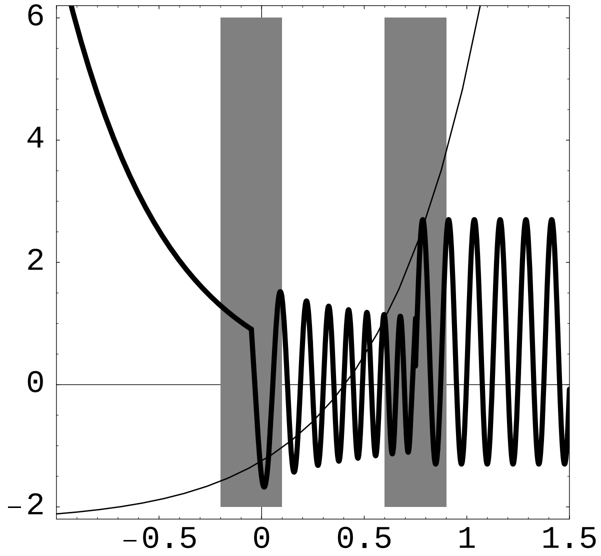

Figure 4.2: Standard WKB approximation.

order results less accurate than the leading ones [36].

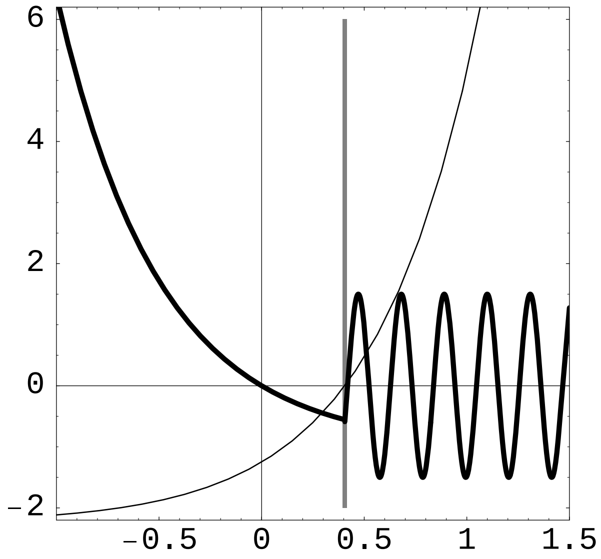

Figure 4.3: Improved WKB approximation.

The improved WKB approach, that we shall present in detail in the next section, will give us an approximation which is also valid at the turnig point. The solution will be divided into only two branches and the procedure of matching will be clearer and more accurate. Actually, the match will be performed exactly at the turning point, which is well located, and, without ambiguous matching regions, the results at next-to-leading order are always improved (see Fig. 4.3).

Finally, the Method of Comparison Equations, presented in the last part of this chapter, is a generalised WKB method that will not need any matching between branches of solutions. The solution will be valid on the whole range of the independent variable and could be used in every problems where we need a global solution of our differential equation (see Fig. 4.4).

So far we haven only considered one turning point, since this is the case for the equations governing cosmological perturbations we shall solve for later. We however note that, if the frequency has two, or more, turning points the solution of this problem could be enormously complicated (a case with two turning points will be described in Appendix G).

4.3 Improved WKB approximation

We shall now describe a method to improve the WKB approximation for equations of the form in Eq. (4.6) to all orders in the adiabatic parameter δ by following the scheme outlined in Ref. [37] (see also Ref. [38]). The basic idea is to use approximate expressions which are valid for all values of the coordinate x and then expand around them. Two

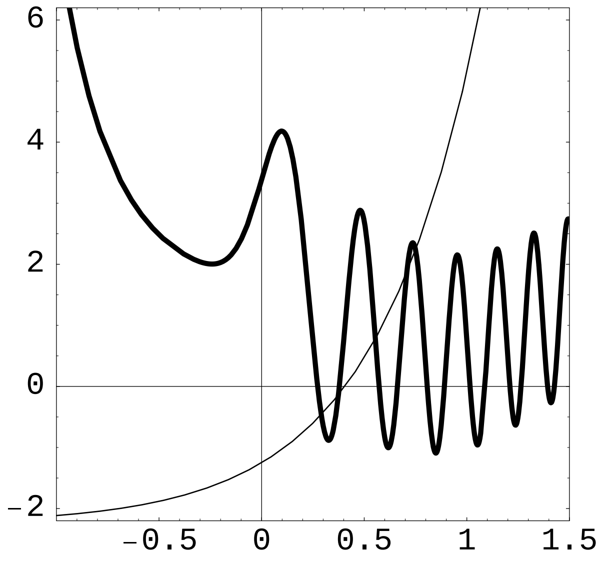

Figure 4.4: MCE approximation.

different such expansions we shall consider, namely one based on the Green's function technique and the other on the usual adiabatic expansion [37].

Let us first illustrate the main idea of Ref. [37] for the particular case $\omega^2 = C\ (x - x_0)^n$, with C a positive costant. All the solutions to Eq. (4.6) for $x > x_0$ can be written as linear combinations of the two functions

$$u_\pm(x) = \sqrt{\frac{\xi(x)}{\omega(x)}}\, J_{\pm m}\left[\xi(x)\right]\ , \tag{4.7}$$

where

$$\xi(x) \equiv \int_{x_0}^{x} \omega(y)\,\mathrm{d}y\ , \qquad m = \frac{1}{n+2}\ , \tag{4.8}$$

and J_ν are Bessel functions [39]. Moreover, for a general frequency ω, the expressions in Eq. (4.7) satisfy

$$\left[\frac{\mathrm{d}^2}{\mathrm{d}x^2} + \omega^2(x) - \sigma(x)\right] u_\pm = 0\ , \tag{4.9}$$

where the quantity (primes will denote derivatives with respect to the argument of the given function from here on)

$$\sigma(x) = \frac{3}{4}\,\frac{(\omega')^2}{\omega^2} - \frac{\omega''}{2\,\omega} + \left(m^2 - \frac{1}{4}\right)\frac{\omega^2}{\xi^2} = Q_\omega + \left(m^2 - \frac{1}{4}\right)\frac{\omega^2}{\xi^2}\ , \tag{4.10}$$

contains the term Q defined in Eq. (4.4), whose divergent behavior at the turning point $x = x_0$ we identified as the possible cause of failure of the standard WKB approach. For a general (finite) frequency, which can be expanded in powers of $x - x_0$ [1],

$$\omega^2(x) = C\ (x - x_0)^n \left[1 + \sum_{q \geq 1} c_q\,(x - x_0)^q\right] \ , \tag{4.11}$$

one finds that the extra term in Eq. (4.10) precisely "removes" the divergence in Q at the turning point. In fact, the residue

$$\lim_{x \to x_0} \sigma(x) = \frac{3\,(n+5)\,c_1^2}{2\,(n+4)\,(n+6)} - \frac{3\,c_2}{n+6} \ , \tag{4.12}$$

is finite [37, 38]. The finiteness of σ at the turning point is crucial in order to extend the WKB method to higher orders. For slowly varying frequencies, with $|\sigma(x)|$ small everywhere, the functions (4.7) are thus expected to be good approximations to the solutions of Eq. (4.6) for the whole range of x, including the turning point.

We can now introduce both the adiabatic expansion of the previous Section and a new formal expansion of the mode functions by replacing Eq. (4.6) by

$$\left[\delta\,\frac{\mathrm{d}^2}{\mathrm{d}x^2} + \omega^2(x) - \delta\,\sigma(x)\right]\,\chi = -\delta\,\varepsilon\,\sigma(x)\,\chi \ , \tag{4.13}$$

where δ and ε are "small" positive parameters. For clarity, we shall refer to expressions proportional to δ^n as the n-th adiabatic order and to those proportional to ε^n as the n-th perturbative order.

It is convenient to consider the solutions to Eq. (4.13) to the left and right of the turning point x_0 separately. We shall call:

region I) where $\omega^2 > 0$ (on the right of x_0), with

$$\omega_{\mathrm{I}}(x) \equiv \sqrt{\omega^2(x)} \ , \quad \xi_{\mathrm{I}}(x) \equiv \int_{x_0}^{x} \omega_{\mathrm{I}}(y)\,\mathrm{d}y \ , \tag{4.14a}$$

and the solutions to the corresponding homogeneous equation (4.9) are given in Eq. (4.7);

region II) where $\omega^2 < 0$ (on the left of x_0), with

$$\omega_{\mathrm{II}}(x) \equiv \sqrt{-\omega^2(x)} \ , \quad \xi_{\mathrm{II}}(x) \equiv \int_{x}^{x_0} \omega_{\mathrm{II}}(y)\,\mathrm{d}y \ , \tag{4.14b}$$

and the solutions to the corresponding homogeneous equation (4.9) are obtained from those in Eq. (4.7) by replacing the J_ν with the I_ν [39].

---

[1] In the following we shall consider the general case in Eq. (4.11), although one might restrict to $n = 1$, since the frequencies for cosmological perturbations usually exhibit a linear turning point.

Corresponding expressions are obtained for all relevant quantities, for example $\sigma_{\rm I}$ and $\sigma_{\rm II}$, and we shall omit the indices I and II whenever it is not ambiguous.

Although it is possible to expand in both parameters, so as to obtain terms of order $\delta^p\,\varepsilon^q$ (with p and q positive integers), in the following we shall just consider each expansion separately, that is we shall set $\delta = 1$ in the perturbative expansion (see Section 4.3.1) and $\varepsilon = 1$ in the adiabatic expansion (see Section 4.3.2).

4.3.1 Perturbative expansion

For $\delta = 1$, the limit $\varepsilon \to 0$ is exactly solvable and yields the solutions (4.7), whereas the case of interest (4.6) is recovered in the limit $\varepsilon \to 1$, which must always be taken at the end of the computation. The solutions to Eq. (4.13) can be further cast in integral form as

$$\chi(x) = u(x) - \varepsilon \int G(x,y)\,\sigma(y)\,\chi(y)\,{\rm d}y \ , \tag{4.15}$$

where $u(x) = A_+\,u_+(x) + A_-\,u_-(x)$ is a linear combination of solutions (4.7) to the corresponding homogeneous equation (4.9), and $G(x,y)$ is the Green's function determined by

$$\left[\frac{{\rm d}^2}{{\rm d}x^2} + \omega^2(x) - \sigma(x)\right]\,G(x,y) = \varepsilon\,\delta(x-y) \ . \tag{4.16}$$

The solutions of the homogeneous equation (4.9) in the two regions are then given by

$$\begin{aligned} u_{\rm I}(x) &= \sqrt{\frac{\xi_{\rm I}(x)}{\omega_{\rm I}(x)}}\,\left\{A_+\,J_{+m}\left[\xi_{\rm I}(x)\right] + A_-\,J_{-m}\left[\xi_{\rm I}(x)\right]\right\} \equiv A_+\,u_{{\rm I}+}(x) + A_-\,u_{{\rm I}-}(x) \\ u_{\rm II}(x) &= \sqrt{\frac{\xi_{\rm II}(x)}{\omega_{\rm II}(x)}}\,\left\{B_+\,I_{+m}\left[\xi_{\rm II}(x)\right] + B_-\,I_{-m}\left[\xi_{\rm II}(x)\right]\right\} \equiv B_+\,u_{{\rm II}+}(x) + B_-\,u_{{\rm II}-}(x) \end{aligned} \tag{4.17}$$

and the Green's functions can be written as

$$\begin{aligned} G_{\rm I}(x,y) &= -\frac{\pi}{\sqrt{3}}\,\theta(x-y)\,u_{{\rm I}-}(x)\,u_{{\rm I}+}(y) - \frac{\pi}{\sqrt{3}}\,\theta(y-x)\,u_{{\rm I}+}(x)\,u_{{\rm I}-}(y) \\ G_{\rm II}(x,y) &= \frac{i\,\pi}{\sqrt{3}}\,\theta(x-y)\,u_{{\rm II}-}(x)\,u_{{\rm II}+}(y) + \frac{i\,\pi}{\sqrt{3}}\,\theta(y-x)\,u_{{\rm II}+}(x)\,u_{{\rm II}-}(y) \ . \end{aligned} \tag{4.18}$$

With the ansatz

$$\begin{aligned} \chi_{\rm I}(x) &= A_+\,a_+(x)\,u_{{\rm I}+}(x) + A_-\,a_-(x)\,u_{{\rm I}-}(x) \\ \chi_{\rm II}(x) &= B_+\,b_+(x)\,u_{{\rm II}+}(x) + B_-\,b_-(x)\,u_{{\rm II}-}(x) \ , \end{aligned} \tag{4.19}$$

from Eqs. (4.17) and (4.18), the problem is now reduced to the determination of the x-dependent coefficients

$$\begin{aligned} a_+(x) &\equiv \left[1+\varepsilon\, J^{+}_{+-}(x,x_i)\right] + \varepsilon\,\frac{A_-}{A_+}\,J^{-}_{--}(x,x_i) \\ a_-(x) &\equiv \left[1+\varepsilon\, J^{-}_{+-}(x_0,x)\right] + \varepsilon\,\frac{A_+}{A_-}\,J^{+}_{++}(x_0,x) \\ b_+(x) &\equiv \left[1-i\,\varepsilon\, I^{+}_{+-}(x,x_0)\right] - i\,\varepsilon\,\frac{B_-}{B_+}\,I^{-}_{--}(x,x_0) \\ b_-(x) &\equiv \left[1-i\,\varepsilon\, I^{-}_{+-}(x_f,x)\right] - i\,\varepsilon\,\frac{B_+}{B_-}\,I^{+}_{++}(x_f,x)\ , \end{aligned} \tag{4.20}$$

in which, for the sake of brevity (and clarity), we have introduced a shorthand notation for the following integrals

$$\begin{aligned} J^{w}_{s\bar s}(x_1,x_2) &\equiv \frac{\pi}{\sqrt 3}\int_{x_1}^{x_2}\sigma_{\rm I}(y)\,a_w(y)\,u_{{\rm I}s}(y)\,u_{{\rm I}\bar s}(y)\,{\rm d}y \\ &= \frac{\pi}{\sqrt 3}\int_{x_1}^{x_2}\sigma_{\rm I}(y)\,\frac{\xi_{\rm I}(y)}{\omega_{\rm I}(y)}\,a_w(y)\;J_{sm}\left[\xi_{\rm I}(y)\right]\;J_{\bar s m}\left[\xi_{\rm I}(y)\right]{\rm d}y \\ I^{w}_{s\bar s}(x_1,x_2) &\equiv \frac{\pi}{\sqrt 3}\int_{x_1}^{x_2}\sigma_{\rm II}(y)\,b_w(y)\,u_{{\rm II}s}(y)\,u_{{\rm II}\bar s}(y)\,{\rm d}y \\ &= \frac{\pi}{\sqrt 3}\int_{x_1}^{x_2}\sigma_{\rm II}(y)\,\frac{\xi_{\rm II}(y)}{\omega_{\rm II}(y)}\,b_w(y)\;I_{sm}\left[\xi_{\rm II}(y)\right]\;I_{\bar s m}\left[\xi_{\rm II}(y)\right]{\rm d}y\,, \end{aligned} \tag{4.21}$$

where the symbols w, s and $\bar s$ are $+$ or $-$.

Before tackling this problem, we shall work out relations which allow us to determine the constant coefficients $A_\pm$ and $B_\pm$ uniquely.

4.3.2 Adiabatic expansion

Let us now apply the usual adiabatic expansion with the assumption that the leading order be given by the functions (4.7) [rather than the more common expression (4.2)]. This leads one to replace

$$\xi(x) \to \frac{\xi(x)}{\sqrt\delta} \equiv \frac{1}{\sqrt\delta}\int^{x}\omega(y)\,{\rm d}y\ , \tag{4.22}$$

and consider the forms [37].

$$U_\pm = F_\pm(x;\delta)\,u_\pm(x) + G_\pm(x;\delta)\,u'_\pm(x)\ , \tag{4.23a}$$

where the x-dependent coefficients F and G must now be determined. The particular case of a linear turning point [40] (precisely the one which mostly concerns us here), can then be fully analyzed as follows.

Recursive (adiabatic) relations

The x-dependent coefficients F and G can be expanded in powers of δ as

$$\begin{aligned} F(x;\delta) &= \sum_{j\geq 0} \delta^j\, \phi_{(j)}(x) \\ G(x;\delta) &= \sum_{j\geq 0} \delta^j\, \gamma_{(j)}(x)\ . \end{aligned} \tag{4.23b}$$

Upon substituting into Eq. (4.13) with $\varepsilon = 1$, one therefore obtains that the coefficients $\phi_{(j)}$ and $\gamma_{(j)}$ are given recursively by the formulae

$$\begin{aligned} \phi_{(j)}(x) &= -\frac{1}{2}\int^x \left[\gamma''_{(j)}(y) + \sigma(y)\,\gamma_{(j)}(y)\right] \mathrm{d}y \\ \gamma_{(j)}(x) &= \frac{1}{2\,\omega(x)}\int^x \Big\{\sigma(y)\ \left[2\,\gamma'_{(j-1)}(y) + \phi_{(j-1)}(y)\right] \\ &\qquad +\sigma'(y)\,\gamma_{(j-1)}(y) + \phi''_{(j-1)}(y)\Big\}\,\frac{\mathrm{d}y}{\omega(y)}\ , \end{aligned} \tag{4.23c}$$

where it is understood that the integration must be performed from x_0 to x in region I and from x to x_0 in region II. Let us also remark that, for $\omega^2 \sim (x - x_0)$ near the turning point, the above expressions are finite [40], whereas for more general cases one expects divergences as with the more standard WKB approach.

Leading order

The lowest order solutions (4.7) are correctly recovered on setting

$$\phi_{(0)} = 1 \quad \text{and} \quad \gamma_{(0)} = 0\ , \tag{4.24}$$

in the limit $\delta = 1$. The relevant leading order perturbations are therefore obtained on imposing the initial conditions (5.13) and matching conditions between region I and region II at the turning point, which therefore yield for χ_{I} and χ_{II} the same linear combinations u_{I} of Eq. (5.25a) and u_{II} of Eq. (5.25b) previously obtained.

Higher orders

The condition (4.24) makes the formal expressions of the coefficients $\phi_{(1)}$ and $\gamma_{(1)}$ particularly simple,

$$\begin{aligned} \phi_{(1)}(x) &= -\frac{1}{2}\int^x \left[\gamma''_{(1)}(y) + \sigma(y)\,\gamma_{(1)}(y)\right]\,\mathrm{d}y \\ \gamma_{(1)}(x) &= \frac{1}{2\,\omega(x)}\int^x \frac{\sigma(y)}{\omega(y)}\,\mathrm{d}y\ , \end{aligned} \tag{4.25}$$

and the first order solutions are then given by linear combinations of the two functions

$$U_\pm(x) = \left[1 + \delta\,\phi_{(1)}(x)\right]\; u_\pm(x) + \delta\,\gamma_{(1)}(x)\,u'_\pm(x)\ . \tag{4.26}$$

4.4 Method of Comparison Equation

In this Section we briefly review the Method of Comparison Equation (MCE). The name is due to Dingle and it was independently introduced in Refs. [41, 42] and applied to wave mechanics by Berry and Mount in Ref. [43]. The standard WKB approximation and its improvement by Langer [37] are just particular cases of this method. In Section 4.4.1 we shall also present the connection of the MCE with the Ermakov-Pinney equation.

We start from the well-known second-order differential equation (4.6) and suppose that we know an exact solution to a similar second-order differential equation,

$$\left[\frac{\mathrm{d}^2}{\mathrm{d}\sigma^2} + \Theta^2(\sigma)\right]\, U(\sigma) = 0\ , \tag{4.27}$$

where Θ is the "comparison function". One can then represent an exact solution of Eq. (4.6) in the form

$$\chi(x) = \left(\frac{\mathrm{d}\sigma}{\mathrm{d}x}\right)^{-1/2}\, U(\sigma)\ , \tag{4.28}$$

provided the variables x and σ are related by

$$\omega^2(x) = \left(\frac{\mathrm{d}\sigma}{\mathrm{d}x}\right)^{2}\Theta^2(\sigma) - \left(\frac{\mathrm{d}\sigma}{\mathrm{d}x}\right)^{1/2}\frac{\mathrm{d}^2}{\mathrm{d}x^2}\left(\frac{\mathrm{d}\sigma}{\mathrm{d}x}\right)^{-1/2}\ . \tag{4.29}$$

Eq. (4.29) can be solved by using some iterative scheme, in general cases as [44] and Appendix C or Refs. [45, 46] for specific problems. If we choose the comparison function sufficiently similar to ω, the second term in the right hand side of Eq. (4.29) will be negligible with respect to the first one, so that

$$\omega^2(x) \simeq \left(\frac{\mathrm{d}\sigma}{\mathrm{d}x}\right)^{2}\Theta^2(\sigma)\ . \tag{4.30}$$

On selecting a pair of values x_0 and σ_0 such that $\sigma_0 = \sigma(x_0)$, the function $\sigma(x)$ can be implicitly expressed as

$$-\,\xi(x) \equiv \int_{x_0}^{x}\sqrt{\pm\,\omega^2(y)}\,\mathrm{d}\,y \simeq \int_{\sigma_0}^{\sigma}\sqrt{\pm\,\Theta^2(\rho)}\,\mathrm{d}\,\rho\ , \tag{4.31}$$

where the signs are chosen conveniently [2]. The result in Eq. (4.28) leads to a uniform approximation for $\chi(x)$, valid in the whole range of the variable x, including "turning points". The similarity between Θ and ω is clearly very important in order to implement this method.

---

[2] Here $\xi(x)$ corresponds to the quantity $\xi_{\mathrm{II}}(x)$ used in Section 4.3 when the signs are both chosen as minus.

4.4.1 MCE vs Ermakov&Pinney

In Ref. [47], we studied the relation between the MCE [41, 42] and the Ermakov - Pinney equation [48, 49]. Let us consider again the second-order differential equation (4.6) but with the small parameter ε defined by [3]

$$\frac{d^2\chi(x)}{dx^2} = \frac{1}{\varepsilon}\omega^2(x)\chi(x) \ . \tag{4.32}$$

Let us suppose that one knows the solution of another second-order differential equation

$$\frac{d^2U(\sigma)}{d\sigma^2} = \frac{1}{\varepsilon}\Theta^2(\sigma)U(\sigma) \ . \tag{4.33}$$

In this case one can represent an *exact* solution of Eq. (4.32) in the form

$$\chi(x) = \left(\frac{d\sigma}{dx}\right)^{-1/2} U(\sigma) \ , \tag{4.34}$$

where the relation between the variables x and σ is given by the equation

$$\omega^2(x) = \left(\frac{d\sigma}{dx}\right)^2 \Theta^2(\sigma) + \varepsilon \left(\frac{d\sigma}{dx}\right)^{1/2} \frac{d^2}{dx^2}\left(\frac{d\sigma}{dx}\right)^{-1/2} \ . \tag{4.35}$$

On solving Eq. (4.35) for $\sigma(x)$ and substituting for it into Eq. (4.34) one finds the solution to Eq. (4.32). Eq. (4.35) can be solved by using some iterative scheme. The application of such a scheme is equivalent to the application of the MCE or, in other words, to the construction of the uniform asymptotic expansion for the solution of Eq. (4.32). The method of construction of the solution to Eq. (4.32) by means of the solutions of Eqs. (4.33) and (4.35) is called the method of comparison equations and the function $\Theta^2(\sigma)$ is called the comparison function [42].

The iterative scheme of solution of Eq. (4.35) depends essentially on the form of the comparison function $\Theta(\sigma)$. A reasonable approach consists in the elimination of σ from Eq. (4.35) and its reduction to a form, where the only unknown function is $(d\sigma/dx)$. The equation obtained for the case of the simple comparison function $\Theta^2(\sigma) = 1$ coincides with the Ermakov-Pinney equation, this will be explicitly shown in the next section. For more complicated forms of the comparison function $\Theta^2(\sigma)$ useful for the description of various physical problems the corresponding equation will acquire a more intricate form and we shall call it a generalised Ermakov-Pinney equation. The role of an unknown function in this equation is played by the function

$$y(x) \equiv \left(\frac{d\sigma}{dx}\right)^{-1/2} \ , \tag{4.36}$$

---

[3] With respect to Eq. (4.6), we have absorbed a minus sign in ε, as this change of sign is irrelevant for the present topic and for its application in Appendix C.

while the equation itself has the form

$$K\left(y, \frac{dy}{dx}\right) = \varepsilon L\left(y, \frac{dy}{dx}, \frac{d^2y}{dx^2}, \frac{d^3y}{dx^3}\right) \ , \tag{4.37}$$

where the explicit forms for the functions K and L will be defined in the next sections. We shall represent the function $y(x)$ as a series

$$y = \sum_{n=0}^{\infty} y_n \varepsilon^n \ , \tag{4.38}$$

and the general recurrence relation connecting the different coefficient functions y_n can be represented as

$$\left.\left(\frac{d^n K}{d\varepsilon^n} - \frac{d^{n-1}L}{d\varepsilon^{n-1}}\right)\right|_{\varepsilon=0} = 0 \ . \tag{4.39}$$

To implement this formula one may use the combinatorial relation [50]

$$\frac{d^n(uv)}{dx^n} = (u+v)^{(n)} \ , \tag{4.40}$$

where on the right-hand side one has a binomial expression wherein the powers are replaced by the derivatives of the same order. When the function $y(x)$ is constructed up to some level of approximation one can, in principle, find $\sigma(x)$ and substitute for it into Eq. (4.34).

We shall consider the implementation of this scheme for four choices of the comparison function: $\Theta^2(\sigma) = 1, \Theta^2(\sigma) = \sigma, \Theta^2(\sigma) = \exp(\sigma) - 1$ and $\Theta^2(\sigma) = \sigma^2 - a^2$. At the end we shall discuss the relation between the different WKB-type methods and equations of the Ermakov-Pinney type. In Appendix C we shall give a pure numerical example of application of the method of comparison equations.

No turning points

In the case for which the function $\omega^2(x)$ does not have zeros (turning points) it is convenient to choose a comparison function $\Theta^2(\sigma) = 1$. In this case the function $U(\sigma)$ is simply an exponent, while Eq. (4.35) can be rewritten as

$$\varepsilon\frac{d^2y(x)}{dx^2} = \omega^2(x)y(x) - \frac{1}{y^3(x)} \ , \tag{4.41}$$

where the function $y(x)$ is defined by Eq. (4.36). The above equation is nothing more then the well known Pinney or Ermakov-Pinney Eq. [48, 49], which can be solved perturbatively with respect to the parameter ε [51]. We shall give here some general formulae for such a solution. It is convenient to rewrite Eq. (4.41) as

$$\omega^2 y^4 - 1 = \varepsilon y^3 \ddot{y} \ , \tag{4.42}$$

where a "dot" denotes the derivative with respect to x. We shall search for the solution of Eq. (4.42) in the form (4.38). The zero-order solution of Eq. (4.42) is

$$y_0 = \omega^{-1/2} \ , \tag{4.43}$$

and the general recurrence relation following from Eq. (4.42) for $n \geq 1$ is

$$\begin{aligned} y_n &= \frac{1}{4y_0^3} \sum_{k_1=0}^{n-1} \cdots \sum_{k_4=0}^{n-1} \left\{ \frac{1}{\omega^2} \delta\left[(n-1) - (k_1+k_2+k_3+k_4)\right] \ddot{y}_{k_1} y_{k_2} y_{k_3} y_{k_4} \right. \\ &\left. \qquad - \delta\left[n - (k_1+k_2+k_3+k_4)\right] y_{k_1} y_{k_2} y_{k_3} y_{k_4} \right\} \ , \end{aligned} \tag{4.44}$$

where $\delta()$ is the Kronecker delta symbol. It is now easy to obtain from the general expression (4.44) expressions for particular values of y_n

$$y_1 = \frac{\ddot{y}_0}{4\omega^2} \tag{4.45a}$$

$$y_2 = -\frac{3y_1^2}{2y_0} + \frac{\ddot{y}_1}{4\omega^2} + \frac{3\ddot{y}_0 y_1}{4\omega^2 y_0} \tag{4.45b}$$

$$y_3 = -\frac{y_1^3}{y_0^2} - \frac{3y_2 y_1}{y_0} + \frac{\ddot{y}_2}{4\omega^2} + \frac{3\ddot{y}_0 y_2}{4\omega^2 y_0} + \frac{3\ddot{y}_1 y_1}{4\omega^2 y_0} + \frac{3\ddot{y}_0 y_1^2}{4\omega^2 y_0^2} \ . \tag{4.45c}$$

Let us end by noting that the standard WKB approximation corresponds to the case discussed here and is, of course, only valid away from turning points.

One turning point: the Langer solution

In the case of the presence of a linear zero in the function $\omega^2(x)$ one can use the Langer solution [37]. In terms of the method of comparison equations it means that one chooses the comparison function $\Theta^2(\sigma) = \sigma$. In this case Eq. (4.35) becomes

$$\omega^2(x) = \left(\frac{d\sigma}{dx}\right)^2 \sigma + \varepsilon \left(\frac{d\sigma}{dx}\right)^{1/2} \frac{d^2}{dx^2} \left(\frac{d\sigma}{dx}\right)^{-1/2} \ . \tag{4.46}$$

Dividing this equation by $(d\sigma/dx)^2$ and differentiating the result with respect to x we get an equation which depends only on the derivative $\dot{\sigma}$ and not on the function σ. Such an equation can be rewritten in the form

$$2\dot{\omega}\omega y^6 + 4\omega^2 \dot{y} y^5 = 1 + \varepsilon \left(3\ddot{y}\dot{y}y^4 + y^{(3)} y^5\right) \ , \tag{4.47}$$

where the function $y(x)$, as in the preceding section, is defined by Eq. (4.36). Again we shall search for the solution of Eq. (4.47) in the form (4.38). The equation for y_0 is

$$2\dot{\omega}\omega y_0^6 + 4\omega^2 \dot{y}_0 y_0^5 = \left(\omega^2 y_0^4\right)^{\cdot} y_0^2 = 1 \ . \tag{4.48}$$

This equation may be rewritten as

$$\sqrt{\omega^2 y_0^4} \, \frac{d}{dx} \left(\omega^2 y_0^4\right) = \omega \ , \tag{4.49}$$

and integrated

$$\omega^2 y_0^4 = \left(\frac{3}{2}\int \omega dx\right)^{2/3} \quad . \tag{4.50}$$

Finally

$$y_0 = \frac{1}{\omega^{1/2}}\left(\frac{3}{2}\int \omega dx\right)^{\frac{1}{6}} \quad . \tag{4.51}$$

Comparing the coefficients of ε^n with $n \geq 1$ in Eq. (4.47) we have

$$4\omega^2 y_0^5 \dot{y}_n + \left(12\dot{\omega}\omega y_0^5 + 20\omega^2 \dot{y}_0 y_0^4\right) y_n = 4\omega^{-1}\left(\omega^3 y_0^5 y_n\right)^{\cdot} \equiv F_n \ , \tag{4.52}$$

where F_n contains the terms which depend on $y_k, 0 \leq k \leq n-1$, and can be written as

$$\begin{aligned} F_n \ &= \sum_{k_1=0}^{n-1}\cdots\sum_{k_6=0}^{n-1}\left\{-\delta\left[n-(k_1+k_2+k_3+k_4+k_5+k_6)\right]\left(4\omega^2\dot{y}_{k_1} + 2\dot{\omega}\omega y_{k_1}\right) y_{k_2}\cdots y_{k_6}\right. \\ &\left. + \ \delta[(n-1)-(k_1+k_2+k_3+k_4+k_5+k_6)]\left(3\ddot{y}_{k_1}\dot{y}_{k_2} + y_{k_1}^{(3)} y_{k_2}\right) y_{k_3}\cdots y_{k_6}\right\} \ . \end{aligned} \tag{4.53}$$

The general expression for y_n is

$$y_n = \frac{1}{4\omega^3 y_0^5}\int dx\omega F_n \ . \tag{4.54}$$

Let us also give the explicit expressions for the first terms in the expansion (4.38)

$$y_1 \ = \ \frac{1}{4\omega^3 y_0^5}\int dx\omega\left(3\ddot{y}_0\dot{y}_0 y_0^4 + y_0^{(3)} y_0^5\right) \tag{4.55a}$$

$$\begin{aligned} y_2 \ = \ \frac{1}{4\omega^3 y_0^5}\int dx\omega & \left(-30\dot{\omega}\omega y_1^2 y_0^4 - 20\omega^2\dot{y}_1 y_1 y_0^4 - 40\omega^2\dot{y}_0 y_1^2 y_0^3\right. \\ & \left. + \ 3\ddot{y}_1\dot{y}_0 y_0^4 + 3\ddot{y}_0\dot{y}_1 y_0^4 + y_1^{(3)} y_0^5 + 5y_0^{(3)} y_1 y_0^4 + 12\ddot{y}_0\dot{y}_0 y_1 y_0^3\right) \end{aligned} \tag{4.55b}$$

$$\begin{aligned} y_3 \ = \ \frac{1}{4\omega^3 y_0^5}\int dx\omega & \left(-60\dot{\omega}\omega y_2 y_1 y_0^4 - 40\dot{\omega}\omega y_1^3 y_0^3 - 20\omega^2\dot{y}_2 y_1 y_0^4 - 80\omega^2\dot{y}_0 y_2 y_1 y_0^3\right. \\ & -40\omega^2\dot{y}_0 y_1^3 y_0^2 - 40\omega^2\dot{y}_1 y_1^2 y_0^3 - 20\omega^2\dot{y}_1 y_2 y_0^4 + 3\ddot{y}_2\dot{y}_0 y_0^4 + 3\ddot{y}_0\dot{y}_2 y_0^4 \\ & +12\ddot{y}_0\dot{y}_0 y_2 y_0^3 + 3\ddot{y}_1\dot{y}_1 y_0^4 + 12\ddot{y}_1\dot{y}_0 y_1 y_0^3 + 12\ddot{y}_0\dot{y}_1 y_1 y_0^3 + 18\ddot{y}_0\dot{y}_0 y_1^2 y_0^2 \\ & \left. +y_2^{(3)} y_0^5 + 5y_0^{(3)} y_2 y_0^4 + 5y_1^{(3)} y_1 y_0^4 + 10y_0^{(3)} y_1^2 y_0^3\right) \ . \end{aligned} \tag{4.55c}$$

Before closing this section we may compare our results with some formulae, obtained by Dingle [42]. In the vicinity of the turning point, which we choose as $x = 0$, the function $\omega^2(x)$ can be represented as

$$\omega^2(x) = \gamma_1 x + \frac{\gamma_2}{2}x^2 + \frac{\gamma_3}{3!}x^3 + \frac{\gamma_4}{4!}x^4 + \cdots \tag{4.56}$$

while the function $\sigma(x)$ looks like

$$\sigma(x) = \sigma_0 + \sigma_1 x + \frac{\sigma_2}{2}x^2 + \frac{\sigma_3}{3!}x^3 + \frac{\sigma_4}{4!}x^4 + \cdots \tag{4.57}$$

In reference [42] the first five coefficients $\sigma_0, \sigma_1, \sigma_2, \sigma_3$ and σ_4, as functions of the coefficients $\gamma_1, \gamma_2, \gamma_3$ and γ_4, were obtained in the lowest approximation by using a system of recurrence relations. We can reproduce all these formulae on only using the general formula (4.51). Indeed, on writing

$$\frac{d\sigma}{dx} = \frac{1}{y^2} = \frac{\omega(x)}{\left[\frac{3}{2}\int \omega(x)\right]^{1/3}} \tag{4.58}$$

using expansions (4.56) and (4.57) and comparing the coefficients of different powers of x we get the formulae

$$\begin{aligned} \sigma_0 &= 0 \\ \sigma_1 &= \gamma_1^{1/3} \\ \sigma_2 &= \frac{1}{5}\gamma_1^{-2/3}\gamma_2 \\ \sigma_3 &= \frac{1}{7}\gamma_1^{-2/3}\gamma_3 - \frac{12}{175}\gamma_1^{-5/3}\gamma_2^2 \\ \sigma_4 &= \frac{1}{9}\gamma_1^{-2/3}\gamma_4 - \frac{44}{315}\gamma_1^{-5/3}\gamma_2\gamma_3 + \frac{148}{2625}\gamma_1^{-8/3}\gamma_2^3 \, , \end{aligned} \tag{4.59}$$

which coincide with those obtained in [42]. The value of σ_0 comes directly from Eq. (4.46) on ignoring the ϵ-term and using the relations (4.56) and (4.57).

We can also find the ε-dependent corrections to the function $\sigma(x)$ in the neighbourhood of the point $x = 0$ by using the results (4.59) and the recurrence relations (4.55a) etc. We shall only give here the first correction, proportional to ε, to the coefficients σ_0 and σ_1. The value of σ_0 comes directly from Eq. (4.46) using the relations (4.56), (4.57) and (4.59)

$$\sigma_0 = \varepsilon\left(\frac{\gamma_3\gamma_1^{-5/3}}{14} - \frac{9\gamma_2^2\gamma_1^{-8/3}}{140}\right) \, . \tag{4.60}$$

In order to obtain σ_1 we introduce into the definition of the function $y(x)$, Eq. (4.36), the expansion (4.57) and

$$y_0 = \sigma_1^{-1/2}\left[1 - \frac{\sigma_2}{2\sigma_1}x + \left(\frac{3\sigma_2^2}{8\sigma_1^2} - \frac{\sigma_3}{4\sigma_1}\right)x^2 + \left(\frac{3\sigma_2\sigma_3}{8\sigma_1^2} - \frac{\sigma_4}{12\sigma_1} - \frac{5\sigma_2^3}{16\sigma_1^3}\right)x^3\right] + \cdots \tag{4.61}$$

Now, on using the recurrence formula (4.55a) we find the leading (constant) term in the expression for y_1

$$y_1 = \frac{1}{\gamma_1}\left(-\frac{1}{2}\sigma_2^3\sigma_1^{-7/2} + \frac{1}{2}\sigma_3\sigma_2\sigma_1^{-5/2} - \frac{\sigma_4\sigma_1^{-3/2}}{12}\right) + \cdots \tag{4.62}$$

From the formula

$$\frac{d\sigma}{dx} = \frac{1}{y^2} = \frac{1}{(y_0 + \varepsilon y_1)^2} \tag{4.63}$$

it is easy to find the first correction to the first coefficient σ_1 in the expansion (4.57)

$$\sigma_1 = \gamma_1^{1/3} - 2\varepsilon \frac{y_1}{y_0^3} \ . \tag{4.64}$$

Substituting into Eq. (4.64) the leading term of y_1 from Eq. (4.62), of y_0 from (4.61) and using the explicit expressions for the coefficients σ_i from Eq. (4.59) we finally obtain

$$\sigma_1 = \gamma_1^{1/3} + \varepsilon \left(\frac{7}{225}\gamma_2^3\gamma_1^{-11/3} - \frac{7}{135}\gamma_3\gamma_2\gamma_1^{-8/3} + \frac{1}{54}\gamma_4\gamma_1^{-5/3} \right) \ . \tag{4.65}$$

The results (4.60) and (4.65) was found by Dingle [42], but in his article there were two sign errors in the second line of equation (69).

One turning point: more complicated comparison function

Let us consider the differential Eq. (4.32), when the function $\omega^2(x)$ has a linear turning point, but instead of Langer's comparison function $\Theta^2(\sigma) = \sigma$ consider a more complicated comparison function, also having linear turning point, namely

$$\Theta^2(\sigma) = e^{\sigma} - 1 \ . \tag{4.66}$$

Now, Eq. (4.35) will have the form

$$\omega^2(x) = \left(\frac{d\sigma}{dx}\right)^2 (e^{\sigma} - 1) + \varepsilon \left(\frac{d\sigma}{dx}\right)^{1/2} \frac{d^2}{dx^2} \left(\frac{d\sigma}{dx}\right)^{-1/2} \ . \tag{4.67}$$

On isolating the function e^{σ}, taking its logarithm and differentiating it with respect to x we finally get an equation which involves only the derivative $\dot{\sigma}$. This equation can be written as

$$\omega^2 y^4 - 2\dot{\omega}\omega y^6 - 4\omega^2 \dot{y} y^5 + 1 = \varepsilon \left(\ddot{y} y^3 - 3\ddot{y}\dot{y} y^4 - y^{(3)} y^5 \right) \ . \tag{4.68}$$

To find the function y_0 one should solve the equation

$$\omega^2 y_0^4 - 2\dot{\omega}\omega y_0^6 - 4\omega^2 \dot{y}_0 y_0^5 + 1 = 0 \ . \tag{4.69}$$

On introducing the new variable

$$z \equiv \omega^2 y_0^4 \tag{4.70}$$

one can rewrite Eq. (4.69) as

$$\dot{z} = \frac{(z+1)\omega}{z^{1/2}} \ . \tag{4.71}$$

It is also convenient to introduce the variable

$$v \equiv \sqrt{z} \ . \tag{4.72}$$

Eq. (4.71) now becomes

$$\frac{2v^2\dot{v}}{1+v^2} = \omega \tag{4.73}$$

which can be integrated, obtaining

$$2v - 2\arctan v = \int \omega dx \ . \tag{4.74}$$

Finally, for y_0 we have the implicit representation

$$y_0^2 - \frac{1}{\omega}\arctan \omega y_0^2 = \frac{1}{2\omega}\int \omega dx \ . \tag{4.75}$$

We may now write the equation defining the recurrence relation for $y_n, n \geq 1$

$$-4\omega^2 y_0^5 \dot{y}_n + \left(4\omega^2 y_0^3 - 20\omega^2 \dot{y}_0 y_0^4 - 12\dot{\omega}\omega y_0^5\right) y_n = -4\frac{(\omega^3\, y_0^5\, G\, y_n)^{\cdot}}{\omega\, G} \equiv F_n \ , \tag{4.76}$$

where

$$\begin{aligned} F_n \ = \ & \sum_{k_1=0}^{n-1}\cdots\sum_{k_4=0}^{n-1} \{\delta\,[(n-1)-(k_1+k_2+k_3+k_4)]\ \ddot{y}_{k_1} y_{k_2} y_{k_3} y_{k_4} \\ & \qquad\qquad -\omega^2\,\delta\,[n-(k_1+k_2+k_3+k_4)]\, y_{k_1} y_{k_2} y_{k_3} y_{k_4}\} \\ + \ & \sum_{k_1=0}^{n-1}\cdots\sum_{k_6=0}^{n-1} \Big\{\delta\,[n-(k_1+k_2+k_3+k_4+k_5+k_6)]\big(2\,\dot{\omega}\,\omega\, y_{k_1} + 4\,\omega^2\,\dot{y}_{k_1}\big) y_{k_2}\cdots y_{k_6} \\ & -\delta\,[(n-1)-(k_1+k_2+k_3+k_4+k_5+k_6)]\Big(3\,\ddot{y}_{k_1}\dot{y}_{k_2} + y_{k_1}^{(3)} y_{k_2}\Big) y_{k_3}\cdots y_{k_6}\Big\} \ , \end{aligned} \tag{4.77}$$

and

$$G = \exp\left(-\int^x \frac{dx'}{y_0^2(x')}\right) \ . \tag{4.78}$$

The solution for y_n is

$$y_n = -\frac{1}{4\omega^3 y_0^5 G}\int dx\, \omega G F_n \ , \tag{4.79}$$

Here we give the explicit expressions for the first two functions F_1 and F_2

$$F_1 \ = \ \ddot{y}_0 y_0^3 - 3\ddot{y}_0\dot{y}_0 y_0^4 - y_0^{(3)} y_0^5 \tag{4.80a}$$

$$\begin{aligned} F_2 \ = \ & -6\omega^2 y_1^2 y_0^2 + 30\dot{\omega}\omega y_1^2 y_0^4 + 20\omega^2 \dot{y}_1 y_1 y_0^4 + 40\omega^2 \dot{y}_0 y_1^2 y_0^3 + \ddot{y}_1 y_0^3 \\ + \ & 3\ddot{y}_0 y_1 y_0^2 - 3\ddot{y}_1\dot{y}_0 y_0^4 - 3\ddot{y}_0\dot{y}_1 y_0^4 - 12\ddot{y}_0\dot{y}_0 y_1 y_0^3 - y_1^{(3)} y_0^5 - 5y_0^{(3)} y_1 y_0^4 \ . \end{aligned} \tag{4.80b}$$

Two turning points

Let us now consider the differential Eq. (4.32), when the function $\omega^2(x)$ has two turning points. This situation, describing the tunneling through a potential barrier was considered in [41, 43]. In this case the comparison function can be chosen to be

$$\Theta^2(\sigma) = \sigma^2 - a^2 \ . \tag{4.81}$$

The solutions $U(\sigma)$ of Eq. (4.33) are the well-known parabolic functions [43]. Substituting $\Theta^2(\sigma)$ of Eq. (4.81) into Eq. (4.35) one can isolate σ and after the subsequent differentiation one can write down the equation for the function $y(x)$

$$2\sqrt{\omega^2 y^4 + a^2 - \varepsilon \ddot{y} y^3} = 2\dot{\omega}\omega y^6 + 4\omega^2 \dot{y} y^5 - \varepsilon\left(3\ddot{y}\dot{y}y^4 + y^{(3)}y^5\right) \ . \tag{4.82}$$

The lowest-approximation y_0 can be found from the equation

$$2\sqrt{\omega^2 y_0^4 + a^2} = 2\dot{\omega}\omega y_0^6 + 4\omega^2 \dot{y}_0 y_0^5 \ . \tag{4.83}$$

This equation can be integrated and the solution y_0 can be written down in the implicit form

$$\omega y_0^3 - \frac{a^2}{\omega}\text{arcsinh}\frac{\omega y_0}{a} = \frac{2}{\omega}\int \omega dx \ . \tag{4.84}$$

To get the recurrence relations for the functions $y_n, n \geq 1$ it is convenient to take the square of Eq. (4.82)

$$\begin{aligned}
&4\dot{\omega}^2\omega^2 y^{12} + 16\omega^4\dot{y}^2 y^{10} + 16\dot{\omega}\omega^3\dot{y}y^{11} - 4\omega^2 y^4 - 4a^2 = \\
&\qquad -\varepsilon(4\ddot{y}y^3 - 12\dot{\omega}\omega\ddot{y}\dot{y}y^{10} - 24\omega^2\ddot{y}\dot{y}^2 y^9 - 4\dot{\omega}\omega y^{(3)}y^{11} - 8\omega^2 y^{(3)}\dot{y}y^{10}) \\
&\qquad -\varepsilon^2(9\ddot{y}^2\dot{y}^2 y^8 + {y^{(3)}}^2 y^{10} + 6y^{(3)}\ddot{y}\dot{y}y^9) \ .
\end{aligned} \tag{4.85}$$

On comparing the terms containing the n^{th} power of the small parameter ε one obtains

$$f\dot{y}_n + g y_n = \frac{f}{G}\,(G\,y_n)^{\cdot} \equiv F_n \ , \tag{4.86}$$

where

$$\begin{aligned}
f &= 32\omega^4\dot{y}_0y_0^{10} + 16\dot{\omega}\omega^3y_0^{11} && (4.87a)\\
g &= 48\dot{\omega}^2\omega^2y_0^{11} + 160\omega^4\dot{y}_0^2y_0^9 + 176\dot{\omega}\omega^3\dot{y}_0y_0^{10} - 16\omega^2y_0^3 && (4.87b)\\
F_n &= 4\sum_{k_1=0}^{n-1}\cdots\sum_{k_4=0}^{n-1}\left\{\omega^2\delta\left[n-(k_1+k_2+k_3+k_4)\right]y_{k_1}y_{k_2}y_{k_3}y_{k_4}\right.\\
&\qquad\qquad \left.-\delta\left[(n-1)-(k_1+k_2+k_3+k_4)\right]\ddot{y}_{k_1}y_{k_2}y_{k_3}y_{k_4}\right\}\\
&- 4\sum_{k_1=0}^{n-1}\cdots\sum_{k_{12}=0}^{n-1}\left\{\delta\left[n-(k_1+\cdots+k_{12})\right]\right.\\
&\times\left(\dot{\omega}^2\omega^2y_{k_1}y_{k_2}+4\omega^4\dot{y}_{k_1}\dot{y}_{k_2}+4\dot{\omega}\omega^3\dot{y}_{k_1}y_{k_2}\right)y_{k_3}\cdots y_{k_{12}}\\
&\qquad\qquad -\delta\left[(n-1)-(k_1+\cdots+k_{12})\right]\\
&\times\left.\left(3\dot{\omega}\omega\ddot{y}_{k_1}\dot{y}_{k_2}y_{k_3}+6\omega^2\ddot{y}_{k_1}\dot{y}_{k_2}\dot{y}_{k_3}+\dot{\omega}\omega y^{(3)}y_{k_2}y_{k_3}+2\omega^2y_{k_1}^{(3)}\dot{y}_{k_2}y_{k_3}\right)y_{k_4}\cdots y_{k_{12}}\right\}\\
&- \sum_{k_1=0}^{n-2}\cdots\sum_{k_{12}=0}^{n-2}\delta\left[(n-2)-(k_1+\cdots+k_{12})\right]\\
&\times\left(9\ddot{y}_{k_1}\ddot{y}_{k_2}\dot{y}_{k_3}\dot{y}_{k_4}+y_{k_1}^{(3)}y_{k_2}^{(3)}y_{k_3}y_{k_4}+6y_{k_1}^{(3)}\ddot{y}_{k_2}\dot{y}_{k_3}y_{k_4}\right)y_{k_5}\cdots y_{k_{12}}\ . && (4.87c)\\
G &= \exp\left(\int^x dx'\frac{g}{f}\right)\ . && (4.87d)
\end{aligned}$$

The integration of Eq. (4.86) gives

$$y_n = \frac{1}{G}\int dx\frac{GF_n}{f}\ . \qquad (4.88)$$

The explicit expressions for the coefficients F_n are rather cumbersome and we shall only write down the coefficient F_1

$$F_1 = 12\dot{\omega}\omega\ddot{y}_0\dot{y}_0y_0^{10} + 24\omega^2\ddot{y}_0\dot{y}_0^2y_0^9 + 4\dot{\omega}\omega y_0^{(3)}y_0^{11} + 8\omega^2y_0^{(3)}\dot{y}_0y_0^{10} - 4\ddot{y}_0y_0^3\ . \qquad (4.89)$$

Historical and physical remarks

We have seen that, for some non-trivial applications of the MCE, instead of the standard form of the Ermakov-Pinney equation, one is lead to its generalizations which are rather different from the known generalizations of Ermakov systems. Let us note that although the Ermakov equation was already reproduced in the MCE context (first of all in the important paper by Milne [52]), its generalizations arising in the process of application of the MCE [41, 42] were not yet studied, at least to the best of our knowledge. We shall therefore try to give a short review of the history of the Ermakov-Pinney equation and its applications to quantum mechanics and to similar WKB-type problems and discuss the physical significance of its non-trivial generalization (for a more detailed account of the history of the Eramkov-Pinney equation see e.g. [53]).

The relation between the second-order linear differential equation

$$\frac{d^2u}{dx^2} + \omega^2(x)\chi(x) = 0 \tag{4.90}$$

and the non-linear differential equation

$$\frac{d^2\rho}{dx^2} + \omega^2(x)\rho(x) = \frac{\alpha}{\rho^3(x)} \ , \tag{4.91}$$

where α is some constant was noticed by Ermakov [48], who showed that any two solutions ρ and u of the above equations are connected by the formula

$$C_1 \int \frac{dx}{u^2} + C_2 = \sqrt{C_1 \frac{\rho^2}{u^2} - \alpha} \ . \tag{4.92}$$

The couple of Eqs. (4.90) and (4.91) constitute the so called Ermakov system. An important corollary was derived [48] from the formula (4.92). Namely, on having a particular solution $\rho(x)$ of Eq. (4.91) one can construct the general solution of Eq. (4.90) which is given by

$$\chi(x) = c_1\rho(x) \exp\left[\sqrt{-\alpha} \int \frac{dx}{\rho^2(x)}\right] + c_2\rho(x) \exp\left[-\sqrt{-\alpha} \int \frac{dx}{\rho^2(x)}\right] \ . \tag{4.93}$$

It is easy to see that the function $\rho(x)$ plays of the role of an “amplitude” of the function $\chi(x)$, while the integral $\int [dx/\rho^2(x)]$ represents some kind of “phase”. Thus, it is not surprising that the Ermakov equation was re-discovered by Milne [52] in a quantum-mechanical context. On introducing the amplitude obeying Eq. (4.91) and the phase, Milne constructed a formalism for the solution of the Schrödinger equation which was equivalent to the MCE. Milne’s MCE technique was extensively used for the solution of quantum mechanical problems (see e.g. [54]). In the paper by Pinney [49] the general form of the solution of the Ermakov equation was presented, while the most general expression for this solution was written down by Lewis [51].

A very simple physical example rendering trasparent the derivation of the Ermakov-Pinney equation and its solutions was given in the paper by Eliezer and Gray [55]. The motion of a two-dimensional oscillator with time-dependent frequency was considered. In this case the second-order linear differential Eq. (4.90) describes the projection of the motion of this two-dimensional oscillator on one of its Cartesian coordinates, while the Ermakov-Pinney Eq. (4.91) describes the evolution of the radial coordinate ρ. The parameter α is nothing more than the square of the conserved angular momentum of the two-dimensional oscillator. Thus, the notion of the amplitude and phase acquire in this example a simple geometrical and physical meaning. Similarly, the supersymmetric generalization of the Ermakov-Pinney equation was considered in the paper by Ioffe and Korsch [56].

An additional generalization of the notion of an Ermakov system of equations was suggested in the paper by Ray and Reid [57]. Thy consider the system of two equations

$$\frac{d^2u}{dx^2} + \omega^2(x)\chi(x) = \frac{1}{\rho x^2} g\left(\frac{\rho}{x}\right) \tag{4.94}$$

and

$$\frac{d^2\rho}{dx^2} + \omega^2(x)\rho(x) = \frac{1}{x\rho^2(x)} f\left(\frac{x}{\rho}\right) \ , \tag{4.95}$$

where g and f are arbitrary functions of their arguments. The standard Ermakov system (4.90), (4.91) corresponds to the choice of functions $g(\xi) = 0$ and $f(\xi) = \alpha\xi$. One can show that the generalized Ermakov system (4.94), (4.95) has an invariant (zero total time derivative)

$$I_{f,g} = \frac{1}{2}\left[\phi\left(\frac{u}{\rho}\right) + \theta\left(\frac{\rho}{u}\right) + \left(u\frac{d\rho}{dx} - \rho\frac{du}{dx}\right)^2\right] \ , \tag{4.96}$$

where

$$\phi\left(\frac{u}{\rho}\right) = 2\int^{\frac{u}{\rho}} f(x)dx \tag{4.97a}$$

$$\theta\left(\frac{\rho}{u}\right) = 2\int^{\frac{\rho}{u}} g(x)dx \ . \tag{4.97b}$$

The invariant (4.96) establishes the connection between the solutions of Eqs. (4.94) and (4.95) and sometimes allows one to find the solution of one of these equations provided the solution of the other one is known (just as in the case of the standard Ermakov system). However, for the case of an arbitrary couple of functions f and g a simple physical or geometrical interpretation of the Ermakov system analogous to that given in [55] is not known.

Here we have established the connection between the generalized WKB method (MCE [41, 42]) and the Ermakov - Pinney equation and on the other hand we have obtained a generalization of the Ermakov - Pinney equation, different to those studied in the literature. One has two second-order differential Eqs. (4.32) and (4.33) and the solution of one of them (4.33) is well known and described. Using the previous convenient analogy [55], one can say that in this case one has two time-dependent oscillators, evolving with two different time-parameters. One can try to find the solution of Eq. (4.32) by representing it as a known solution of Eq. (4.33) multiplied by a correction factor. This correction factor plays the role of the prefactor in the standard WKB approach while the known solution of Eq. (4.33) represents some kind of generalized phase term. Further, the prefactor is expressed in terms of the derivative between two variables x and σ (or in terms of the oscillator analogy, between two times). On writing down the equation definining this factor, which we have denoted by $y(x)$ (see Eq. (4.36)) we arrive to Eq. (4.35) which could be called a generalized Ermakov-Pinney equation. For the case when the function $\omega^2(x)$ does not have turning points the comparison function $\Theta^2(\sigma)$ can be chosen constant (the second oscillator has a time-independent frequency) and the the equation defining the prefactor becomes the standard Ermakov-Pinney Eq. (4.41). In terms of the two-dimensional oscillator analogy [55] this means that we exclude from the equation for the radial coordinate the dependence on the angle coordinate σ by using its cyclicity, i.e. the conservation of the angular moment.

In cases for which the function $\omega^2(x)$ has turning points, as in Secs. 4.4.1, 4.4.1 and 4.4.1, the comparison functions are non-constant and instead of the standard Ermakov-Pinney equation we have its non-trivial generalizations. The common feature of these generalizations consists in the fact that the corresponding equations for the variable y also depend explicitly on the parameter σ which does not disappear automatically. To get a differential equation for y, one should isolate the parameter σ and subsequently differentiate ti with respect to x. As a result one gets a differential equation of higher-order for the function $y(x)$. Remarkably, for the perturbative solution of these equations one can again construct a reasonable iterative procedure.

Again, it is interesting to look at the generalized Ermakov-Pinney equation as an equation describing a two-dimensional physical system in the spirit of the reference [55]. In our case one has

$$\frac{d^2y(x)}{dx^2} + \omega^2(x)y(x) = \frac{\Theta^2(\sigma)}{y^3(x)} , \tag{4.98}$$

where y plays the role of a radial coordinate, σ resembles a phase or an angle (e.g. the position of a hand of a clock) and x is a time parameter. It is important to notice that according to the definition of the variable y (4.36) there is a relation between the radial and angle coordinates

$$\frac{d\sigma}{dx} = \frac{1}{y^2} , \tag{4.99}$$

which on interpreting σ as a phase corresponds to constant (unit) angular momentum. In our case however the right-hand side of the radial Eq. (4.98) contains an explicit dependence on the "angle" σ. Thus, the couple of Eqs. (4.98) and (4.99) cannot be represented as a system of equations of motion corresponding to some Lagrangian or Hamiltonian as in Ref. [55]. Perhaps, this system could be described in terms of non-Hamiltonian dissipative dynamics, but this question requires a further study.

Chapter 5

Analysis of Cosmological Perturbations

In this chapter, we shall apply the different WKB approaches reviewed previously to the equations that drive the scalar and tensorial cosmological perturbations. In the first Section, we recall the main expressions and review one fo the first applications of the WKB approximation to cosmolgical perturbations [58]. In the second Section, we present the improved version of the WKB analysis [59] and, in the last part, we employ the MCE [60]

5.1 Standard WKB approximation

In this Section we begin by recalling that the straightforward application of the standard WKB method leads to a poor approximation and that the results can be improved to first adiabatic order by means of the transformation (5.9), as was shown in Ref. [58]. However, the extension to higher orders is more subtle, as we shall discuss in some details.

We have seen that the general equation for cosmological perturbations is

$$\left[\delta\,\frac{\mathrm{d}^2}{\mathrm{d}\eta^2}+\Omega_j^2(k,\eta)\right]\,\mu_j=0\ , \tag{5.1}$$

where

$$\Omega_j^2(k,\eta)=k^2-\frac{z_j''}{z_j}\ , \tag{5.2}$$

with $j=S$ for scalar perturbations and $j=T$ for tensorial ones, so $z_S=z$ and $z_T=a$. We can now solve Eq. (5.1) together with the condition that the modes are initially plane waves for wavelengths much shorter than the Hubble radius,

$$\lim_{\frac{k}{a\,H}\to+\infty}\mu(k,\eta)=d\,\frac{\mathrm{e}^{-i\,k\,\eta}}{\sqrt{2\,k}}\ , \tag{5.3}$$

where $d = d_{\mathrm{S}} = 1$ and $d = d_{\mathrm{T}} = \sqrt{8\,\pi}/m_{\mathrm{Pl}}$ for scalar and tensor perturbations (m_{Pl} is the Planck mass). So the dimensionless power spectra of scalar and tensor fluctuations are given by the usual definitions

$$\mathcal{P}_\zeta = \frac{k^3}{2\,\pi^2} \left|\frac{\mu_{\mathrm{S}}}{z_{\mathrm{S}}}\right|^2 \ , \quad \mathcal{P}_h = \frac{4\,k^3}{\pi^2} \left|\frac{\mu_{\mathrm{T}}}{z_{\mathrm{T}}}\right|^2 \ . \tag{5.4}$$

The spectral indices and their runnings give the standard parametrization for the power spectra. They are usually defined at an arbitrary pivot scale k_* [1] as

$$n_{\mathrm{S}} - 1 = \left.\frac{\mathrm{d}\ln\mathcal{P}_\zeta}{\mathrm{d}\ln k}\right|_{k=k_*} \ , \quad n_{\mathrm{T}} = \left.\frac{\mathrm{d}\ln\mathcal{P}_h}{\mathrm{d}\ln k}\right|_{k=k_*} \ , \tag{5.5}$$

and

$$\alpha_{\mathrm{S}} = \left.\frac{\mathrm{d}^2\ln\mathcal{P}_\zeta}{(\mathrm{d}\ln k)^2}\right|_{k=k_*} \ , \quad \alpha_{\mathrm{T}} = \left.\frac{\mathrm{d}^2\ln\mathcal{P}_h}{(\mathrm{d}\ln k)^2}\right|_{k=k_*} \ . \tag{5.6}$$

We also define the tensor-to-scalar ratio

$$R = \frac{\mathcal{P}_h}{\mathcal{P}_\zeta} \ . \tag{5.7}$$

In the following we shall drop the subscript j, S and T if they are not necessary. On using the potentials in Eqs. (3.68) and (3.69) in terms of a and H, one finds, for the quantities defined in Eq. (4.5)

$$\Delta_{\mathrm{S,T}} = \begin{cases} \left(\dfrac{a\,H}{k}\right)^4 \mathcal{O}(\epsilon_n) \sim 0 & \text{sub-horizon scales} \\[2ex] \dfrac{1}{8} + \mathcal{O}(\epsilon_n) & \text{super-horizon scales.} \end{cases} \tag{5.8}$$

The result for super-horizon scales suggests that a change of variable and function are necessary in order to obtain better accuracy.

A convenient change of dependent variable and funtion is the Langer transformation [37]

$$x \equiv \ln\left(\frac{k}{H\,a}\right) \ , \quad \chi \equiv (1-\epsilon_1)^{1/2}\,\mathrm{e}^{-x/2}\,\mu \ , \tag{5.9}$$

introduced in Ref. [61] is used [2] in order to improve the accuracy. Such a transformation bring Eqs. (3.4) and (3.64) into the form

$$\left[\frac{\mathrm{d}^2}{\mathrm{d}x^2} + \omega^2(x)\right] \chi = 0 \ , \tag{5.10}$$

---

[1] Sometimes the spectral indices and their runnings are defined without assuming $k = k_*$. We shall always make it clear where we use this assumption.

[2] Note that we define x with the opposite sign with respect to that in Ref. [58]. This of course implies that our $x_i \to +\infty$ and $x_f \to -\infty$, whereas $x_i \to -\infty$ and $x_f \to +\infty$ in Ref. [58].

where the (new) frequency $\omega(x)$ in general vanishes at the classical "turning point" $x = x_0$. In fact, on employing the transformation (5.9), one finds (for $\delta = 1$) the new equations of motion (5.10), which explicitly read

$$\frac{\mathrm{d}^2\chi_{\mathrm{S}}}{\mathrm{d}x^2}+\left[\frac{\mathrm{e}^{2\,x}}{(1-\epsilon_1)^2}-\left(\frac{3-\epsilon_1}{2-2\,\epsilon_1}\right)^2-\frac{(3-2\,\epsilon_1)\,\epsilon_2}{2\,(1-\epsilon_1)^2}-\frac{(1-2\,\epsilon_1)\,\epsilon_2\,\epsilon_3}{2\,(1-\epsilon_1)^3}-\frac{(1-4\,\epsilon_1)\,\epsilon_2^2}{4\,(1-\epsilon_1)^4}\right]\chi_{\mathrm{S}}=0 \tag{5.11}$$

$$\frac{\mathrm{d}^2\chi_{\mathrm{T}}}{\mathrm{d}x^2}+\left[\frac{\mathrm{e}^{2\,x}}{(1-\epsilon_1)^2}+\left(\frac{3-\epsilon_1}{2-2\epsilon_1}\right)^2+\frac{\epsilon_1\,\epsilon_2}{2\,(1-\epsilon_1)^2}+\frac{\epsilon_1\,\epsilon_2\,\epsilon_3}{2\,(1-\epsilon_1)^3}+\frac{(2+\epsilon_1)\,\epsilon_1\,\epsilon_2^2}{4\,(1-\epsilon_1)^4}\right]\chi_{\mathrm{T}}=0\ .$$

From $\omega_{\mathrm{S}}^2(x)$ and $\omega_{\mathrm{T}}^2(x)$, respectively given by the expressions in the square brackets of Eqs. (5.11), we now obtain

$$\begin{cases}\Delta_{\mathrm{S,T}}=e^{-2\,x}\mathcal{O}(\epsilon_n)\sim 0 & \text{sub-horizon scales}\\[2ex] \Delta_{\mathrm{S}}=\dfrac{4}{27}\left(\epsilon_1\,\epsilon_2^2+\epsilon_1\,\epsilon_2\,\epsilon_3+\dfrac{\epsilon_2\,\epsilon_3^2}{2}+\dfrac{\epsilon_2\,\epsilon_3\,\epsilon_4}{2}\right)+\mathcal{O}(\epsilon_n^4) & \text{super-horizon scales}\\[2ex] \Delta_{\mathrm{T}}=\dfrac{4}{27}\left(\epsilon_1\,\epsilon_2^2+\epsilon_1\,\epsilon_2\,\epsilon_3\right)+\mathcal{O}(\epsilon_n^4) & \text{super-horizon scales}\ ,\end{cases} \tag{5.12}$$

and it is thus obvious that Δ becomes very small for any inflationary potential satisfying the slow-roll conditions [61] in both limits of interest (but, remarkably, not at the turning point). As a consequence, the WKB approximation is now also valid on super-horizon scales.

One might naively expect that the transformation (5.9) will improve the WKB approach to all orders (in the formal expansion in δ), thus yielding increasingly better results. However, since Q diverges at the turning point $x = x_0$, whether the function μ_{WKB} can still be regarded as a solution to Eq. (5.1) for $x \sim x_0$ in the adiabatic limit $\delta \to 0$ becomes a subtle issue. It is precisely for this reason that one usually considers particular solutions around the turning point (for example, combinations of Airy functions for a linear turning point) which must then be matched with the asymptotic form (4.2) on both sides of the turning point. The problem with this standard procedure is that there is no general rule to determine the actual matching points (which cannot be x_0 where Q diverges) in such a way that the overall error be small. As a consequence, the standard adiabatic expansion for $\delta \ll 1$ may not lead to a reliable approximation around the turning point, which would then result in large errors to higher orders and a questionable further extension of all the expressions to the interesting case $\delta = 1$.

It was in fact shown in Ref. [36] that a simple extension to higher orders of the above procedure [32] actually seems to reduce the accuracy with respect to the leading order results of Ref. [58]. We shall see in the next Section that one can overcome this problem by introducing mode functions which remain good approximations also around the turning point.

5.2 Improved WKB approximation

We consider here the formalism given in Section 4.3 and apply it to cosmological perturbations. The basic idea is to use approximate expressions which are valid for all values of the coordinate x and then expand around them. It is also easy to show that, for the cosmological case, $|\sigma/\omega^2| \simeq \Delta$ as given in Eq. (5.12) for $x \to \pm\infty$, so that the new approximate solutions remain very accurate for large $|x|$.

5.2.1 Perturbative expansion

We start by considering the initial conditions and the matching procedure for the perturbative expansion given in Section 4.3.

Initial and matching conditions

We first use the initial conditions (5.3) in order to fix the constant coefficients $A_\pm$.

For the function χ such conditions become

$$\lim_{x \to x_i} \chi(x) = d\sqrt{\frac{1-\epsilon_1(x_i)}{2k}}\,\mathrm{e}^{-i\,k\,\eta_i - x_i/2} = d\sqrt{\frac{1-\epsilon_1(x_i)}{2k}}\,\mathrm{e}^{i\,\xi_{\mathrm{I}}(x_i) - x_i/2}\ , \tag{5.13}$$

where, from the definitions of η and x, $k\,\eta_i \simeq -i\,\xi_{\mathrm{I}}(x_i)$. We then recall the asymptotic form of the Bessel functions J_ν for $x \to +\infty$ [39, 38] [3],

$$J_{\pm m}\left[\xi_{\mathrm{I}}(x)\right] \sim \sqrt{\frac{2}{\pi\,\xi_{\mathrm{I}}(x)}}\,\cos\left(\xi_{\mathrm{I}}(x) \mp \frac{\pi}{2}\,m - \frac{\pi}{4}\right)\ , \tag{5.14}$$

from which we obtain the asymptotic expression of the mode function in region I,

$$\begin{aligned}
\chi_{\mathrm{I}}(x_i) \sim & \sqrt{\frac{1-\epsilon_1(x_i)}{2\,\pi}}\,\mathrm{e}^{-x_i/2}\ \times \\
& \Big\{\mathrm{e}^{+i\,\xi_{\mathrm{I}}(x_i)}\,\Big[\mathrm{e}^{-i\left(\frac{1}{4}+\frac{m}{2}\right)\pi}\,A_+ + \mathrm{e}^{-i\left(\frac{1}{4}-\frac{m}{2}\right)\pi}\left(A_- + \varepsilon\,A_-\,J^-_{+-}(x_0,x_i) + \varepsilon\,A_+\,J^+_{++}(x_0,x_i)\right)\Big] \\
& +\mathrm{e}^{-i\,\xi_{\mathrm{I}}(x_i)}\,\Big[\mathrm{e}^{+i\left(\frac{1}{4}+\frac{m}{2}\right)\pi}\,A_+ + \mathrm{e}^{+i\left(\frac{1}{4}-\frac{m}{2}\right)\pi}\,\left(A_- + \varepsilon\,A_-\,J^-_{+-}(x_0,x_i) + \varepsilon\,A_+\,J^+_{++}(x_0,x_i)\right)\Big]\Big\}\ .
\end{aligned} \tag{5.15}$$

The initial conditions (5.13) therefore yield

$$A_+ = d\sqrt{\frac{\pi}{k}}\,\frac{\mathrm{e}^{+i\left(\frac{1}{4}+\frac{m}{2}\right)\pi}}{1-\mathrm{e}^{2\,i\,m\,\pi}}\ ,\ A_- = -A_+\,\frac{\mathrm{e}^{+i\,m\,\pi} + \varepsilon\,J^+_{++}(x_0,x_i)}{1+\varepsilon\,J^-_{+-}(x_0,x_i)}\ . \tag{5.16}$$

Note that A_+ does not depend on ε, so it holds to all orders.

---

[3] Since the initial conditions must be imposed at x in deep region I, we can consider $x_i \sim +\infty$.

We next impose continuity at the turning point in order to determine the coefficients $B_\pm$. For this we shall need the (asymptotic) expressions of Bessel functions for $x \to x_0$ [39, 38] [4]. In particular,

$$\begin{aligned} J_{\pm m}\left[\xi_{\rm I}(x)\right] &\simeq \left[\frac{\xi_{\rm I}(x)}{2}\right]^{\pm m} \frac{1}{\Gamma\left(1 \pm m\right)} \quad \text{for } x \to x_0^+ \\ I_{\pm m}\left[\xi_{\rm II}(x)\right] &\simeq \left[\frac{\xi_{\rm II}(x)}{2}\right]^{\pm m} \frac{1}{\Gamma\left(1 \pm m\right)} \quad \text{for } x \to x_0^- \ , \end{aligned} \tag{5.17}$$

where Γ is Euler's gamma function. Near the turning point, we just keep the leading term in the expansion (4.11), so that

$$\omega(x) \simeq \sqrt{C}\,|x-x_0|^{\frac{1-2m}{2m}} \ , \ \xi(x) \simeq 2\,m\,\sqrt{C}\,|x-x_0|^{\frac{1}{2m}} \ . \tag{5.18}$$

We thus obtain the following forms of the mode functions near the turning point,

$$\begin{aligned} \chi_{\rm I}(x \simeq x_0) \ \simeq \ & A_+\,a_+(x_0)\,\frac{\sqrt{2\,m}\,\left(m\,\sqrt{C}\right)^{m}}{\Gamma\left(1+m\right)}\,(x-x_0) \\ & + A_-\,a_-(x_0)\,\frac{\sqrt{2\,m}\,\left(m\,\sqrt{C}\right)^{-m}}{\Gamma\left(1-m\right)} \end{aligned} \tag{5.19a}$$

$$\begin{aligned} \chi_{\rm II}(x \simeq x_0) \ \simeq \ & B_+\,b_+(x_0)\,\frac{\sqrt{2\,m}\,\left(m\,\sqrt{C}\right)^{m}}{\Gamma\left(1+m\right)}\,(x_0-x) \\ & + B_-\,b_-(x_0)\,\frac{\sqrt{2\,m}\,\left(m\,\sqrt{C}\right)^{-m}}{\Gamma\left(1-m\right)} \ . \end{aligned} \tag{5.19b}$$

Continuity across x_0 then implies that

$$B_+\,b_+(x_0) = -A_+\,a_+(x_0) \ , \quad B_-\,b_-(x_0) = A_-\,a_-(x_0) \ . \tag{5.20}$$

From the definitions (4.20) at $x = x_0$, Eqs. (5.16) and the relations (5.20) we therefore obtain

$$\begin{aligned} \frac{B_+}{A_+} &= -1 + \varepsilon\,\frac{{\rm e}^{+i\,m\,\pi} + \varepsilon\,J^+_{++}(x_0,x_i)}{1+\varepsilon\,J^-_{+-}(x_0,x_i)}\,J^-_{--}(x_0,x_i) - \varepsilon\,J^+_{+-}(x_0,x_i) \\ \frac{B_-}{A_+} &= -\frac{{\rm e}^{+i\,m\,\pi} + \varepsilon\,J^+_{++}(x_0,x_i)}{1+\varepsilon\,J^-_{+-}(x_0,x_i)}\,\frac{1-i\,\varepsilon^2\,J^-_{--}(x_0,x_i)\,I^+_{++}(x_f,x_0)}{1-i\,\varepsilon\,I^-_{+-}(x_f,x_0)} \\ & \quad -i\,\varepsilon\,\frac{1+\varepsilon\,J^+_{+-}(x_0,x_i)}{1-i\,\varepsilon\,I^-_{+-}(x_f,x_0)}\,I^+_{++}(x_f,x_0) \ . \end{aligned} \tag{5.21}$$

---

[4] The Bessel functions are actually regular around $x = x_0$, therefore the following expressions are just the leading terms in the Taylor expansion of J_ν and I_ν.

It is apparent from the above derivation that, since the matching between approximate solutions in the two regions is always performed at $x = x_0$, no ambiguity hinders the evaluation of the coefficients $B_\pm$ and the accuracy of the approximate solution is therefore expected to increase with increasing order.

Recursive (perturbative) relations

We can finally obtain expressions for the coefficients $a_\pm(x)$ and $b_\pm(x)$ by solving the integral relations (4.20). We remark that the r.h.s.'s of such equations contain $a_\pm(x)$ and $b_\pm(x)$, which can therefore be determined recursively by expanding them (as well as any function of them) in ε, that is

$$a_\pm(x) = 1 + \sum_{q\geq 1} \varepsilon^q \, a_\pm^{(q)} \ , \quad b_\pm(x) = 1 + \sum_{q\geq 1} \varepsilon^q \, b_\pm^{(q)} \ . \tag{5.22}$$

It will also be useful to define the following integrals

$$\begin{aligned} J_{s\bar{s}}^{w(q)}(x_1, x_2) &\equiv \frac{\pi}{\sqrt{3}} \int_{x_1}^{x_2} \sigma_{\rm I}(y)\, a_w^{(q)}(y)\, u_{Is}(y)\, u_{I\bar{s}}(y)\, {\rm d}y \\ I_{s\bar{s}}^{w(q)}(x_1, x_2) &\equiv \frac{\pi}{\sqrt{3}} \int_{x_1}^{x_2} \sigma_{\rm II}(y)\, b_w^{(q)}(y)\, u_{IIs}(y)\, u_{II\bar{s}}(y)\, {\rm d}y \, , \end{aligned} \tag{5.23}$$

where again w, s and $\bar{s} = \pm$, and q is a non-negative integer.

Leading order

We begin by considering the leading (ε^0) order

$$a_\pm^{(0)}(x) = b_\pm^{(0)}(x) = 1 \ . \tag{5.24}$$

The corresponding solutions are simply given by

$$\chi_{\rm I}(x) \simeq u_{\rm I}(x) = A_+ \sqrt{\frac{\xi_{\rm I}(x)}{\omega_{\rm I}(x)}} \, \left\{ J_{+m}\left[\xi_{\rm I}(x)\right] - \, {\rm e}^{+i\,m\,\pi} \, J_{-m}\left[\xi_{\rm I}(x)\right] \right\} \tag{5.25a}$$

$$\chi_{\rm II}(x) \simeq u_{\rm II}(x) = -A_+ \sqrt{\frac{\xi_{\rm II}(x)}{\omega_{\rm II}(x)}} \, \left\{ I_{+m}\left[\xi_{\rm II}(x)\right] + {\rm e}^{+i\,m\,\pi} \, I_{-m}\left[\xi_{\rm II}(x)\right] \right\} \ , \tag{5.25b}$$

where we used the zero order forms of Eqs. (5.16) and (5.21),

$$A_- = B_- = -A_+ \, {\rm e}^{+i\,m\,\pi} \ , \quad B_+ = -A_+ \ . \tag{5.26}$$

We know that these expressions are also good solutions of Eq. (5.10) near the turning point and, deep in region II, we can use the asymptotic form of I_ν for $x \sim x_f \to -\infty$ [38, 39],

$$I_{\pm m}\left[\xi_{\rm II}(x)\right] \ \sim \ \frac{1}{\sqrt{2\,\pi\,\xi_{\rm II}(x)}} \, \left[{\rm e}^{\xi_{\rm II}(x)} + {\rm e}^{-\xi_{\rm II}(x) - i\left(\frac{1}{2} \pm m\right)\pi} \right] \ . \tag{5.27}$$

On neglecting the non-leading mode $\mathrm{e}^{-\xi_{\mathrm{II}}(x)}$, we then obtain

$$\chi_{\mathrm{II}}(x_f) \sim -A_+ \, \frac{(1+\mathrm{e}^{+i\,m\,\pi})}{\sqrt{2\,\pi\,\omega_{\mathrm{II}}(x_f)}} \, \mathrm{e}^{\xi_{\mathrm{II}}(x_f)} \ . \tag{5.28}$$

If we now use Eqs. (5.4), (5.16) and (5.28), and the values of d, we recover the results of Ref. [58] for all quantities of interest, i.e. power spectra, spectral indices and α-runnings

$$\mathcal{P}_\zeta \simeq \frac{H^2}{\pi\,\epsilon_1\,m_{\mathrm{Pl}}^2}\left(\frac{k}{a\,H}\right)^3 \frac{\mathrm{e}^{2\,\xi_{\mathrm{II,S}}(k,\eta)}}{[1-\epsilon_1(\eta)]\;\omega_{\mathrm{II,S}}(k,\eta)} \equiv \mathcal{P}_\zeta^{(0)} \tag{5.29a}$$

$$n_{\mathrm{S}} - 1 \simeq 3 + 2\,\left.\frac{\mathrm{d}\,\xi_{\mathrm{II,S}}}{\mathrm{d}\,\ln k}\right|_{k=k_*} \tag{5.29b}$$

$$\alpha_{\mathrm{S}} \simeq 2\,\left.\frac{\mathrm{d}^2\,\xi_{\mathrm{II,S}}}{(\mathrm{d}\,\ln k)^2}\right|_{k=k_*} \ , \tag{5.29c}$$

and

$$\mathcal{P}_h \simeq \frac{16\,H^2}{\pi\,m_{\mathrm{Pl}}^2}\left(\frac{k}{a\,H}\right)^3 \frac{\mathrm{e}^{2\,\xi_{\mathrm{II,T}}(k,\eta)}}{[1-\epsilon_1(\eta)]\;\omega_{\mathrm{II,T}}(k,\eta)} \equiv \mathcal{P}_h^{(0)} \tag{5.29d}$$

$$n_{\mathrm{T}} \simeq 3 + 2\,\left.\frac{\mathrm{d}\,\xi_{\mathrm{II,T}}}{\mathrm{d}\,\ln k}\right|_{k=k_*} \tag{5.29e}$$

$$\alpha_{\mathrm{T}} \simeq 2\,\left.\frac{\mathrm{d}^2\,\xi_{\mathrm{II,T}}}{(\mathrm{d}\,\ln k)^2}\right|_{k=k_*} \ , \tag{5.29f}$$

where we have transformed back to the original variables k and η, and all quantities are evaluated in the super-horizon limit (i.e. for $k \ll a\,H$).

Next-to-leading order

We now insert the leading order expressions (5.24) into the integral relations (4.20) to compute the next-to-leading order expressions

$$\begin{aligned}
a_+^{(1)}(x) &= J_{+-}^{(0)}(x,x_i) - \mathrm{e}^{+i\,m\,\pi}\,J_{--}^{(0)}(x,x_i) \\
a_-^{(1)}(x) &= J_{+-}^{(0)}(x_0,x) - \mathrm{e}^{-i\,m\,\pi}\,J_{++}^{(0)}(x_0,x) \\
b_+^{(1)}(x) &= -i\,I_{+-}^{(0)}(x,x_0) - i\,\mathrm{e}^{+i\,m\,\pi}\,I_{--}^{(0)}(x,x_0) \\
b_-^{(1)}(x) &= -i\,I_{+-}^{(0)}(x_f,x) - i\,\mathrm{e}^{-i\,m\,\pi}\,I_{++}^{(0)}(x_f,x) \ ,
\end{aligned} \tag{5.30}$$

where we used the simplified notation $J_{s\bar{s}}^{+(0)} = J_{s\bar{s}}^{-(0)} \equiv J_{s\bar{s}}^{(0)}$ and $I_{s\bar{s}}^{+(0)} = I_{s\bar{s}}^{-(0)} \equiv I_{s\bar{s}}^{(0)}$, and also expanded the coefficients A_- and $B_\pm$ to zero order in ε.

From Eq. (5.27), again neglecting the non-leading mode $\mathrm{e}^{-\xi_{\mathrm{II}}(x)}$, we obtain the mode function at $x = x_f$ to first order in ε,

$$\begin{aligned}\chi_{\mathrm{II}}(x_f) \sim & -\frac{A_+\,\mathrm{e}^{\xi_{\mathrm{II}}(x_f)}}{\sqrt{2\,\pi\,\omega_{\mathrm{II}}(x_f)}}\,\Big\{1+\mathrm{e}^{+i\,m\,\pi}+i\,\varepsilon\,\Big[I^{(0)}_{++}(x_f,x_0)-I^{(0)}_{+-}(x_f,x_0)\Big] \\ & -i\,\varepsilon\,\mathrm{e}^{+i\,m\,\pi}\,\Big[I^{(0)}_{--}(x_f,x_0)-I^{(0)}_{+-}(x_f,x_0)\Big]-\varepsilon\,\mathrm{e}^{+i\,m\,\pi}\,\Big[J^{(0)}_{+-}(x_0,x_i)+J^{(0)}_{--}(x_0,x_i)\Big] \\ & +\varepsilon\,\Big[J^{(0)}_{+-}(x_0,x_i)+J^{(0)}_{++}(x_0,x_i)\Big]\Big\}\ ,\end{aligned} \tag{5.31}$$

which, using Eqs. (5.4), (5.16), (5.31) and the values of d, yields all quantities of interest to first order in ε. For the spectra we obtain

$$\mathcal{P}_\zeta \simeq \mathcal{P}^{(0)}_\zeta\,\left[1+g^{\mathrm{GREEN}}_{(1)\,\mathrm{S}}(x_f)\right]\ ,\quad \mathcal{P}_h \simeq \mathcal{P}^{(0)}_h\,\left[1+g^{\mathrm{GREEN}}_{(1)\,\mathrm{T}}(x_f)\right]\ , \tag{5.32}$$

where the relative corrections to the leading order expressions (5.29a) and (5.29d) are now given by

$$\begin{aligned}g^{\mathrm{GREEN}}_{(1)\,\mathrm{S,T}}(x) \;=\; & \Big\{J^{(0)}_{++}(x_0,x_i)-J^{(0)}_{--}(x_0,x_i) \\ & +\frac{1}{\sqrt{3}}\,\Big[I^{(0)}_{++}(x,x_0)-2\,I^{(0)}_{+-}(x,x_0)+I^{(0)}_{--}(x,x_0)\Big]\Big\}_{\mathrm{S,T}}\ ,\end{aligned} \tag{5.33}$$

in which we set $\varepsilon = 1$ and $n = 1$ as required, and write S and T to recall the use of the corresponding frequencies. The expressions for the spectral indices and their runnings to this order can finally be derived from the definitions (5.5) and (5.6).

Higher orders

The above procedure can be extended to all orders. The coefficients up to $a^{(q)}_\pm$ and $b^{(q)}_\pm$ must be used to compute the integrals $J^{w(q)}_{s\bar{s}}$ and $I^{w(q)}_{s\bar{s}}$ which determine $a^{(q+1)}_\pm$ and $b^{(q+1)}_\pm$. However, general expressions soon become very involved, and we shall test the effectiveness of our method by applying it to several cases of interest.

5.2.2 Adiabatic expansion

It is important to observe that the initial conditions (5.13) and matching conditions at the turning point to first order in the adiabatic parameter δ yield different results with respect to the perturbative expansion in ε. First of all, the coefficient A_+, which was left unaffected by the expansion in ε [see Eq. (5.16)], acquires a correction. The relations between A_-, $B_\pm$ and A_+ instead remain those given in Eq. (5.26) to all orders, whereas in the perturbative expansion they were modified [see Eqs. (5.16) and (5.21)]. To summarize, to first order in δ, one obtains

$$\begin{aligned}A_+ \;&\simeq\; d\,\sqrt{\frac{\pi}{k}}\,\frac{\mathrm{e}^{i\left(\frac{1}{4}+\frac{m}{2}\right)\pi}}{1-\mathrm{e}^{2\,i\,m\,\pi}}\,\left\{1-\delta\,\left[\phi_{\mathrm{I}(1)}(x_i)+\gamma_{\mathrm{I}(1)}(x_i)\,\left(i\,\omega_{\mathrm{I}}(x_i)-\frac{1}{2}\right)\right]\right\} \\ A_- \;&=\; -A_+\,\mathrm{e}^{+i\,m\,\pi}\ ,\quad B_\pm = \mp A_\pm\ ,\end{aligned} \tag{5.34}$$

and the perturbation modes deep in Region II (at $x \ll x_0$) are finally given by

$$\chi_{\rm II}(x) \simeq u_{\rm II}(x) \left\{1 + \delta \left[\phi_{\rm II(1)}(x) - \gamma_{\rm II(1)}(x) \left(\omega_{\rm II}(x) + \frac{\omega'_{\rm II}(x)}{2\,\omega_{\rm II}(x)}\right) \right.\right.$$
$$\left.\left. -\phi_{\rm I(1)}(x_i) + \gamma_{\rm I(1)}(x_i) \left(\frac{1}{2} - i\,\omega_{\rm I}(x_i)\right)\right]\right\} \; . \qquad (5.35)$$

We note that, in order to obtain the above result, one must first take the asymptotic expansion of the functions $u_\pm$ and then take the derivative, since the reverse order would lead to larger errors. The corrected power spectra are then given by

$$\mathcal{P}_\zeta \simeq \mathcal{P}_\zeta^{(0)} \left[1 + g^{\rm AD}_{(1){\rm S}}(x_f)\right] \; , \quad \mathcal{P}_h \simeq \mathcal{P}_h^{(0)} \left[1 + g^{\rm AD}_{(1){\rm T}}(x_f)\right] \; , \qquad (5.36a)$$

in which we set $\delta = 1$ at the end [5]. The spectral indices are also given by

$$\begin{aligned} n_{\rm S} - 1 &= 3 + 2\,\frac{{\rm d}\,\xi_{\rm II,S}}{{\rm d}\,\ln k} + \frac{{\rm d}\,g^{\rm AD}_{(1){\rm S}}}{{\rm d}\,\ln k} \\ n_{\rm T} &= 3 + 2\,\frac{{\rm d}\,\xi_{\rm II,T}}{{\rm d}\,\ln k} + \frac{{\rm d}\,g^{\rm AD}_{(1){\rm T}}}{{\rm d}\,\ln k} \; , \end{aligned} \qquad (5.36b)$$

and their runnings by

$$\begin{aligned} \alpha_{\rm S} &= 2\,\frac{{\rm d}^2\,\xi_{\rm II,S}}{({\rm d}\,\ln k)^2} + \frac{{\rm d}^2\,g^{\rm AD}_{(1){\rm S}}}{({\rm d}\,\ln k)^2} \\ \alpha_{\rm T} &= 2\,\frac{{\rm d}^2\,\xi_{\rm II,T}}{({\rm d}\,\ln k)^2} + \frac{{\rm d}^2\,g^{\rm AD}_{(1){\rm T}}}{({\rm d}\,\ln k)^2} \; . \end{aligned} \qquad (5.36c)$$

Finally, the tensor-to-scalar ratio takes the form

$$R = 16\,\epsilon_1\,\frac{{\rm e}^{2\,\xi_{\rm II,T}}\left(1 + g^{\rm AD}_{(1){\rm T}}\right)\,\omega_{\rm II,S}}{{\rm e}^{2\,\xi_{\rm II,S}}\left(1 + g^{\rm AD}_{(1){\rm S}}\right)\,\omega_{\rm II,T}} \; , \qquad (5.36d)$$

where all quantities are evaluated in the super-horizon limit ($x \ll x_0$) and we used the results

$$g^{\rm AD}_{(1){\rm S,T}}(x) = 2\left[\phi_{\rm II(1)}(x) - \gamma_{\rm II(1)}(x)\left(\omega_{\rm II}(x) + \frac{\omega'_{\rm II}(x)}{2\,\omega_{\rm II}(x)}\right) + \frac{\gamma_{\rm I(1)}(x_i)}{2} - \phi_{\rm I(1)}(x_i)\right]_{\rm S,T} , \qquad (5.37)$$

where the indices S and T recall the use of the corresponding frequencies.

---

[5] Since our method has some similarity with that of Ref. [62] (see also Ref. [63]), it is worth pointing out that the first order corrections shown here differ from those of Ref. [62] (at least) in that they contain contributions from both Regions I and II.

Given the complicated expressions for ω, it is usually impossible to carry out the double integration that yields $\phi_{(1)}$ analytically, let alone higher order terms. One must therefore rely on numerical computations. In the context of power-law inflation we can compare results obtained in next-to-leading order from the two expansions with the exact result.

5.3 Method of Comparison Equation

In order to apply the MCE to cosmological perturbations, we note that the frequency $\omega^2(x)$ is

$$\omega^2(x) = \frac{\mathrm{e}^{2\,x}}{\left[1-\epsilon_1(x)\right]^2} - \nu^2(x)\ , \tag{5.38}$$

with $\nu^2(x)$ given, respectively for scalar and tensor perturbations, by

$$\begin{aligned}
\nu_{\mathrm{S}}^2(x) &= \frac{1}{4}\left(\frac{3-\epsilon_1}{1-\epsilon_1}\right)^2 + \frac{(3-2\,\epsilon_1)\,\epsilon_2}{2\,(1-\epsilon_1)^2} + \frac{(1-2\,\epsilon_1)\,\epsilon_2\,\epsilon_3}{2\,(1-\epsilon_1)^3} + \frac{(1-4\,\epsilon_1)\,\epsilon_2^2}{4\,(1-\epsilon_1)^4} && \text{(5.39a)}\\
\nu_{\mathrm{T}}^2(x) &= \frac{1}{4}\left(\frac{3-\epsilon_1}{1-\epsilon_1}\right)^2 - \frac{\epsilon_1\,\epsilon_2}{2\,(1-\epsilon_1)^2} - \frac{\epsilon_1\,\epsilon_2\,\epsilon_3}{2\,(1-\epsilon_1)^3} - \frac{(2+\epsilon_1)\,\epsilon_1\,\epsilon_2^2}{4\,(1-\epsilon_1)^4}\ , && \text{(5.39b)}
\end{aligned}$$

where we omit the dependence on x in the ϵ_i for the sake of brevity. From Eqs. (5.38), (5.39a) and (5.39b) we can recognise our second-order differential basic equations (5.11). The point $x = x_0$ where the frequency vanishes, $\omega(x_0) = 0$ (i.e. the classical "turning point"), is given by the expression

$$x_0 = \ln\left[\bar{\nu}\ (1-\bar{\epsilon}_1)\right]\ , \tag{5.40}$$

where we have defined $\bar{\nu} \equiv \nu(x_0)$ and $\bar{\epsilon}_1 \equiv \epsilon_1(x_0)$. We now choose the comparison function

$$\Theta^2(\sigma) = \frac{\mathrm{e}^{2\,\sigma}}{(1-\bar{\epsilon}_1)^2} - \bar{\nu}^2\ , \tag{5.41}$$

and note that then $\sigma_0 = x_0$. Solutions to Eq. (4.6) can now be expressed, by means of Eqs. (4.27), (4.30) and (5.41), as

$$\chi_{\pm}(x) \simeq \sqrt{\frac{\Theta(\sigma)}{\omega(x)}}\, J_{\pm\bar{\nu}}\left(\frac{\mathrm{e}^{\sigma}}{1-\bar{\epsilon}_1}\right)\ , \tag{5.42}$$

where the J's are Bessel functions [39], and the initial condition (5.3) can be satisfied by taking a linear combination of them. However, in contrast with the improved WKB method presented in Section 4.3, MCE solutions need not be matched at the turning point, since the functions (5.42) are valid solutions for the whole range of the variable x. Eq. (4.31) at the end of inflation, $x = x_{\mathrm{f}}$, becomes

$$\begin{aligned}
\xi(x_{\mathrm{f}}) &\simeq -\Theta(\sigma_{\mathrm{f}}) - \frac{\bar{\nu}}{2}\ln\left[\frac{\bar{\nu}-\Theta(\sigma_{\mathrm{f}})}{\bar{\nu}+\Theta(\sigma_{\mathrm{f}})}\right] \\
&\simeq -\bar{\nu}\left[1+\ln\left(\frac{\mathrm{e}^{\sigma_{\mathrm{f}}}}{1-\bar{\epsilon}_1}\right)-\ln\left(2\,\bar{\nu}\right)\right] ,
\end{aligned} \tag{5.43}$$

where the super-horizon limit $x_{\mathrm{f}} \ll x_0$ ($\sigma_{\mathrm{f}} \to -\infty$) has been taken in the second line. One then has

$$\frac{\mathrm{e}^{\sigma_{\mathrm{f}}}}{1-\bar{\epsilon}_1} \simeq \frac{2\,\bar{\nu}}{\mathrm{e}}\exp\left[-\frac{\xi(x_{\mathrm{f}})}{\bar{\nu}}\right] . \tag{5.44}$$

Finally, on using Eq. (5.44), we obtain the general expressions for the power spectra to leading MCE order,

$$\mathcal{P}_\zeta = \left[\frac{H^2}{\pi\,\epsilon_1\,m_{\mathrm{Pl}}^2}\left(\frac{k}{a\,H}\right)^3\frac{\mathrm{e}^{2\,\xi_{\mathrm{S}}}}{(1-\epsilon_1)\,\omega_{\mathrm{S}}}\right]_{x=x_{\mathrm{f}}} g_{\mathrm{S}}(x_0) \tag{5.45a}$$

$$\mathcal{P}_h = \left[\frac{16\,H^2}{\pi\,m_{\mathrm{Pl}}^2}\left(\frac{k}{a\,H}\right)^3\frac{\mathrm{e}^{2\,\xi_{\mathrm{T}}}}{(1-\epsilon_1)\,\omega_{\mathrm{T}}}\right]_{x=x_{\mathrm{f}}} g_{\mathrm{T}}(x_0) , \tag{5.45b}$$

where m_{Pl} is the Planck mass and the quantities inside the square brackets are evaluated in the super-horizon limit, whereas the functions

$$g(x_0) \equiv \frac{\pi\,e^{2\,\bar{\nu}}\,\bar{\nu}^{1-2\,\bar{\nu}}}{\left[1-\cos\left(2\,\pi\,\bar{\nu}\right)\right]\,\left[\Gamma\left(1-\bar{\nu}\right)\right]^2} , \tag{5.45c}$$

describe corrections that just depend on quantities evaluated at the turning point and represent the main result of the MCE applied to cosmological perturbations [6]. The expression in Eq. (5.45c) is obtained by simply making use of the approximate solutions (5.42) and their asymptotic expansion at $x \to \infty$ to impose the initial conditions (5.3). In Section 5.2 one finds a similar factor but, in that case, using the Bessel functions of order 1/3 leads to a large error in the amplitudes. The MCE instead uses Bessel functions of order $\bar{\nu}$, with $\bar{\nu} = 3/2$ to leading order in the HFF (i.e. the right index for the de Sitter model), which yields a significantly better value for the amplitudes of inflationary spectra.

The MCE allows one to compute approximate perturbation modes with errors in the asymptotic regions (i.e. in the sub- and super-horizon limits) which are comparable with those of the standard (or improved) WKB approximation (see Sec. 5.1). Since these methods usually give large errors at the turning point (which produce equally large errors in the amplitude of the power spectra) it will suffice to estimate the error at the turning point in order to show that the MCE is indeed an improvement. To leading order (that is, on using the approximate solution (5.42)), the MCE gives an error at the turning point of the second order in the HFF, which means that we have a small error in the amplitudes of the power spectra. Unfortunately, this error remains of second order in the HFF also for next-to-leading order in the MCE. We shall see this by applying Dingle's analysis [42] for linear frequencies to our case (5.38). We start by rewriting Eq. (4.29) as

---

[6] Inside the square brackets we recognize the general results $\mathcal{P}_\zeta^{(0)}$ and $\mathcal{P}_h^{(0)}$ given by the WKB (leading-order) approximation in Section 5.2. The "correction" $g(x_0)$ accounts for the fact that Θ^2 in Eq. (5.41) is a better approximation than Langer's [59, 37].

$$\left\{\omega^2-\sigma_1^2\left[\frac{\mathrm{e}^{2\,\sigma}}{(1-\bar{\epsilon}_1)^2}-\bar{\nu}^2\right]\right\}+\left[\frac{3}{4}\frac{\sigma_2^2}{\sigma_1^2}-\frac{1}{2}\frac{\sigma_3}{\sigma_1}\right]=0\ , \tag{5.46}$$

where we dropped the x dependence in ω and σ and the order of the derivatives is given by their subscripts ($\sigma_1\equiv\mathrm{d}\sigma/\mathrm{d}x$, $\omega_1^2\equiv\mathrm{d}\omega^2/\mathrm{d}x$, etc.). Note that the term in square brackets is the error obtained on using the solutions (5.42). We then evaluate Eq. (5.46) and its subsequent derivatives at the turning point (i.e. at $x=x_0$),

$$\left\{\omega^2-\sigma_1^2\,\Theta^2\left(\sigma\right)\right\}+\left[\frac{3}{4}\frac{\sigma_2^2}{\sigma_1^2}-\frac{1}{2}\frac{\sigma_3}{\sigma_1}\right]=0 \tag{5.47a}$$

$$\left\{\omega_1^2-2\,\sigma_2\,\sigma_1\,\Theta^2\left(\sigma\right)-\frac{2\,\mathrm{e}^{2\,\sigma}\,\sigma_1^3}{\left(1-\bar{\epsilon}_1\right)^2}\right\}+\left[2\,\frac{\sigma_3\,\sigma_2}{\sigma_1^2}-\frac{3}{2}\frac{\sigma_2^3}{\sigma_1^3}-\frac{1}{2}\frac{\sigma_4}{\sigma_1}\right]=0 \tag{5.47b}$$

$$\begin{aligned}&\left\{\omega_2^2-2\,\left(\sigma_3\,\sigma_1+\sigma_2^2\right)\,\Theta^2\left(\sigma\right)-\frac{2\,\sigma_1^2\,\mathrm{e}^{2\,\sigma}}{\left(1-\bar{\epsilon}_1\right)^2}\,\left(2\,\sigma_1^2+5\,\sigma_2\right)\right\}\\&+\left[\frac{9}{2}\frac{\sigma_2^4}{\sigma_1^4}-\frac{17}{2}\frac{\sigma_3\,\sigma_2^2}{\sigma_1^3}+\frac{5}{2}\frac{\sigma_4\,\sigma_2}{\sigma_1^2}+2\,\frac{\sigma_3^2}{\sigma_1^2}-\frac{1}{2}\frac{\sigma_5}{\sigma_1}\right]=0\end{aligned} \tag{5.47c}$$

$$\begin{aligned}&\left\{\omega_3^2-2\,\left(\sigma_4\,\sigma_1+3\,\sigma_2\,\sigma_3\right)\,\Theta^2\left(\sigma\right)-\frac{2\,\sigma_1\,\mathrm{e}^{2\,\sigma}}{\left(1-\bar{\epsilon}_1\right)^2}\,\left(4\,\sigma_1^4+18\,\sigma_2\,\sigma_1^2+7\,\sigma_3\,\sigma_1+12\,\sigma_2^2\right)\right\}\\&+\left[\frac{87}{2}\frac{\sigma_3\,\sigma_2^3}{\sigma_1^4}-18\,\frac{\sigma_2^5}{\sigma_1^5}-\frac{27}{2}\frac{\sigma_4\,\sigma_2^2}{\sigma_1^3}-21\,\frac{\sigma_3^2\,\sigma_2}{\sigma_1^3}+3\,\frac{\sigma_5\,\sigma_2}{\sigma_1^2}+\frac{13}{2}\frac{\sigma_3\,\sigma_4}{\sigma_1^2}-\frac{1}{2}\frac{\sigma_6}{\sigma_1}\right]=0\ ,\end{aligned} \tag{5.47d}$$

where $\Theta^2\left(\sigma\right)$ was defined in Eq. (5.41) and we omit two equations for brevity. In order to evaluate the error at the turning point

$$\Delta_{\mathrm{TP}}=\left[\frac{3}{4}\frac{\sigma_2^2}{\sigma_1^2}-\frac{1}{2}\frac{\sigma_3}{\sigma_1}\right]_{x=x_0}\ , \tag{5.48}$$

we ignore the terms in square brackets and equate to zero the expressions in the curly brackets in Eqs. (5.47a)-(5.47d) and so on. This leads to

$$\sigma = \ln\left[\left(1-\bar{\epsilon}_1\right)\,\bar{\nu}\right] \tag{5.49a}$$

$$\sigma_1 = \left(\frac{\omega_1^2}{2\,\bar{\nu}^2}\right)^{1/3} \tag{5.49b}$$

$$\sigma_2 = \frac{1}{5\,\left(2\,\bar{\nu}^2\right)^{1/3}}\left[\frac{\omega_2^2}{\left(\omega_1^2\right)^{2/3}} - \left(2\,\frac{\omega_1^2}{\bar{\nu}}\right)^{2/3}\right] \tag{5.49c}$$

$$\sigma_3 = -\frac{6\left(2^{1/3}\,\omega_2^2\right)^2}{175\,\left(\bar{\nu}^{2/5}\,\omega_1^2\right)^{5/3}} - \frac{3\cdot 2^{1/3}\,\omega_2^2}{25\,\left(\bar{\nu}^4\,\omega_1^2\right)^{1/3}} + \frac{16\,\omega_1^2}{175\,\bar{\nu}^2} + \frac{\omega_3^2}{7\,\left(2^{1/2}\,\bar{\nu}\,\omega_1^2\right)^{2/3}}\ , \tag{5.49d}$$

and similar expressions for σ_4, σ_5, and σ_6 which we again omit for brevity. On inserting Eqs. (5.38), (5.39a) and (5.39b) in the above expressions, we find the errors to leading MCE order

$$\Delta^{(0)}_{\mathrm{TP,S}} = -\frac{32}{315}\,\epsilon_1\,\epsilon_2 - \frac{22}{315}\,\epsilon_2\,\epsilon_3 \tag{5.50a}$$

$$\Delta^{(0)}_{\mathrm{TP,T}} = -\frac{32}{315}\,\epsilon_1\,\epsilon_2\ , \tag{5.50b}$$

for scalar and tensor modes respectively.

On iterating this procedure we can further obtain the errors for the next-to-leading MCE order $\Delta^{(1)}_{\mathrm{TP}}$. We first compute next-to-leading solutions to Eqs. (5.47a)-(5.47d) and so on by inserting the solutions found to leading order for $\sigma_1, \sigma_2, \ldots, \sigma_6$ into the corrections (i.e. the square brackets) and into all terms containing $\Theta^2(\sigma)$ [42]. This leads to

$$\Delta^{(1)}_{\mathrm{TP,S}} = -\frac{31712}{331695}\,\epsilon_1\,\epsilon_2 - \frac{21598}{331695}\,\epsilon_2\,\epsilon_3 \tag{5.51a}$$

$$\Delta^{(1)}_{\mathrm{TP,T}} = -\frac{31712}{331695}\,\epsilon_1\,\epsilon_2\ , \tag{5.51b}$$

which show that the next-to-leading MCE solutions lead to an error of second order in the HFF, too. We suspect that this remains true for higher MCE orders, since there is no *a priori* relation between the MCE and the slow-roll expansions. Let us however point out that the above expressions were obtained without performing a slow-roll expansion and therefore do not require that the ϵ_i be small.

Chapter 6

Applications

We shall now apply the formalism developed in the previous chapter to some models of inflation. We shall start by considering the so called Power-law inflation as a benchmark. We shall then proceed by expanding our general expressions to second order in the HFF and compare with the results obtained from other approximation methods used in the literature.

6.1 Power-law Inflation

In this model, the scale factor is given in conformal time by

$$a(\eta) = \ell_0 |\eta|^{1+\beta} \ , \tag{6.1}$$

with $\beta \leq -2$. The case $\beta = -2$ is special, since it corresponds to the de Sitter space-time with constant Hubble radius equal to $\ell_0 = H^{-1}$. The frequency is given, both for scalar and tensor modes, by

$$\omega^2(x) = (1+\beta)^2 \, \mathrm{e}^{2\,x} - \left(\beta + \frac{1}{2}\right)^2 \ , \tag{6.2}$$

and the horizon flow functions read

$$\epsilon_1 = \frac{2+\beta}{1+\beta} \ , \quad \epsilon_n = 0 \ , \quad n > 1 \ . \tag{6.3}$$

Eq. (5.1) with the initial conditions (5.3) can be solved analytically and the exact power spectra at $x_f \to -\infty$ are given by (see, e.g. Refs. [64, 58, 65, 66])

$$\begin{aligned} \mathcal{P}_\zeta &= \frac{1}{\pi \, \epsilon_1 \, m_{\mathrm{Pl}}^2} \, \frac{1}{l_0^2} \, f(\beta) \, k^{2\,\beta+4} \\ \mathcal{P}_h &= \frac{16}{\pi \, m_{\mathrm{Pl}}^2} \, \frac{1}{l_0^2} \, f(\beta) \, k^{2\,\beta+4} \ , \end{aligned} \tag{6.4a}$$

where

$$f(\beta) := \frac{1}{\pi}\left[\frac{\Gamma\left(|\beta+1/2|\right)}{2^{\beta+1}}\right]^2 , \tag{6.4b}$$

and $f(\beta=-2)=1$ [1]. The spectral indices and their runnings can also be calculated from Eqs. (5.5) and (5.6) and one finds $n_{\mathrm{S}}-1=n_{\mathrm{T}}=2\,\beta+4$ and $\alpha_{\mathrm{S}}=\alpha_{\mathrm{T}}=0$. Exact scale-invariance is obtained for $\beta=-2$. For this particular case, we plot the frequency in Fig. 6.1, the function $\xi(x)$ in Fig. 6.2 and the perturbation $\sigma(x)$ in Fig. 6.3.

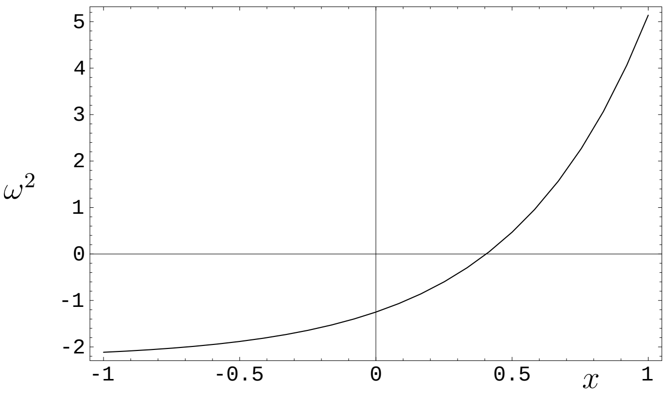

Figure 6.1: The frequency ω^2 for $\beta=-2$. The turning point is at $x_*=\ln(3/2)\simeq 0.4$

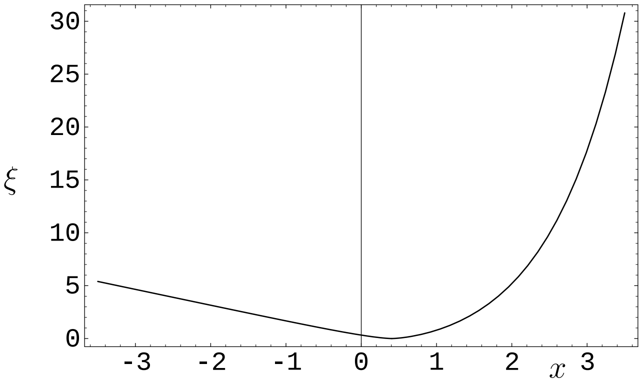

Figure 6.2: The function ξ for $\beta=-2$.

---

[1] The case $\beta=-2$ is singular ($\epsilon_1=0$ and the expression of the scalar power spectrum blows up) and should be considered separately. However, there are no scalar perturbations in De Sitter space-time to first order.

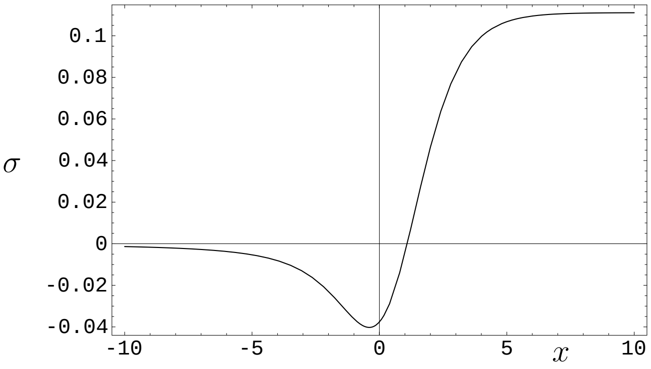

Figure 6.3: The "perturbation" σ for $\beta = -2$.

6.1.1 Improved WKB leading order results

The leading order expressions in the perturbative expansion of Section 4.3.1, as well as the adiabatic expansion of Section 5.2.2, lead to the same result as in Ref. [58],

$$\begin{aligned}\mathcal{P}_\zeta &\simeq \frac{1}{\pi\,\epsilon_1\,m_{\mathrm{Pl}}^2}\,\frac{1}{l_0^2}\,g^{(0)}(\beta)\,k^{2\beta+4}\\ \mathcal{P}_h &\simeq \frac{16}{\pi\,m_{\mathrm{Pl}}^2}\,\frac{1}{l_0^2}\,g^{(0)}(\beta)\,k^{2\beta+4}\ ,\end{aligned} \tag{6.5a}$$

where the function $g^{(0)}(\beta)$ is given by

$$g^{(0)}(\beta) := \frac{2\,e^{2\beta+1}}{|2\,\beta+1|^{2\beta+2}}\ . \tag{6.5b}$$

This yields a relative error for the amplitude of the power spectrum

$$\Delta_P^{(0)} := 100\,\left|\frac{f(\beta)-g^{(0)}(\beta)}{f(\beta)}\right|\%\ , \tag{6.6}$$

which decreases for increasing $|\beta|$, as can be seen from Fig. 6.4, but is rather large (about 10%) for the de Sitter space-time. The spectral indices and their runnings are instead predicted exactly as $n_{\mathrm{S}}-1 = n_{\mathrm{T}} = 2\,\beta+4$ and $\alpha_{\mathrm{S}} = \alpha_{\mathrm{T}} = 0$.

6.1.2 Improved WKB next-to-leading order results

We shall now compare the corrections to the amplitude of the power spectra coming from the two different expansions we described in Chapter 5.

Perturbative expansion

From the next-to-leading expressions in Section 4.3.1, we obtain that the relative correction to the power spectra is given by the function $g_{(1)}^{\mathrm{GREEN}} := g_{(1)\,\mathrm{S}}^{\mathrm{GREEN}} = g_{(1)\,\mathrm{T}}^{\mathrm{GREEN}}$ in

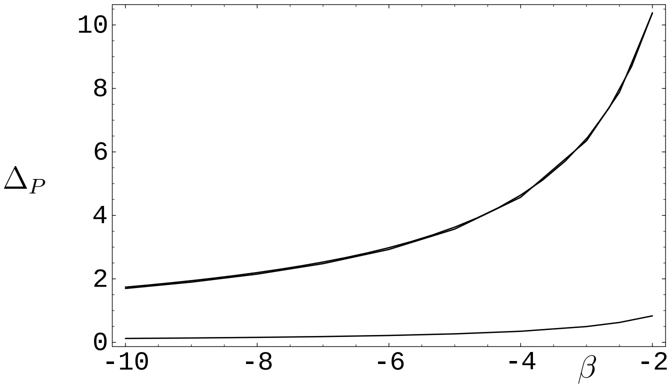

Figure 6.4: The total error on the power spectrum to leading order and to next-to-leading order for the perturbative correction (superposed upper lines) and to next-to-leading order for the adiabatic correction (lower line).

Eq. (5.33) evaluated at $x = x_f \ll x_*$. This quantity can be determined numerically and one finds that it approaches an asymptotical finite value for $x_f \to -\infty$. Some examples are given in Table 6.1 for $x_f = -13$, from which it is clear that the improvement over the leading order is small.

β	-2	-3	-4	-5	-6	-7
$g_{(1)}^{\mathrm{GREEN}}$	$+9.6 \cdot 10^{-5}$	$+7.3 \cdot 10^{-4}$	$+7.1 \cdot 10^{-4}$	$+6.4 \cdot 10^{-4}$	$+5.8 \cdot 10^{-4}$	$+5.2 \cdot 10^{-4}$
$\Delta_P^{(0)}$	10.4%	6.4%	4.6%	3.6%	3.0%	2.5%
$\Delta_P^{(1)}$	10.4%	6.3%	4.6%	3.6%	2.9%	2.5%

Table 6.1: Next-to-leading order improvement for the power spectra ($g_{(1)}^{\mathrm{GREEN}}$) and total final error ($\Delta_P^{(1)}$) to first order in ε. The latter is essentially the same as to leading order ($\Delta_P^{(0)}$).

Once the correction has been included, the total relative error on the power spectra (denoted by $\Delta_P^{(1)}$) therefore remains of the same order as the leading order error $\Delta_P^{(0)}$.

Adiabatic expansion

We analogously evaluate the coefficients $\phi_{(1)}$ and $\gamma_{(1)}$ numerically. For the case $\beta = -2$, the result is plotted in Fig. 6.5, from which it appears that the functions $\phi_{(1)}(x)$ and $\gamma_{(1)}(x)$ converge to finite asymptotic values for $x \to \pm\infty$. Since the same behavior is also found for all $\beta < -2$, we exhibit the values of such coefficients (with $x_i = 20$ and $x_f = -13$) in Table 6.2, together with the corresponding next-to-leading order relative improvement [$g_{(1)}^{\mathrm{AD}}(x_f)$ as defined in Eq. (5.37)] and the total error on the power spectra ($\Delta_P^{(1)}$).

On comparing with the last row in Table 6.1, we can therefore conclude that the adiabatic corrections are significantly better than those obtained from the perturbative expan-

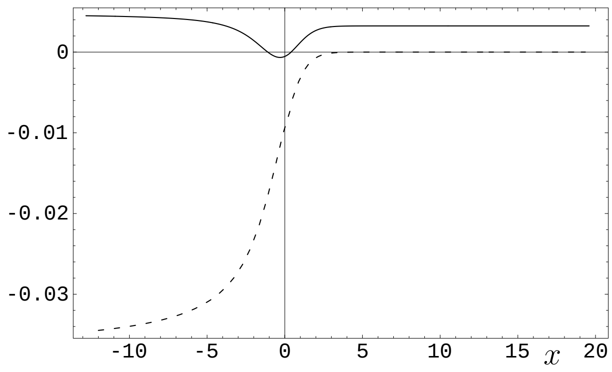

Figure 6.5: The functions $\phi_{(1)}(x)$ (solid line) and $\gamma_{(1)}(x)$ (dotted line) for $\beta = -2$.

sion and, in fact, yield the amplitudes with extremely high accuracy (see also Fig. 6.4). In fact, this method seems (at least) as accurate as the next-to-leading order in the uniform approximation employed in Ref. [62].

β	-2	-3	-4	-5	-6	-7
$\phi_{\mathrm{I}(1)}$	$+3.2 \cdot 10^{-3}$	$+1.1 \cdot 10^{-3}$	$+6.0 \cdot 10^{-4}$	$+3.6 \cdot 10^{-4}$	$+2.4 \cdot 10^{-4}$	$+1.7 \cdot 10^{-4}$
$\gamma_{\mathrm{I}(1)}$	$-2.4 \cdot 10^{-19}$	$-5.9 \cdot 10^{-20}$	$-2.6 \cdot 10^{-20}$	$-1.5 \cdot 10^{-20}$	$-9.4 \cdot 10^{-21}$	$-6.6 \cdot 10^{-21}$
$\phi_{\mathrm{II}(1)}$	$+4.5 \cdot 10^{-3}$	$+1.6 \cdot 10^{-3}$	$+8.2 \cdot 10^{-4}$	$+5.0 \cdot 10^{-4}$	$+3.3 \cdot 10^{-4}$	$+2.4 \cdot 10^{-4}$
$\gamma_{\mathrm{II}(1)}$	$-3.5 \cdot 10^{-2}$	$-1.2 \cdot 10^{-2}$	$-6.4 \cdot 10^{-3}$	$-3.8 \cdot 10^{-3}$	$-2.6 \cdot 10^{-3}$	$-1.8 \cdot 10^{-3}$
$g_{(1)}^{\mathrm{AD}}$	$+1.1 \cdot 10^{-1}$	$+6.3 \cdot 10^{-2}$	$+4.5 \cdot 10^{-2}$	$+3.5 \cdot 10^{-2}$	$+2.9 \cdot 10^{-2}$	$+2.4 \cdot 10^{-2}$
$\Delta_P^{(1)}$	0.83%	0.50%	0.35%	0.27%	0.22%	0.18%

Table 6.2: First order coefficients $\phi_{(1)}$ and $\gamma_{(1)}$, correction ($g_{(1)}^{\mathrm{AD}}$) and total relative error ($\Delta_P^{(1)}$) for the power spectrum to first order in δ.

6.1.3 MCE results

The MCE (developed in Scection 5.3) yields the exact power spectra, spectral indices and runnings,

$$\mathcal{P}_\zeta = \frac{\ell_{\mathrm{Pl}}^2}{\ell_0^2\,\pi\,\epsilon_1}\,f(\beta)\,k^{2\beta+4} \tag{6.7a}$$

$$\mathcal{P}_h = \frac{16\,\ell_{\mathrm{Pl}}^2}{\ell_0^2\,\pi}\,f(\beta)k^{2\beta+4} \tag{6.7b}$$

where $\ell_{\mathrm{Pl}} = m_{\mathrm{Pl}}^{-1}$ is the Planck length and

$$f(\beta) = \frac{\pi}{2^{2\beta+1}}\,\frac{1}{\left[1-\cos\left(2\,\pi\left|\beta+\frac{1}{2}\right|\right)\right]\,\Gamma^2\left(\beta+\frac{3}{2}\right)} \equiv \frac{1}{\pi}\left[\frac{\Gamma\left(\left|\beta+\frac{1}{2}\right|\right)}{2^{\beta+1}}\right]^2\,, \tag{6.7c}$$

with Γ the Gamma function. The spectral indices are $n_{\rm S} - 1 = n_{\rm T} = 2\beta + 4$ and their runnings $\alpha_{\rm S} = \alpha_{\rm T} = 0$. Finally, the tensor-to-scalar ratio becomes

$$R = 16\,\frac{2+\beta}{1+\beta}\ , \tag{6.8}$$

which is constant as well.

6.2 Slow-Roll Inflation

Let us briefly recall the known results obtained from the slow-roll approximation [67, 68, 69]. To first order in the slow-roll parameters (3.65), we have the PS

$$\begin{aligned} \mathcal{P}_\zeta &= \frac{H^2}{\pi\,\epsilon_1\,m_{\rm Pl}^2}\left[1 - 2\,(C+1)\,\epsilon_1 - C\,\epsilon_2 - (2\,\epsilon_1 + \epsilon_2)\,\ln\left(\frac{k}{k_*}\right)\right] \\ \mathcal{P}_h &= \frac{16\,H^2}{\pi\,m_{\rm Pl}^2}\left[1 - 2\,(C+1)\,\epsilon_1 - 2\,\epsilon_1\,\ln\left(\frac{k}{k_*}\right)\right]\ , \end{aligned} \tag{6.9a}$$

where $C \equiv \gamma_{\rm E} + \ln 2 - 2 \approx -0.7296$, $\gamma_{\rm E}$ being the Euler-Mascheroni constant, and all quantities are evaluated at the Hubble crossing η_*, that is the moment of time when $k_* = (a\,H)(N_*) \equiv (a\,H)_*$. (The number k_* is usually called "pivot scale".) From Eqs. (6.9a), we can also obtain the spectral indices and α-runnings,

$$n_S - 1 = -2\,\epsilon_1 - \epsilon_2\ , \quad n_T = -2\,\epsilon_1 \tag{6.9b}$$

$$\alpha_S = \alpha_T = 0\ , \tag{6.9c}$$

on using respectively Eqs. (5.5) and (5.6). From Eq. (5.7), the tensor-to-scalar ratio becomes

$$R = 16\,\epsilon_1\left[1 + C\,\epsilon_2 + \epsilon_2\,\ln\left(\frac{k}{k_*}\right)\right]\ . \tag{6.9d}$$

6.2.1 Improved WKB leading and second slow-roll order

We now consider the possibility of obtaining consistent second order results in the parameters ϵ_i's from the leading WKB approximation.

We first set $g^{\rm AD}_{(1)}(x) \equiv 0$ in Eqs. (5.36a), (5.36b), (5.36c) and (5.36d). We then find it convenient to re-express all relevant quantities in terms of the conformal time η. For this purpose, we employ the relation

$$\begin{aligned} -\,k\,\eta &= \frac{k}{a\,H\,(1-\epsilon_1)}\left[1 + \epsilon_1\,\epsilon_2 + \mathcal{O}\left(\epsilon_i^3\right)\right] && (6.10a) \\ &= \frac{{\rm e}^x}{(1-\epsilon_1)}\left[1 + \epsilon_1\,\epsilon_2 + \mathcal{O}\left(\epsilon_i^3\right)\right]\ . && (6.10b) \end{aligned}$$

We can now expand the frequencies to second order in the HFF,

$$\begin{aligned}
\omega_{\mathrm{S}}^2(\eta) &= k^2\,\eta^2\,(1-2\,\epsilon_1\,\epsilon_2)-\left(\frac{9}{4}+3\,\epsilon_1+4\,\epsilon_1^2+\frac{3}{2}\,\epsilon_2+2\,\epsilon_1\,\epsilon_2+\frac{1}{4}\,\epsilon_2^2+\frac{1}{2}\,\epsilon_2\,\epsilon_3\right)\\
\omega_{\mathrm{T}}^2(\eta) &= k^2\,\eta^2\,(1-2\,\epsilon_1\,\epsilon_2)-\left(\frac{9}{4}+3\,\epsilon_1+4\,\epsilon_1^2-\frac{1}{2}\,\epsilon_1\,\epsilon_2\right)\ ,
\end{aligned} \tag{6.11}$$

and the PS become

$$\begin{aligned}
\mathcal{P}_\zeta &= \frac{H_{\mathrm{f}}^2}{\pi\,\epsilon_{1,\mathrm{f}}\,m_{\mathrm{Pl}}^2}\,(-k\,\eta_{\mathrm{f}})^3\,\frac{2}{3}\left(1-\frac{8}{3}\,\epsilon_{1,\mathrm{f}}-\frac{1}{3}\,\epsilon_{2,\mathrm{f}}+\frac{19}{9}\,\epsilon_{1,\mathrm{f}}^2-\frac{19}{9}\,\epsilon_{1,\mathrm{f}}\,\epsilon_{2,\mathrm{f}}\right.\\
&\qquad\left.+\frac{1}{9}\,\epsilon_{2,\mathrm{f}}^2-\frac{1}{9}\,\epsilon_{2,\mathrm{f}}\,\epsilon_{3,\mathrm{f}}\right)\,\mathrm{e}^{2\xi_{\mathrm{II,S}}}\\
\mathcal{P}_h &= \frac{16\,H_{\mathrm{f}}^2}{\pi\,m_{\mathrm{Pl}}^2}\,(-k\,\eta_{\mathrm{f}})^3\,\frac{2}{3}\left(1-\frac{8}{3}\,\epsilon_{1,\mathrm{f}}+\frac{19}{9}\,\epsilon_{1,\mathrm{f}}^2-\frac{26}{9}\,\epsilon_{1,\mathrm{f}}\,\epsilon_{2,\mathrm{f}}\right)\,\mathrm{e}^{2\xi_{\mathrm{II,T}}}\ .
\end{aligned} \tag{6.12}$$

From now on, the subscript f will denote that the given quantity is evaluated in the super-horizon limit.

We must now compute the arguments of the exponentials in the above expressions, which are in general of the form

$$\xi_{\mathrm{II}}(\eta_0,\eta_{\mathrm{f}};k)=\int_{\eta_{\mathrm{f}}}^{\eta_0}\sqrt{A^2(\eta)-k^2\,\eta^2}\,\frac{\mathrm{d}\,\eta}{\eta}\ , \tag{6.13}$$

where the function $A^2(\eta)$ contains the HFF, but does not depend on k, and we have used

$$\mathrm{d}\,x=\frac{\mathrm{d}\,\eta}{\eta}\,\left[1+\epsilon_1(\eta)\,\epsilon_2(\eta)+\mathcal{O}(\epsilon_i^3)\right]\ . \tag{6.14}$$

Let us also note that, at the turning point $\eta=\eta_0$, one has

$$A(\eta_0)=-k\,\eta_0\ . \tag{6.15}$$

It is now clear that, in order to obtain consistent results to second order in the slow-roll parameters, we must consider the time-dependence of the ϵ_i's, and the function $A^2(\eta)$ may not be approximated by a constant. This does not allow us to perform the integral unless the scale factor $a=a(\eta)$ is given explicitly or, as we shall see, some further approximation is employed.

In Refs. [70, 71], we proposed a procedure which will now be described in detail. Let us start with the general exact relation

$$\begin{aligned}\int_{\eta_1}^{\eta_2} \sqrt{A^2(\eta) - k^2\,\eta^2}\,\frac{\mathrm{d}\,\eta}{\eta} \quad = \quad & \sqrt{A^2(\eta) - k^2\,\eta^2}\Big|_{\eta_1}^{\eta_2} \\ & + \frac{A(\eta)}{2}\,\ln\left(\frac{A(\eta) - \sqrt{A^2(\eta) - k^2\,\eta^2}}{A(\eta) + \sqrt{A^2(\eta) - k^2\,\eta^2}}\right)\Bigg|_{\eta_1}^{\eta_2} \\ & - \int_{\eta_1}^{\eta_2} \ln\left(\frac{A(\eta) - \sqrt{A^2(\eta) - k^2\,\eta^2}}{A(\eta) + \sqrt{A^2(\eta) - k^2\,\eta^2}}\right)\,\frac{[A^2(\eta)]'}{4\,A(\eta)}\,\mathrm{d}\,\eta\ , \qquad (6.16)\end{aligned}$$

which holds for every function $A^2(\eta)$. We can derive this relation by initially considering the integral in Eq. (6.13) with A constant (i.e. independent of η, which is just power-law inflation). In this case, the integration can be performed and yields the first and second term in the r.h.s. of Eq. (6.16) with the function A independent of η, whereas the third term vanishes identically. If we then reinstate the η-dependence of A in the two non-vanishing terms and differentiate them with respect to η, we obtain the original integrand in Eq. (6.13) plus another term, originating from $A^2(\eta)$. We then obtain the result (6.16) by (formally) integrating the latter term and subtracting it from the previous two.

One can also repeat the above procedure for the new integral in the r.h.s. of Eq. (6.16). To do this, we define

$$\left[A^2(\eta)\right]' \equiv -\frac{1}{\eta}\,B(\eta)\ , \qquad (6.17)$$

and, after several simplifications, we can write the general relation as

$$\begin{aligned}-\int_{\eta_1}^{\eta_2} \ln\left(\frac{A(\eta) - \sqrt{A^2(\eta) - k^2\,\eta^2}}{A(\eta) + \sqrt{A^2(\eta) - k^2\,\eta^2}}\right)\,\frac{[A^2(\eta)]'}{4\,A(\eta)}\,\mathrm{d}\,\eta = & \ Y(\eta)\,\frac{B(\eta)}{8\,A(\eta)}\Big|_{\eta_1}^{\eta_2} \\ & - \int_{\eta_1}^{\eta_2} Y(\eta)\,\left(\frac{B^2(\eta)}{16\,\eta\,A^3(\eta)} + \frac{B'(\eta)}{8\,A(\eta)}\right)\,\mathrm{d}\eta \\ & - \int_{\eta_1}^{\eta_2} \ln\left(\frac{A(\eta) - \sqrt{A^2(\eta) - k^2\,\eta^2}}{A(\eta) + \sqrt{A^2(\eta) - k^2\,\eta^2}}\right)\,\frac{B^2(\eta)}{8\,\eta\,A^3(\eta)}\,\mathrm{d}\eta\ , \qquad (6.18)\end{aligned}$$

with

$$\begin{aligned}Y(\eta) \quad \equiv \quad & \ln\left(\frac{-k\,\eta}{2\,A(\eta)}\right)\,\ln\left(\frac{A(\eta) - \sqrt{A^2(\eta) - k^2\,\eta^2}}{A(\eta) + \sqrt{A^2(\eta) - k^2\,\eta^2}}\right) \\ & + \mathrm{Li}_2\left(\frac{A(\eta) - \sqrt{A^2(\eta) - k^2\,\eta^2}}{2\,A(\eta)}\right) \\ & - \mathrm{Li}_2\left(\frac{A(\eta) + \sqrt{A^2(\eta) - k^2\,\eta^2}}{2\,A(\eta)}\right)\ , \qquad (6.19)\end{aligned}$$

and $\mathrm{Li}_2(z)$ is the dilogarithm function (see, e.g. Ref. [72]),

$$\mathrm{Li}_2(z) \equiv \sum_{k=1}^{\infty} \frac{z^k}{k^2} = -\int_0^z \frac{\ln(1-z')}{z'}\,\mathrm{d}z' \ . \tag{6.20}$$

On putting together all the pieces, we finally obtain

$$\begin{aligned}
\int_{\eta_1}^{\eta_2} \sqrt{A^2(\eta) - k^2\,\eta^2}\,\frac{\mathrm{d}\,\eta}{\eta} \;=\;& \sqrt{A^2(\eta) - k^2\,\eta^2}\Big|_{\eta_1}^{\eta_2} + Y(\eta)\,\frac{B(\eta)}{8\,A(\eta)}\Big|_{\eta_1}^{\eta_2} \\
&+ \frac{A(\eta)}{2}\,\ln\left(\frac{A(\eta) - \sqrt{A^2(\eta) - k^2\,\eta^2}}{A(\eta) + \sqrt{A^2(\eta) - k^2\,\eta^2}}\right)\Bigg|_{\eta_1}^{\eta_2} \\
&- \int_{\eta_1}^{\eta_2} Y(\eta)\,\left(\frac{B^2(\eta)}{16\,\eta\,A^3(\eta)} + \frac{B'(\eta)}{8\,A(\eta)}\right)\,\mathrm{d}\eta \qquad (6.21) \\
&- \int_{\eta_1}^{\eta_2} \ln\left(\frac{A(\eta) - \sqrt{A^2(\eta) - k^2\,\eta^2}}{A(\eta) + \sqrt{A^2(\eta) - k^2\,\eta^2}}\right)\,\frac{B^2(\eta)}{8\,\eta\,A^3(\eta)}\,\mathrm{d}\eta \ .
\end{aligned}$$

For the cases of interest to us [i.e. for the frequencies (6.11)], the functions A for scalar and tensor perturbations to second order in the HFF are given by

$$\begin{aligned}
A_{\mathrm{S}}^2 &= \frac{9}{4} + 3\,\epsilon_1 + \frac{3}{2}\,\epsilon_2 + 4\,\epsilon_1^2 + \frac{13}{2}\,\epsilon_1\,\epsilon_2 + \frac{1}{4}\,\epsilon_2^2 + \frac{1}{2}\,\epsilon_2\,\epsilon_3 \\
A_{\mathrm{T}}^2 &= \frac{9}{4} + 3\,\epsilon_1 + 4\,\epsilon_1^2 + 4\,\epsilon_1\,\epsilon_2 \ ,
\end{aligned} \tag{6.22a}$$

so that

$$B_{\mathrm{S}} = 3\,\epsilon_1\,\epsilon_2 + \frac{3}{2}\,\epsilon_2\,\epsilon_3 \ , \quad B_{\mathrm{T}} = 3\,\epsilon_1\,\epsilon_2 \ . \tag{6.22b}$$

For the results to second order in the HFF, we can neglect the last two integrals in Eq. (6.21), since $B'(\eta) = \mathcal{O}\left(\epsilon_i^3\right)$ and $B^2(\eta) = \mathcal{O}\left(\epsilon_i^4\right)$. Thus our approximation consists in neglecting such terms and not in assuming the HFF be constant (or any specific functional form for them). We can finally write $\xi_{\mathrm{II,S}}(\eta_0, \eta_{\mathrm{f}}; k)$ and $\xi_{\mathrm{II,T}}(\eta_0, \eta_{\mathrm{f}}; k)$ as

$$\begin{aligned}
\xi_{\mathrm{II,S}} \simeq & -\frac{3}{2} + \frac{3\,\ln 3}{2} + \ln 3\,\epsilon_{1,\mathrm{f}} + \frac{\ln 3}{2}\,\epsilon_{2,\mathrm{f}} + \left(\ln 3 + \frac{1}{3}\right)\,\epsilon_{1,\mathrm{f}}^2 + \frac{1}{12}\,\epsilon_{2,\mathrm{f}}^2 \\
& + \left(\frac{11\,\ln 3}{6} - \frac{\ln^2 3}{2} + \frac{\pi^2}{24} + \frac{1}{3}\right)\,\epsilon_{1,\mathrm{f}}\,\epsilon_{2,\mathrm{f}} + \left(\frac{\ln 3}{6} - \frac{\ln^2 3}{4} + \frac{\pi^2}{48}\right)\,\epsilon_{2,\mathrm{f}}\,\epsilon_{3,\mathrm{f}} \\
& + \left[-\frac{3}{2} - \epsilon_{1,\mathrm{f}} - \frac{1}{2}\,\epsilon_{2,\mathrm{f}} - \epsilon_{1,\mathrm{f}}^2 + \left(\ln 3 - \frac{11}{6}\right)\,\epsilon_{1,\mathrm{f}}\,\epsilon_{2,\mathrm{f}} + \left(\frac{\ln 3}{2} - \frac{1}{6}\right)\,\epsilon_{2,\mathrm{f}}\,\epsilon_{3,\mathrm{f}}\right]\,\ln\left(-k\,\eta_{\mathrm{f}}\right) \\
& - \frac{1}{2}\,\left(\epsilon_{1,\mathrm{f}}\,\epsilon_{2,\mathrm{f}} + \frac{1}{2}\,\epsilon_{2,\mathrm{f}}\,\epsilon_{3,\mathrm{f}}\right)\,\ln^2\left(-k\,\eta_{\mathrm{f}}\right)
\end{aligned} \tag{6.23a}$$

$$
\begin{aligned}
\xi_{\mathrm{II,T}} \simeq & -\frac{3}{2}+\frac{3\,\ln 3}{2}+\ln 3\,\epsilon_{1,\mathrm{f}}+\left(\ln 3+\frac{1}{3}\right)\epsilon_{1,\mathrm{f}}^2+\left(\frac{4\,\ln 3}{3}-\frac{\ln^2 3}{2}+\frac{\pi^2}{24}\right)\epsilon_{1,\mathrm{f}}\,\epsilon_{2,\mathrm{f}} \\
& +\left[-\frac{3}{2}-\epsilon_{1,\mathrm{f}}-\epsilon_{1,\mathrm{f}}^2+\left(\ln 3-\frac{4}{3}\right)\epsilon_{1,\mathrm{f}}\,\epsilon_{2,\mathrm{f}}\right]\ln\left(-k\,\eta_{\mathrm{f}}\right) \\
& -\frac{1}{2}\,\epsilon_{1,\mathrm{f}}\,\epsilon_{2,\mathrm{f}}\ln^2\left(-k\,\eta_{\mathrm{f}}\right)\ , \qquad (6.23\mathrm{b})
\end{aligned}
$$

where the arguments in ξ_{II} have been omitted. On inserting the above quantities in Eqs. (6.12), we can calculate the PS.

In order to compare the PS from Eqs. (6.12), (6.23a) and (6.23b), with the slow-roll expressions in Eqs. (6.9a), we need a relation between $H(N_{\mathrm{f}})$ and $H(N_*)$, $\epsilon_1(N_{\mathrm{f}})$ and $\epsilon_1(N_*)$, and so on, to second order in the HFF (hereafter, quantities without a subscript will be evaluated at the Hubble crossing η_* corresponding to the pivot scale k_*). We expand the parameters $\epsilon_{i,\mathrm{f}}$ to first order in $\Delta N \equiv N_f - N_*$ in the numerators and to second order in the denominator of the scalar spectrum,

$$
\frac{\epsilon_i(N_{\mathrm{f}})}{\epsilon_i} \simeq 1+\epsilon_{i+1}\Delta N+\frac{1}{2}\left(\epsilon_{i+1}^2+\epsilon_{i+1}\,\epsilon_{i+2}\right)\Delta N^2\ , \qquad (6.24)
$$

and, analogously, we find

$$
\frac{H^2(N_{\mathrm{f}})}{H^2} \simeq 1-2\,\epsilon_1\,\Delta N-\left(\epsilon_1\,\epsilon_2-2\,\epsilon_1^2\right)\Delta N^2\ . \qquad (6.25)
$$

We can eliminate η_{f} in the logarithms by expressing it in terms of $1/(a\,H)_{\mathrm{f}}$,

$$
\begin{aligned}
\ln(-k\,\eta_{\mathrm{f}}) &\simeq \ln\left[\frac{k\ (1+\epsilon_{1,\mathrm{f}}\,\epsilon_{2,\mathrm{f}})}{(a\,H)_{\mathrm{f}}\ (1-\epsilon_{1,\mathrm{f}})}\,\frac{(a\,H)_*}{(a\,H)_*}\right] \\
&\simeq \ln\left(\frac{k}{k_*}\right)-\Delta N+\epsilon_{1,\mathrm{f}}\,\Delta N+\epsilon_{1,\mathrm{f}} \\
&\simeq \ln\left(\frac{k}{k_*}\right)-\Delta N+\epsilon_1\,\Delta N+\epsilon_1\ , \qquad (6.26)
\end{aligned}
$$

where in the first equality we used Eq. (6.10a), in the second one the definition of the pivot scale, and, in the last relation, Eq. (6.24). If we now use the above expressions we obtain the following PS, where the superscript $^{(2)}$ stands for second slow-roll order and the subscript WKB for leading adiabatic order,

$$\begin{aligned}
\mathcal{P}^{(2)}_{\zeta,\mathrm{WKB}} &= \frac{H^2}{\pi\,\epsilon_1\,m_{\mathrm{Pl}}^2}\,A_{\mathrm{WKB}}\left\{1-2\left(D_{\mathrm{WKB}}+1\right)\,\epsilon_1-D_{\mathrm{WKB}}\,\epsilon_2+\left(\frac{1}{2}\,D_{\mathrm{WKB}}^2+\frac{2}{9}\right)\,\epsilon_2^2\right.\\
&+\left(2\,D_{\mathrm{WKB}}^2+2\,D_{\mathrm{WKB}}-\frac{1}{9}\right)\,\epsilon_1^2+\left(D_{\mathrm{WKB}}^2-D_{\mathrm{WKB}}+\frac{\pi^2}{12}-\frac{20}{9}\right)\,\epsilon_1\,\epsilon_2\\
&+\left(-\frac{1}{2}\,D_{\mathrm{WKB}}^2+\frac{\pi^2}{24}-\frac{1}{18}\right)\,\epsilon_2\,\epsilon_3\\
&+\left[-2\,\epsilon_1-\epsilon_2+2\left(2\,D_{\mathrm{WKB}}+1\right)\,\epsilon_1^2+\left(2\,D_{\mathrm{WKB}}-1\right)\,\epsilon_1\,\epsilon_2\right.\\
&\left.+D_{\mathrm{WKB}}\,\epsilon_2^2-D_{\mathrm{WKB}}\,\epsilon_2\,\epsilon_3\right]\,\ln\left(\frac{k}{k_*}\right)\\
&\left.+\frac{1}{2}\,\left(4\,\epsilon_1^2+2\,\epsilon_1\,\epsilon_2+\epsilon_2^2-\epsilon_2\,\epsilon_3\right)\,\ln^2\left(\frac{k}{k_*}\right)\right\}
\end{aligned} \tag{6.27a}$$

$$\begin{aligned}
\mathcal{P}^{(2)}_{h,\mathrm{WKB}} &= \frac{16\,H^2}{\pi\,m_{\mathrm{Pl}}^2}\,A_{\mathrm{WKB}}\left\{1-2\left(D_{\mathrm{WKB}}+1\right)\,\epsilon_1+\left(2\,D_{\mathrm{WKB}}^2+2\,D_{\mathrm{WKB}}-\frac{1}{9}\right)\,\epsilon_1^2\right.\\
&+\left(-D_{\mathrm{WKB}}^2-2\,D_{\mathrm{WKB}}+\frac{\pi^2}{12}-\frac{19}{9}\right)\,\epsilon_1\,\epsilon_2\\
&+\left[-2\,\epsilon_1+2\left(2\,D_{\mathrm{WKB}}+1\right)\,\epsilon_1^2-2\,\left(D_{\mathrm{WKB}}+1\right)\epsilon_1\,\epsilon_2\right]\,\ln\left(\frac{k}{k_*}\right)\\
&\left.+\frac{1}{2}\,\left(4\,\epsilon_1^2-2\,\epsilon_1\,\epsilon_2\right)\,\ln^2\left(\frac{k}{k_*}\right)\right\}\,.
\end{aligned}$$

In the above, we have defined $D_{\mathrm{WKB}}\equiv\frac{1}{3}-\ln 3\approx-0.7653$, which approximates the coefficient C in Eqs. (6.9a) with an error of about 5%, and the factor $A_{\mathrm{WKB}}\equiv 18/e^3\approx 0.896$ which gives an error of about 10% on the amplitudes. An important result is that the PS to second order in the slow-roll parameters do not depend on ΔN, once the laborious dependence on the Hubble crossing has been worked out: this fact is in complete agreement with the constancy of the growing modes of ζ and h on large scales. The spectral indices, from Eqs. (5.36b), and their runnings, from Eqs. (5.36c), are analogously given by

$$\begin{aligned}
n^{(2)}_{\mathrm{S,WKB}}-1 &= -2\,\epsilon_1-\epsilon_2-2\,\epsilon_1^2-\left(2\,D_{\mathrm{WKB}}+3\right)\,\epsilon_1\,\epsilon_2-D_{\mathrm{WKB}}\,\epsilon_2\,\epsilon_3\\
&\quad -2\,\epsilon_1\,\epsilon_2\,\ln\left(\frac{k}{k_*}\right)-\epsilon_2\,\epsilon_3\,\ln\left(\frac{k}{k_*}\right)
\end{aligned} \tag{6.27b}$$

$$n^{(2)}_{\mathrm{T,WKB}} = -2\,\epsilon_1-2\,\epsilon_1^2-2\,\left(D_{\mathrm{WKB}}+1\right)\,\epsilon_1\,\epsilon_2-2\,\epsilon_1\,\epsilon_2\,\ln\left(\frac{k}{k_*}\right)$$

$$\alpha^{(2)}_{\mathrm{S,WKB}}=-2\,\epsilon_1\,\epsilon_2-\epsilon_2\,\epsilon_3\,,\quad \alpha^{(2)}_{\mathrm{T,WKB}}=-2\,\epsilon_1\,\epsilon_2\,. \tag{6.27c}$$

From Eq. (5.36d) the tensor-to-scalar ratio becomes

$$\begin{aligned}R^{(2)}_{\mathrm{WKB}} &= 16\,\epsilon_1\left[1+D_{\mathrm{WKB}}\,\epsilon_2+\left(D_{\mathrm{WKB}}+\frac{1}{9}\right)\epsilon_1\,\epsilon_2+\left(\frac{1}{2}\,D^2_{\mathrm{WKB}}-\frac{2}{9}\right)\epsilon_2^2\right.\\ &\quad+\left(\frac{1}{2}\,D^2_{\mathrm{WKB}}-\frac{\pi^2}{24}+\frac{1}{18}\right)\epsilon_2\,\epsilon_3\\ &\quad+\left(\epsilon_2+\epsilon_1\,\epsilon_2+D_{\mathrm{WKB}}\,\epsilon_2^2+D_{\mathrm{WKB}}\,\epsilon_2\,\epsilon_3\right)\ln\left(\frac{k}{k_*}\right)\\ &\quad\left.+\frac{1}{2}\left(\epsilon_2^2+\epsilon_2\,\epsilon_3\right)\ln^2\left(\frac{k}{k_*}\right)\right]\ . \end{aligned}\tag{6.27d}$$

We note that Eqs. (6.27a), (6.27b) and (6.27c) agree with Ref. [58], to first order in the HFF.

We can also compare the above results with others as we show in Appendix D. For example, one could approximate the HFF by their Taylor expansions around η_0 as in Ref. [73, 62, 74], and give the results in terms of the ϵ_i's calculated at that point (see Table D.2 for results only on spectral indices).

6.2.2 Improved WKB next-to-leading and first slow-roll order

To first order in the HFF, the function A can be taken as constant. In this case, let us then introduce the more convenient notation

$$\begin{aligned}\xi_\pm(x_0,x;k) &= \pm\int_x^{x_0}\sqrt{\mp\,\omega^2(y)}\,\mathrm{d}\,y\\ &\simeq \pm\int_\eta^{\eta_0}\sqrt{\mp\,(k^2\,\tau^2-A^2)}\,\frac{\mathrm{d}\,\tau}{\tau}\\ &= \pm\,A\left[\mathrm{atan}_\pm\left(\Theta_\pm\right)-\Theta_\pm\right]\ ,\end{aligned}\tag{6.28}$$

where we have used $\mathrm{d}\,x=\mathrm{d}\,\tau/\tau$, and

$$\begin{aligned}A^2_{\mathrm{S}}(\epsilon_i) &= \frac{9}{4}+3\epsilon_1+\frac{3}{2}\,\epsilon_2\\ A^2_{\mathrm{T}}(\epsilon_i) &= \frac{9}{4}+3\epsilon_1\end{aligned}\tag{6.29a}$$

$$k\,\eta_0=-A\ ,\tag{6.29b}$$

with ϵ_1 and ϵ_2 constant as well. It is also useful to define

$$\Theta_\pm\equiv\sqrt{\pm\left(1-\frac{\eta^2}{\eta_0^2}\right)}\tag{6.30a}$$

$$\begin{aligned} \mathrm{atan}_+(x) &\equiv \mathrm{arctanh}(x) \\ \mathrm{atan}_-(x) &\equiv \arctan(x)\ , \end{aligned} \tag{6.30b}$$

where the plus (minus) sign corresponds to region II (I). With this notation, the expressions for $\gamma_{(1)}(\eta)$ and $\phi_{(1)}(\eta)$ in Eqs. (4.25) can be explicitly written as

$$\begin{aligned} \gamma_{\pm(1)}(\eta) &= \frac{1}{A^2}\left\{-\frac{5\mp 3\,\Theta_\pm^2}{24\,\Theta_\pm^4} \pm \frac{5}{72\,\Theta_\pm\,\left[\mathrm{atan}_\pm\left(\Theta_\pm\right)-\Theta_\pm\right]}\right\} \\ \phi_{\pm(1)}(\eta) &= \frac{1}{A^2}\left\{\frac{23}{3150} \pm \frac{505\mp 654\,\Theta_\pm^2+153\,\Theta_\pm^4}{1152\,\Theta_\pm^6}\right. \\ &\left. -\frac{5\,\left[\left(102\mp 90\,\Theta_\pm^2\right)\,\mathrm{atan}_\pm\left(\Theta_\pm\right)-\left(102\mp 157\,\Theta_\pm^2\right)\,\Theta_\pm\right]}{10368\,\Theta_\pm^3\,\left[\mathrm{atan}_\pm\left(\Theta_\pm\right)-\,\Theta_\pm\right]^2}\right\}\ . \end{aligned} \tag{6.31}$$

The limits of interest are then given by

$$\lim_{\eta\to-\infty}\gamma_{-(1)}(\eta) = 0 \tag{6.32a}$$

$$\lim_{\eta\to-\infty}\phi_{-(1)}(\eta) = \frac{23}{3150\,A^2} \tag{6.32b}$$

$$\lim_{\eta\to 0^-}\gamma_{+(1)}(\eta) = -\frac{1}{12\,A^2} \tag{6.32c}$$

$$\lim_{\eta\to 0^-}\phi_{+(1)}(\eta) = \frac{181}{16800\,A^2}\ , \tag{6.32d}$$

where we have used

$$\lim_{\eta\to-\infty}\Theta_-(\eta) = \infty \tag{6.32e}$$

$$\lim_{\eta\to 0^-}\Theta_+(\eta) = 1\ , \tag{6.32f}$$

and

$$\lim_{\eta\to 0^-}\left(\omega_{\mathrm{II}}+\frac{\omega'_{\mathrm{II}}}{2\,\omega_{\mathrm{II}}}\right) = A\ . \tag{6.32g}$$

We can now use the values in Eqs. (6.29a) to calculate the correction $g^{\mathrm{AD}}_{(1)}$ in the super-horizon limit ($\eta\to 0^-$) for scalar and tensor perturbations, obtaining

$$\begin{aligned} g^{\mathrm{AD}}_{(1)\mathrm{S}} &= \frac{37}{324}-\frac{19}{243}\left(\epsilon_1+\frac{1}{2}\,\epsilon_2\right) \\ g^{\mathrm{AD}}_{(1)\mathrm{T}} &= \frac{37}{324}-\frac{19}{243}\,\epsilon_1\ . \end{aligned} \tag{6.33}$$

Finally, from Eqs. (5.36a) and (6.33), we can write the expressions for the scalar and tensor PS, with the superscript $^{(1)}$ for first slow-roll order and the subscript WKB$*$ for next-to-leading adiabatic order, as

$$\mathcal{P}^{(1)}_{\zeta,\mathrm{WKB}*} = \frac{H^2}{\pi\,\epsilon_1\,m^2_{\mathrm{Pl}}}\,A_{\mathrm{WKB}*}\left[1-2\,(D_{\mathrm{WKB}*}+1)\,\epsilon_1 - D_{\mathrm{WKB}*}\,\epsilon_2-(2\,\epsilon_1+\epsilon_2)\,\ln\left(\frac{k}{k_*}\right)\right] \tag{6.34a}$$

$$\mathcal{P}^{(1)}_{h,\mathrm{WKB}*} = \frac{16\,H^2}{\pi\,m^2_{\mathrm{Pl}}}\,A_{\mathrm{WKB}*}\left[1-2\,(D_{\mathrm{WKB}*}+1)\,\epsilon_1-2\,\epsilon_1\,\ln\left(\frac{k}{k_*}\right)\right] ,$$

where $D_{\mathrm{WKB}*}\equiv\frac{7}{19}-\ln 3\approx -0.7302$, which approximates the coefficient C in Eqs. (6.9a) with an error of about 0.08%, and the factor $A_{\mathrm{WKB}*}\equiv 361/18\,e^3\approx 0.999$ which gives an error of about 0.1% on the amplitudes. We also obtain the standard slow-roll spectral indices and α-runnings,

$$n^{(1)}_{\mathrm{S,WKB}*}-1=-2\,\epsilon_1-\epsilon_2\ ,\quad n^{(1)}_{\mathrm{T,WKB}*}=-2\,\epsilon_1 \tag{6.34b}$$

$$\alpha^{(1)}_{\mathrm{S,WKB}*}=\alpha^{(1)}_{\mathrm{T,WKB}*}=0\ , \tag{6.34c}$$

on respectively using Eqs. (5.36b) and (5.36c). From Eq. (5.36d) the tensor-to-scalar ratio becomes

$$R^{(1)}_{\mathrm{WKB}*}=16\,\epsilon_1\left[1+D_{\mathrm{WKB}*}\,\epsilon_2+\epsilon_2\,\ln\left(\frac{k}{k_*}\right)\right]\ . \tag{6.34d}$$

6.2.3 Improved WKB next-to-leading and second slow-roll order

In order to give the results to next-to-leading WKB order and second slow-roll order, we should evaluate the corrections $g^{\mathrm{AD}}_{(1)}$ for scalar and tensor perturbations to second order in the ϵ_i's. This, in turn, would require the computation of the functions $\phi_{\pm(1)}$ and $\gamma_{\pm(1)}$, in Eqs. (4.25), whose analytical calculation is extremely difficult. We shall therefore try to give the expressions for the corrections by following a heuristic (and faster) method.

Let us start from the first order slow-roll expressions given in Eqs. (6.33) and add all possible second order terms in the HFF. Some of such terms can then be (partially) fixed by making reasonable requirements, which will be explained below, so that the corrections to the PS read

$$
\begin{aligned}
1+g^{\mathrm{AD}}_{(1)\mathrm{S}} &= \frac{361}{324}\left\{1-\frac{4}{57}\left(\epsilon_{1,\mathrm{f}}+\frac{1}{2}\,\epsilon_{2,\mathrm{f}}\right)-\frac{8}{361}\,\epsilon^2_{1,\mathrm{f}}+\left[\frac{4}{57}\,(b_{\mathrm{S}}-D_{\mathrm{WKB}*})-\frac{262}{3249}\right]\epsilon_{1,\mathrm{f}}\,\epsilon_{2,\mathrm{f}}\right.\\
&\quad +\frac{13}{1083}\,\epsilon^2_{2,\mathrm{f}}+\left[\frac{2}{57}\,(d_{\mathrm{S}}-D_{\mathrm{WKB}*})-\frac{2}{171}\right]\epsilon_{2,\mathrm{f}}\,\epsilon_{3,\mathrm{f}}\\
&\quad \left.-\left(\frac{4}{57}\,\epsilon_{1,\mathrm{f}}\,\epsilon_{2,\mathrm{f}}+\frac{2}{57}\,\epsilon_{2,\mathrm{f}}\,\epsilon_{3,\mathrm{f}}\right)\ln\left(-k\,\eta_{\mathrm{f}}\right)\right\}\\
1+g^{\mathrm{AD}}_{(1)\mathrm{T}} &= \frac{361}{324}\left\{1-\frac{4}{57}\,\epsilon_{1,\mathrm{f}}-\frac{8}{361}\,\epsilon^2_{1,\mathrm{f}}+\left[\frac{4}{57}\,(b_{\mathrm{T}}-D_{\mathrm{WKB}*})-\frac{16}{171}\right]\epsilon_{1,\mathrm{f}}\,\epsilon_{2,\mathrm{f}}\right.\\
&\quad \left.-\frac{4}{57}\,\epsilon_{1,\mathrm{f}}\,\epsilon_{2,\mathrm{f}}\,\ln\left(-k\,\eta_{\mathrm{f}}\right)\right\}\ .
\end{aligned}
\tag{6.35}
$$

First of all, we have factorized the number 361/324 so as to recover the standard slow-roll amplitudes (6.9a) with a very good accuracy. As already mentioned, the first order terms are the same as those in the results (6.33) of Section 6.2.2, evaluated however in the super-horizon limit. The form of the coefficients multiplying the second order monomials in the HFF have been partially determined by using the expressions given in Section 6.2.2 [Eq. (6.32a)-(6.32g)] with Eqs. (6.22a) replacing Eqs. (6.29a). By this procedure, one expects to obtain results correct up to derivatives of A^2, which can just contain mixed terms to second order. The numerical coefficients in front of $\epsilon^2_{1,\mathrm{f}}$ and $\epsilon^2_{2,\mathrm{f}}$ are thus uniquely determined, whereas the coefficients multiplying the mixed terms $\epsilon_{1,\mathrm{f}}\,\epsilon_{2,\mathrm{f}}$ and $\epsilon_{2,\mathrm{f}}\,\epsilon_{3,\mathrm{f}}$ remain partially ambiguous. The last number in each square bracket arises directly from this procedure, whereas the other terms are chosen so as to match the "standard" dependence on $D_{\mathrm{WKB}*}$ in the PS, with $b_{\mathrm{S,T}}$ and d_{S} left undetermined. Finally, we have also required that the PS do not depend on ΔN, consistently with the constancy in time of the growing modes for h and ζ. This requirement fixes the coefficients in front of the logarithms in Eqs. (6.35) uniquely [2], and leads to spectral indices which do not depend on $b_{\mathrm{S,T}}$ and d_{S}.

Proceeding then as in Section 6.2.1, from the above corrections we obtain the expressions for the scalar and tensor PS,

---

[2] For the same reason (i.e. to avoid the appearance of ΔN), we cannot consider terms such as $\mathcal{O}\left(\epsilon_i^2\right)\ln^2\left(-k\,\eta_{\mathrm{f}}\right)$ in Eqs. (6.35).

$$\begin{aligned}
\mathcal{P}^{(2)}_{\zeta,\mathrm{WKB}*} = {} & \frac{H^2}{\pi\,\epsilon_1\,m_{\mathrm{Pl}}^2}\,A_{\mathrm{WKB}*}\,\left\{1-2\left(D_{\mathrm{WKB}*}+1\right)\,\epsilon_1 - D_{\mathrm{WKB}*}\,\epsilon_2 + \left(\frac{1}{2}\,D^2_{\mathrm{WKB}*}+\frac{253}{1083}\right)\,\epsilon_2^2\right.\\
& +\left(D^2_{\mathrm{WKB}*}-D_{\mathrm{WKB}*}+\frac{\pi^2}{12}+b_{\mathrm{S}}\,\frac{4}{57}-\frac{2384}{1083}\right)\,\epsilon_1\,\epsilon_2\\
& +\left(2\,D^2_{\mathrm{WKB}*}+2\,D_{\mathrm{WKB}*}-\frac{71}{1083}\right)\,\epsilon_1^2+\left(-\frac{1}{2}\,D^2_{\mathrm{WKB}*}+\frac{\pi^2}{24}+d_{\mathrm{S}}\,\frac{2}{57}-\frac{49}{722}\right)\,\epsilon_2\,\epsilon_3\\
& +\left[-2\,\epsilon_1-\epsilon_2+2\left(2\,D_{\mathrm{WKB}*}+1\right)\,\epsilon_1^2+\left(2\,D_{\mathrm{WKB}*}-1\right)\,\epsilon_1\,\epsilon_2\right.\\
& \left.+D_{\mathrm{WKB}*}\,\epsilon_2^2-D_{\mathrm{WKB}*}\,\epsilon_2\,\epsilon_3\right]\,\ln\left(\frac{k}{k_*}\right)\\
& \left.+\frac{1}{2}\,\left(4\,\epsilon_1^2+2\,\epsilon_1\,\epsilon_2+\epsilon_2^2-\epsilon_2\,\epsilon_3\right)\,\ln^2\left(\frac{k}{k_*}\right)\right\}
\end{aligned} \tag{6.36a}$$

$$\begin{aligned}
\mathcal{P}^{(2)}_{h,\mathrm{WKB}*} = {} & \frac{16\,H^2}{\pi\,m_{\mathrm{Pl}}^2}\,A_{\mathrm{WKB}*}\,\left\{1-2\left(D_{\mathrm{WKB}*}+1\right)\,\epsilon_1+\left(2\,D^2_{\mathrm{WKB}*}+2\,D_{\mathrm{WKB}*}-\frac{71}{1083}\right)\,\epsilon_1^2\right.\\
& +\left(-D^2_{\mathrm{WKB}*}-2\,D_{\mathrm{WKB}*}+\frac{\pi^2}{12}+b_{\mathrm{T}}\,\frac{4}{57}-\frac{771}{361}\right)\,\epsilon_1\,\epsilon_2\\
& +\left[-2\,\epsilon_1+2\left(2\,D_{\mathrm{WKB}*}+1\right)\,\epsilon_1^2-2\,\left(D_{\mathrm{WKB}*}+1\right)\epsilon_1\,\epsilon_2\right]\,\ln\left(\frac{k}{k_*}\right)\\
& \left.+\frac{1}{2}\,\left(4\,\epsilon_1^2-2\,\epsilon_1\,\epsilon_2\right)\,\ln^2\left(\frac{k}{k_*}\right)\right\}\ .
\end{aligned}$$

We also obtain the spectral indices (5.36b) and their runnings (5.36c),

$$\begin{aligned}
& n^{(2)}_{\mathrm{S},\mathrm{WKB}*}-1=-2\,\epsilon_1-\epsilon_2-2\,\epsilon_1^2-\left(2\,D_{\mathrm{WKB}*}+3\right)\,\epsilon_1\,\epsilon_2-D_{\mathrm{WKB}*}\,\epsilon_2\,\epsilon_3\\
& -2\,\epsilon_1\,\epsilon_2\ln\left(\frac{k}{k_*}\right)-\epsilon_2\,\epsilon_3\ln\left(\frac{k}{k_*}\right)\\
& n^{(2)}_{\mathrm{T},\mathrm{WKB}*}=-2\,\epsilon_1-2\,\epsilon_1^2-2\,\left(D_{\mathrm{WKB}*}+1\right)\,\epsilon_1\,\epsilon_2-2\,\epsilon_1\,\epsilon_2\ln\left(\frac{k}{k_*}\right)
\end{aligned} \tag{6.36b}$$

$$\alpha^{(2)}_{\mathrm{S},\mathrm{WKB}*}=-2\,\epsilon_1\,\epsilon_2-\epsilon_2\,\epsilon_3\ ,\quad \alpha^{(2)}_{\mathrm{T},\mathrm{WKB}*}=-2\,\epsilon_1\,\epsilon_2\ , \tag{6.36c}$$

and the tensor-to-scalar ratio becomes

$$\begin{aligned}
R^{(2)}_{\mathrm{WKB}*} = {} & 16\,\epsilon_1\left\{1+D_{\mathrm{WKB}*}\,\epsilon_2+\left[D_{\mathrm{WKB}*}+\left(b_{\mathrm{T}}-b_{\mathrm{S}}\right)\,\frac{4}{57}+\frac{71}{1083}\right]\,\epsilon_1\,\epsilon_2\right.\\
& +\left(\frac{1}{2}\,D^2_{\mathrm{WKB}*}-\frac{253}{1083}\right)\,\epsilon_2^2+\left(\frac{1}{2}\,D^2_{\mathrm{WKB}*}-\frac{\pi^2}{24}-d_{\mathrm{S}}\,\frac{2}{57}+\frac{49}{722}\right)\,\epsilon_2\,\epsilon_3\\
& \left.+\left(\epsilon_2+\epsilon_1\,\epsilon_2+D_{\mathrm{WKB}*}\,\epsilon_2^2+D_{\mathrm{WKB}*}\,\epsilon_2\,\epsilon_3\right)\,\ln\left(\frac{k}{k_*}\right)+\frac{1}{2}\,\left(\epsilon_2^2+\epsilon_2\,\epsilon_3\right)\,\ln^2\left(\frac{k}{k_*}\right)\right\}\ .
\end{aligned} \tag{6.36d}$$

Let us end this Section with a few remarks. The undetermined coefficients $b_{\rm S,T}$ and $d_{\rm S}$ still appear in the PS (and their ratio R), but not in the spectral indices and runnings, which are therefore uniquely specified by our (heuristic) procedure. In general, one may expect that the complete adiabatic corrections to second order contain HFF calculated both in the super-horizon limit and at the turning points (zeros) of the frequencies. However, this is not relevant in the present context, since the possible numerical coefficients that would multiply such terms can be eventually re-absorbed in the definitions of $b_{\rm S,T}$ and $d_{\rm S}$. This could only be an issue (in particular for the spectral indices) if we considered third order terms (since it would then become important where the second order terms are evaluated).

6.2.4 MCE and second slow-roll order

We now consider the results (5.45a)-(5.45c) given by the MCE to leading order (denoted by the subscript MCE) and evaluate them to second order in the HFF (labelled by the superscript (2)) for a general inflationary scale factor. A crucial point in our method is the computation of the function ξ defined in Eq. (4.31) which can be found in detail in Section III of Ref. [71]. For the sake of brevity, we shall not reproduce that analysis here but it is important to stress that, in contrast with the GFM and other slow-roll approximations, it does not require *a priori* any expansion in the HFF since Eq. (34) of Ref. [71] is exact and higher order terms are discarded *a fortiori*. From that expression, upon neglecting terms of order higher than two in the HFF, we obtain the power spectra

$$\begin{aligned}
\mathcal{P}^{(2)}_{\zeta,{\rm MCE}} = \frac{H^2}{\pi\epsilon_1 m_{\rm Pl}^2}\Bigg\{ & 1-2\left(C+1\right)\epsilon_1 - C\,\epsilon_2 + \left(2C^2+2C+\frac{\pi^2}{2}-5\right)\epsilon_1^2 + \left(\frac{1}{2}C^2+\frac{\pi^2}{8}-1\right)\epsilon_2^2 \\
& +\left(2\,C^2-2\,C\,D_{\rm MCE}+D^2_{\rm MCE}-C-2\,C\,\ln(2)+2\,D_{\rm MCE}\,\ln(2)+\frac{7\pi^2}{12}-\frac{64}{9}\right)\epsilon_1\,\epsilon_2 \\
& +\left(-C\,D_{\rm MCE}+\frac{1}{2}\,D^2_{\rm MCE}-C\,\ln(2)+D_{\rm MCE}\,\ln(2)+\frac{\pi^2}{24}-\frac{1}{18}\right)\epsilon_2\,\epsilon_3 \\
& +\left[-2\,\epsilon_1-\epsilon_2+2\left(2\,C+1\right)\epsilon_1^2+\left(4\,C-2\,D_{\rm MCE}-1\right)\epsilon_1\,\epsilon_2+C\,\epsilon_2^2-D_{\rm MCE}\,\epsilon_2\,\epsilon_3\right]\ln\left(\frac{k}{k_*}\right) \\
& +\frac{1}{2}\left(4\,\epsilon_1^2+2\,\epsilon_1\,\epsilon_2+\epsilon_2^2-\epsilon_2\,\epsilon_3\right)\ln^2\left(\frac{k}{k_*}\right)\Bigg\}
\end{aligned} \tag{6.37a}$$

$$\begin{aligned}
\mathcal{P}^{(2)}_{h,{\rm MCE}} = \frac{16H^2}{\pi m_{\rm Pl}^2}\Bigg\{ & 1-2\left(C+1\right)\epsilon_1+\left(2C^2+2C+\frac{\pi^2}{2}-5\right)\epsilon_1^2 \\
& +\left(-2CD_{\rm MCE}+D^2_{\rm MCE}-2C-2C\ln(2)+2D_{\rm MCE}\ln(2)+\frac{\pi^2}{12}-\frac{19}{9}\right)\epsilon_1\epsilon_2 \\
& +\left[-2\epsilon_1+2\left(2C+1\right)\epsilon_1^2-2\left(D_{\rm MCE}+1\right)\epsilon_1\epsilon_2\right]\ln\left(\frac{k}{k_*}\right) \\
& +\frac{1}{2}\left(4\epsilon_1^2-2\epsilon_1\epsilon_2\right)\ln^2\left(\frac{k}{k_*}\right)\Bigg\}\ ,
\end{aligned} \tag{6.37b}$$

where $D_{\rm MCE} \equiv \frac{1}{3} - \ln 3 \approx -0.7652$ and $C \equiv \ln 2 + \gamma_{\rm E} - 2 \approx -0.7296$, with $\gamma_{\rm E}$ the Euler-Mascheroni constant. A clarification concerning the $g(x_0)$'s is in order. Since the turning point does not coincide with the horizon crossing where the spectra are evaluated [71], we have used the relation

$$\epsilon_i(x_0) \simeq \epsilon_i - \epsilon_i\,\epsilon_{i+1}\,\ln\left(\frac{3}{2}\right) \ , \tag{6.38}$$

in order to express the $g(x_0)$'s as functions of the crossing time (HFF with no explicit argument are evaluated at the horizon crossing). The spectral indices are given by

$$n^{(2)}_{\rm S,MCE} - 1 = -2\,\epsilon_1 - \epsilon_2 - 2\,\epsilon_1^2 - (2\,D_{\rm MCE} + 3)\;\epsilon_1\,\epsilon_2 - D_{\rm MCE}\,\epsilon_2\,\epsilon_3 \tag{6.39a}$$

$$n^{(2)}_{\rm T,MCE} = -2\,\epsilon_1 - 2\,\epsilon_1^2 - 2\;(D_{\rm MCE} + 1)\;\epsilon_1\,\epsilon_2 \ , \tag{6.39b}$$

and their runnings by

$$\alpha^{(2)}_{\rm S,MCE} = -2\,\epsilon_1\,\epsilon_2 - \epsilon_2\,\epsilon_3 \tag{6.39c}$$

$$\alpha^{(2)}_{\rm T,MCE} = -2\,\epsilon_1\,\epsilon_2 \ . \tag{6.39d}$$

The tensor-to-scalar ratio becomes

$$\begin{aligned} \frac{R^{(2)}_{\rm MCE}}{16\,\epsilon_1} \;&=\; 1 + C\,\epsilon_2 + \left(C - \frac{\pi^2}{2} + 5\right)\epsilon_1\,\epsilon_2 + \left(\frac{1}{2}\,C^2 - \frac{\pi^2}{8} + 1\right)\epsilon_2^2 \\ &\quad + \left(C\,D_{\rm MCE} - \frac{1}{2}\,D^2_{\rm MCE} + C\,\ln(2) - D_{\rm MCE}\,\ln(2) - \frac{\pi^2}{24} + \frac{1}{18}\right)\epsilon_2\,\epsilon_3 \ . \end{aligned} \tag{6.40}$$

The polynomial structure in the HFF of the results agrees with that given by the Green Function Method (GFM) [75, 68] and the WKB approximation [58, 59, 70, 71] (the same polynomial structure is also found for the spectral indices by means of the uniform approximation [74]). Let us also note other aspects of our results: first of all, the factors $g(x_0)$ modify the standard WKB leading order amplitudes [58, 59] so as to reproduce the standard first order slow-roll results; secondly, we found that C and $D_{\rm MCE}$ are "mixed" in the numerical factors in front of second order terms (we recall that $D_{\rm MCE}$ differs from C by about 5 %); further, $D_{\rm MCE} = D_{\rm WKB}$ of Refs. [58, 59, 70, 71]. The runnings $\alpha_{\rm S}$ and $\alpha_{\rm T}$ are predicted to be $\mathcal{O}(\epsilon^2)$ [76], and in agreement with those obtained by the GFM [75, 68].

6.2.5 Second slow-roll order MCE and WKB versus GFM

We shall now compare the slow-roll results obtained from the MCE and other methods of approximation previously employed [71] with those obtained using the GFM in the slow-roll expansion.We use the GFM just as a reference for the purpose of comparing the other methods among each other and of illustrating deviations from pure slow-roll results. For a given inflationary "observable" Y evaluated with the method X, we denote the percentage difference with respect to its value given by the GFM as

$$\Delta Y_{\rm X} \equiv 100\,\left|\frac{Y_{\rm X} - Y_{\rm GFM}}{Y_{\rm GFM}}\right|\% \ , \tag{6.41}$$

where X = WKB stands for the first WKB and second slow-roll orders [70], X = WKB$*$ for the second WKB and second slow-roll orders [71] and, of course X = MCE for the result obtained in this paper. Note that for the case X = WKB$*$ we shall set the three undetermined parameters $b_{\mathrm{S}} = b_{\mathrm{T}} = d_{\mathrm{S}} = 2$ in order to minimize the difference with respect to the results of the GFM (see Appendix E and Ref. [71]). In Fig. 6.6 we show,

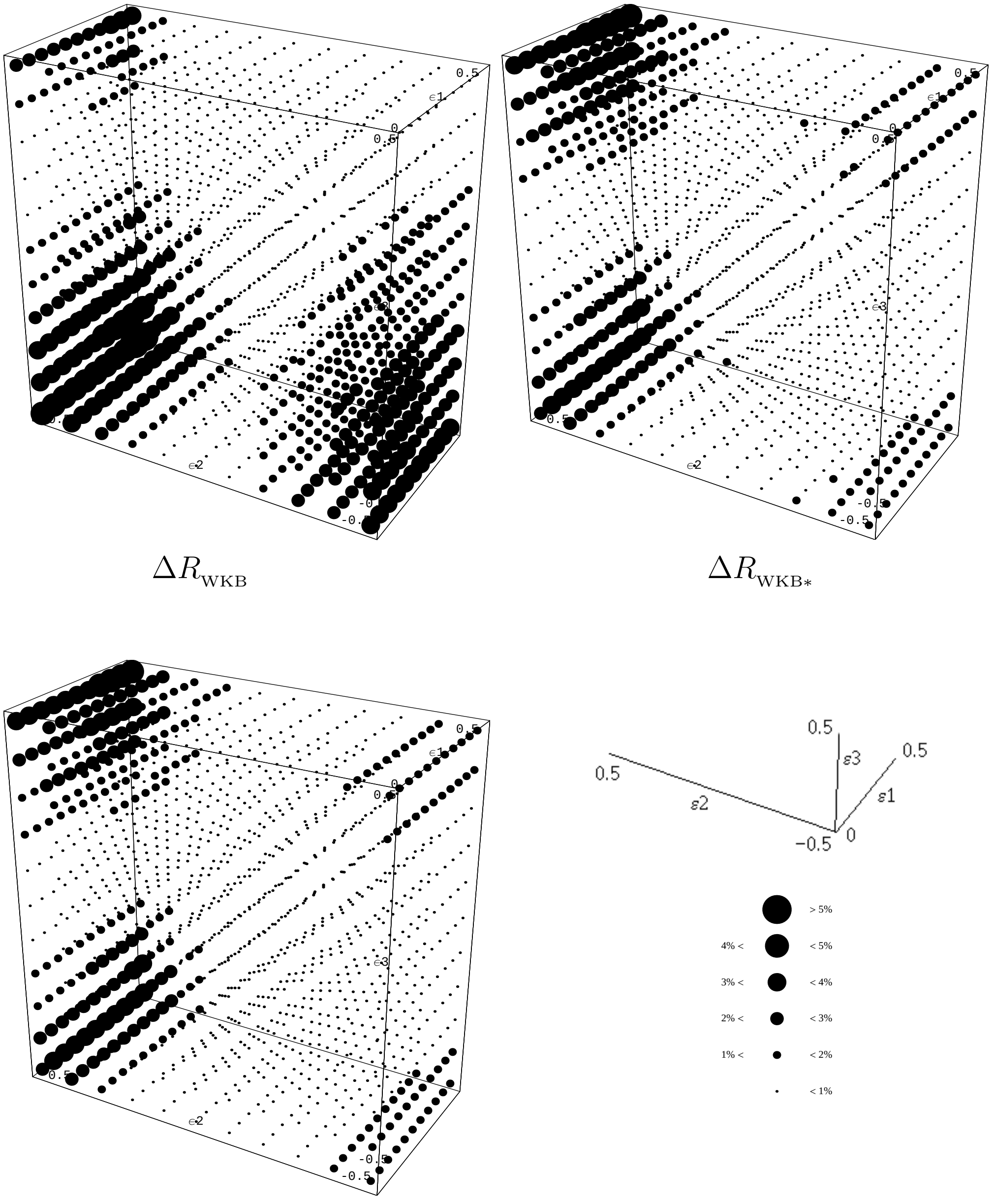

ΔR_{WKB} $\Delta R_{\mathrm{WKB}*}$

ΔR_{MCE}

Figure 6.6: Percentage differences (6.41) between scalar-to-tensor ratios given by the GFM and those obtained from the WKB, WKB$*$ and MCE.

with dots of variable size, the percentage differences (6.41) for the scalar-to-tensor ratios

R at the pivot scale $k = k_*$ for $0 < \epsilon_1 < 0.5$, $|\epsilon_2|$ and $|\epsilon_3| < 0.5$. From the plots it appears that the level of accuracy of the MCE is comparable to that of the WKB$*$ and both are (almost everywhere) more accurate than the WKB. However, the MCE achieves such a precision at leading order and is thus significantly more effective than the WKB$*$. In Fig. 6.7 we show the difference in $n_{\rm S}$ and the relative difference in $P_\zeta(k_*)$ between the MCE and GFM.

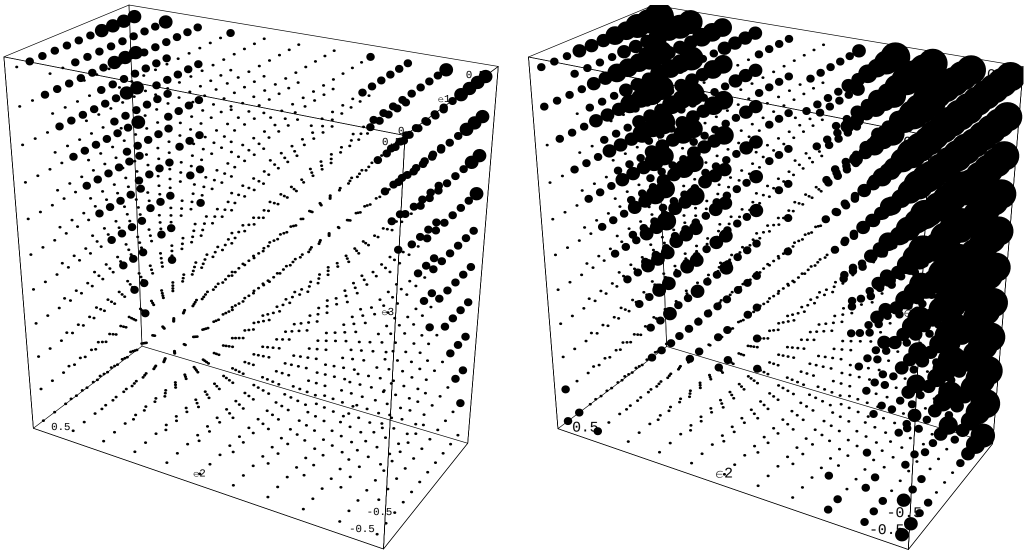

$|n_{\rm S\,MCE} - n_{\rm S\,GFM}| \times 100$ $\Delta P_{\zeta\,\rm MCE}(k_*)$

Figure 6.7: Left box: absolute difference between scalar spectral indeces $n_{\rm S}$ evaluated with the MCE and GFM (rescaled by a factor of 100 for convenience). Note that relevant differences of order 0.05 (shown as 5) occur at the boundaries of the intervals considered for the ϵ_i's. Right box: percentage difference (6.41) for the amplitudes of scalar perturbations P_ζ at the pivot scale $k = k_*$ between the MCE and GFM. See Fig. 6.6 for the meaning of dot size.

In Fig. 6.8 we finally plot the relative difference in $P_\zeta(k_*)$ for $\epsilon_2 = -2\,\epsilon_1$ (the scale invariant case to first order in slow-roll parameters).

6.2.6 GFM and slow-roll approximation

Let us further compare our results with those obtained by the GFM. As we stated before, the most general result of the present work is given by the expressions for the power spectra (5.45a) and (5.45b) with the corrections (5.45c). In fact, the spectral indices and their runnings are the same as found with the standard WKB leading order [58, 71]. On the other hand, the main results of the GFM are the expressions for power spectra, spectral indices and runnings "… in the slow-roll expansion." that is, for small HFF (see, e.g., Eqs. (41) and (43) in Ref. [75]). Here, and in some previous work [58, 59], we instead obtain results which hold for a general inflationary context, independently of

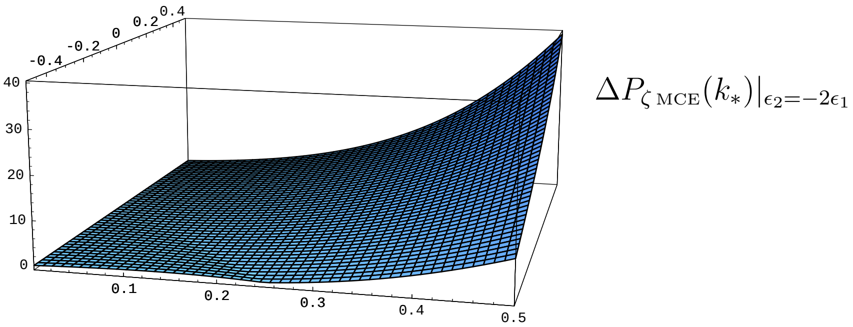

Figure 6.8: Percentage difference (6.41) between the MCE and the GFM for $P_\zeta(k_*)$ restricted on the hypersurface $\epsilon_2 = -2\,\epsilon_1$, which corresponds to a scale-invariant spectrum to first order in the slow-roll expansion. The graph is given for $0 < \epsilon_1 < 0.5$ and $-0.5 < \epsilon_3 < 0.5$.

the "slow-roll conditions" [3] or "slow-roll approximation" [4]. The slow-roll case is just a possible application of our general expressions which can be evaluated for any model by simply specifying the scale factor. Our general, and non-local, expressions in fact take into account all the "history" of the HFF during inflation. For example, we note that the MCE at leading order reproduces the exact result for power-law inflation (see Sec. 6.1), whereas the GFM reproduces those to the next-to-leading order [75].

Chaotic inflation [77] is another example for which a Taylor approximation of the HFF (such as the one required by the GFM [75] or our Green's function perturbative expansion in Appendix F) may lead to inaccurate results. We consider a quadratic potential

$$V(\phi) = \frac{1}{2}\, m^2\, \phi^2 \ , \tag{6.42}$$

where m is the mass of the inflaton ϕ. In a spatially flat Robertson-Walker background, the potential energy dominates during the slow-rollover and the Friedman equation becomes

$$H^2 = \frac{4\,\pi}{3\,m_{\rm Pl}^2}\,\left[\dot\phi^2 + m^2\,\phi^2\right] \simeq \frac{4\,\pi\,m^2\,\phi^2}{3\,m_{\rm Pl}^2} \ . \tag{6.43}$$

The Hubble parameter evolves as

$$\dot H = -\frac{4\,\pi}{m_{\rm Pl}^2}\,\dot\phi^2 \ . \tag{6.44}$$

On using the equation of motion for the scalar field

$$\ddot\phi + 3\,H\,\dot\phi + m^2\,\phi = 0 \ , \tag{6.45}$$

---

[3] Our approximation method does not require small HFF.

[4] We expand instead according to the scheme given in Ref. [71].

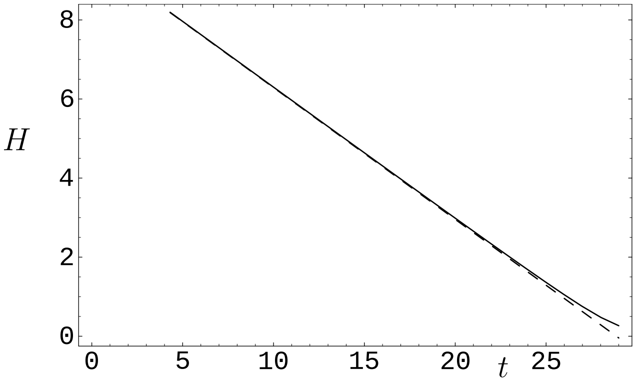

Figure 6.9: Numerical evolution of H (solid line) and its analytic approximation (dashed line). The initial condition corresponds to $H_i \approx 8.2\, m$ (time in units of $1/m$) when the inflaton starts in the slow-roll regime with a value $4\, m_{\rm Pl}$.

and neglecting the second derivative with respect to the cosmic time, we have $3\, H\, \dot{\phi} \simeq -\, m^2\, \phi$. Eq. (6.44) then yields

$$\dot{H} \simeq -\frac{m^2}{3} \equiv \dot{H}_0 \ , \tag{6.46}$$

which leads to a linearly decreasing Hubble parameter and, correspondingly, to an evolution for the scale factor which is not exponentially linear in time, i.e.

$$H(t) \simeq H_0 + \dot{H}_0\, t \ , \tag{6.47a}$$

$$a(t) \simeq a(0)\, \exp\left(H_0\, t + \dot{H}_0\, \frac{t^2}{2}\right) \equiv a(0)\, \exp\left[N(t)\right] \ . \tag{6.47b}$$

In Fig. 6.9 the analytic approximation (6.47a) is shown to be very good on comparing with the exact (numerical) evolution. We are interested in the HFF in the slow-roll regime. From the definitions (3.65) we then have

$$\epsilon_1(t) = -\frac{\dot{H}_0}{\left(H_0 + \dot{H}_0\, t\right)^2} \tag{6.48a}$$

$$\epsilon_n(t) = -\frac{2\, \dot{H}_0}{\left(H_0 + \dot{H}_0\, t\right)^2} = 2\, \epsilon_1(t) \ , \quad n \geq 2 \ , \tag{6.48b}$$

which we plot in Fig. 6.10.

Let us take the end of inflation at $t_{\rm end} \simeq 24/m$ (so that the analytic approximation (6.47a), (6.47b) is very good till the end), corresponding to $N_{\rm end} = 125$ e-folds. We then consider the modes that leave the horizon 60 e-folds before the end of inflation and take that time ($t = t_* \simeq 8/m$ or $N_* = 125 - 60 = 65$) as the starting point for a Taylor

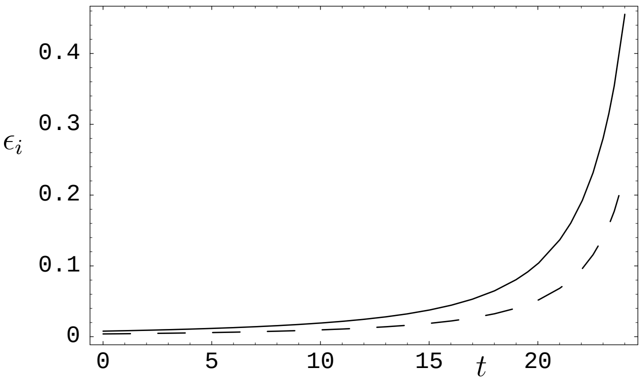

Figure 6.10: HFF in the slow-roll regime: the dashed line is ϵ_1 and the solid line is all the ϵ_n's with $n \geq 2$ (time in units of $1/m$).

expansion to approximate the HFF [5],

$$\epsilon_i\left(\Delta N\right) \simeq \epsilon_i + \epsilon_i\,\epsilon_{i+1}\,\Delta N + \frac{1}{2}\,\epsilon_i\,\left(\epsilon_{i+1}^2 + \epsilon_{i+1}\,\epsilon_{i+2}\right)\,\Delta N^2 \,, \tag{6.49}$$

where the ϵ_i's in the r.h.s. are all evaluated at the time t_* and $\Delta N = N - N_*$. The percentage error with respect to the analytic expressions (6.48a) and (6.48b) ,

$$\delta_i \equiv 100\left|\frac{\epsilon_i(t) - \epsilon_i\left(\Delta N\right)}{\epsilon_i(t)}\right|\% \,, \tag{6.50}$$

with $\Delta N = N(t) - N_*$ is then plotted in Fig. 6.11 for $i = 1$. It obviously becomes large rather quickly away from $t = t_*$ and we can immediately conclude that, had we used a Taylor expansion to approximate the HFF over the whole range of chaotic inflation

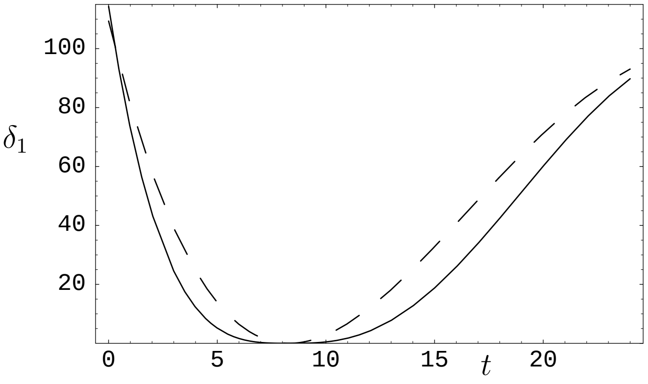

Figure 6.11: Percentage error for ϵ_1 to first and second order in ΔN (dashed and solid line respectively; time in units of $1/m$).

---

[5] One can of course conceive diverse expansions, e.g. using other variables instead of N, however the conclusion would not change as long as equivalent orders are compared.

($-65 < \Delta N < 60$), we would have obtained large errors from the regions both near the beginning and the end of inflation.

In general, we expect that the Taylor expansion of the HFF will lead to a poor determination of the numerical coefficients (depending on C in Eqs. (6.37a) and (6.37b)) in the second slow-roll order terms for those models in which the HFF vary significantly in time. In fact, we can calculate the integral of Eq. (21) in Ref. [75] with ϵ_1 instead of the complete $g(\ln x)$ and $y_0(u)$ instead of $y(u)$. The percentage difference between this integral calculated using the Taylor expansion (6.49) with respect to the same integral calculated with ϵ_1 in Eqs. (6.48a) and (6.48b) is 92 % and 88 % to first and second orders in ΔN, respectively. The MCE method does not require such an expansion and does therefore not suffer from this restriction.

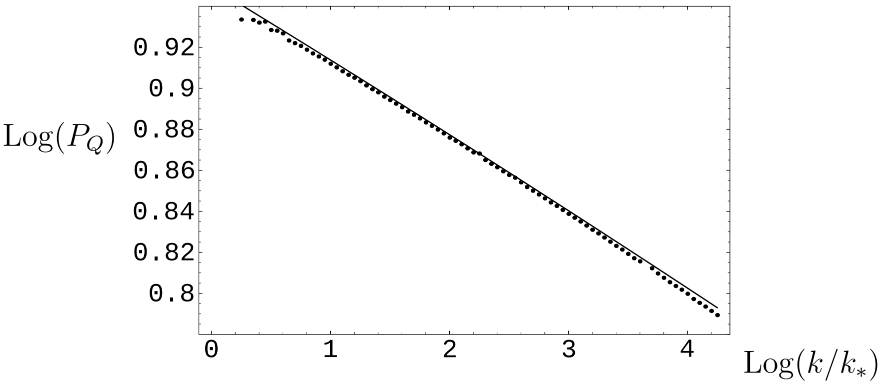

Figure 6.12: Spectrum of the Mukhanov variable Q ($P_Q = k^3\,|Q_k|^2/(2\,\pi^2)$) evaluated at the end of inflation for the chaotic model of Eq. (6.42). The dots represent the numerical values and the solid line the analytic fit based on Eqs. (6.39a) and (6.39c) obtained by the second slow-roll order MCE approximation. The first order and GFM analytic results are not shown since they are almost indistinguishable from the MCE result plotted. k_* crosses the Hubble radius at $\phi_* \simeq 3\,m_{\rm Pl}$ (the lines are normalized at $10^{2.25}\,k_*$).

We have also compared our analytic MCE results in Eqs. (6.39a) and (6.39c) with the numerical evaluation of the spectrum for scalar perturbations. In particular, we have evolved in cosmic time the modulus of the Mukhanov variable Q (recalling that $P_\zeta = k^3\,|Q_k|^2/(2\,\pi^2)$), which satisfies the associated non-linear Pinney equation [78]. The initial conditions for the numerical evolution are fixed for wave-lengths well within the Hubble radius and correspond to the adiabatic vacuum, i.e. $|Q_k(t_i)| = 1/(a(t_i)\,\sqrt{k})$ and $|\dot{Q}_k|(t_i) = -H(t_i)\,|Q_k(t_i)|$ [79]. The agreement of the analytic MCE approximation with the numerical results is good, as shown in Fig. 6.12.

6.2.7 Beyond slow-roll

The slow-roll approximation is quite accurate for a wide class of potentials. However, violations of the slow-roll approximation may occur during inflation, leading to interesting observational effects in the power spectra of cosmological perturbations. An archetypical model to study such violations is given by the potential

$$V(\phi) = V_0 \left[1 - \frac{2}{\pi} \arctan\left(N \frac{\phi}{m_{\rm Pl}} \right) \right] , \tag{6.51}$$

introduced with $N = 5$ in Ref. [61]. In Fig. 6.13 we show that the MCE result expanded to second slow-roll order provides a very good fit for the power spectrum of scalar perturbations even in situations where the slow-roll parameters are not very small (see Fig. 6.14). This example also shows that second slow-roll order results are much better than first order ones (analogous results were also obtained with the GFM in Ref. [68]).

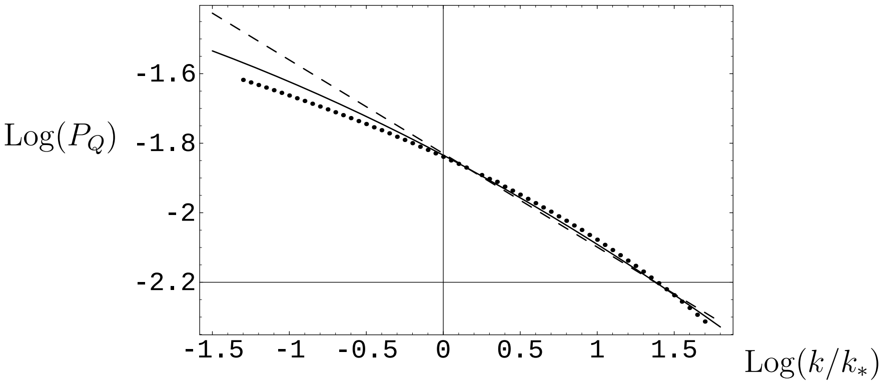

Figure 6.13: Spectrum of the Mukhanov variable Q ($P_Q = k^3\,|Q_k|^2/(2\,\pi^2)$) for the arctan model of Eq. (6.51). The dots represent the numerical values, the solid line the analytic results from Eqs. (6.39a) and (6.39c) obtained by the second slow-roll order MCE approximation and the dashed line those given by the first order slow-roll approximation. k_* crosses the Hubble radius at $\phi_* \simeq -0.3\,m_{\rm Pl}$ (the lines are normalized at $10^{3/20}k_*$) and the spectrum is evaluated at $\simeq 55$ e-folds afterwards.

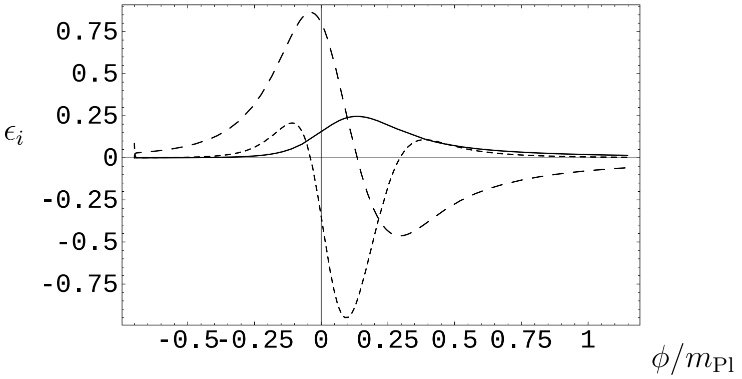

Figure 6.14: Evolution of ϵ_i with the value of the inflaton ϕ (in units of $m_{\rm Pl}$) in the arctan model: ϵ_1 (solid line), ϵ_2 (long-dashed line) and $\dot{\epsilon}_2/H = \epsilon_2\,\epsilon_3$ (short-dashed line).

Conclusions

In this thesis, we have developed some approximations of the WKB type for the purpose of estimating the spectra of cosmological perturbations during inflation. In particular, in Section 5.2 we found general formulae for the amplitudes, spectral indices and α-runnings of the fluctuations to next-to-leading order both in the adiabatic expansion of Ref. [37] and a new perturbative expansion which makes use of the Green's function technique. The most sophisticated Method of Comparison Equations was introduced in Section 4.4 and then applied to cosmological perturbations in Section 5.3. By construction (i.e. by choosing a suitable comparison function), this approach leads to the exact solutions for inflationary models with constant horizon flow functions ϵ_i's (e.g. power-law inflation). The main result is that, on using this approach to leading order, we were able to obtain the general expressions (5.45a)-(5.45c) for the inflationary power spectra which are more accurate than those any other method in the literature can produce at the corresponding order. In fact, the MCE leads to the correct asymptotic behaviours (whereas the standard slow-roll approximation fails [67]) and solves the problems in computing the amplitudes which were encountered with both the standard and improved WKB method analised in Sections 5.1 and 5.2.

In Section 6.1, we have applied our methods to power-law inflation in order to test it against exact results. It is known that the spectral indices and their runnings are obtained exactly at leading order in the WKB approximation, hence we focussed on the spectra to next-to-leading order. For the improved WKB method, we have found that the perturbative corrections remain too small to yield any significant improvement, whereas the adiabatic expansion to next-to-leading order reproduces the exact amplitudes with great accuracy (see Ref. [62] for a similar result with the uniform approximation). This result does not however mean that the perturbative expansion will not lead to significant corrections in different inflationary scenarios. One way of understanding the difference between the two expansions in the power-law case may be the following. It is known that the Born approximation in quantum mechanics (analogous to our perturbative method with the Green's function) is good for high multipoles (angular momenta) ℓ of the expansion in spherical harmonics. In our approach, the parameter β plays the role of the multipole index ℓ for the energy levels of the hydrogen atom, as can be seen on comparing the frequency (6.2) with the expression given in Ref. [37] (see also Ref. [58]). The approximation with the Green's function is therefore expected to yield more significant corrections for large values of $|\beta|$, which coincide with the regime of fast-roll. Indeed, the leading order becomes more and more accurate for increasing $|\beta|$. Since the interesting regime for inflation involves small values of $\beta \sim -2$, it is instead the adiabatic approximation which seems better since the horizon flow functions evolve slowly and/or the states are quasi-classical [6]. This may be the reason whereby the adiabatic approximation works better at the next-to-leading order. However, in more general cases, either or both methods may contribute significant corrections. In this respect, let us remark that the adiabatic expansion can be straightforwardly applied only for a linear turning point [7], whereas the perturbative Green's function method is not so restricted.

In Section 6.2, we have shown that the improved WKB treatment of cosmological perturbations agrees with the standard slow-roll approximation [67] to within 0.1 %, finally resolving the issue of a 10 % error in the prediction of the amplitudes to lowest order which was raised in Ref. [58]. The next issues are the inflationary predictions to second order in the slow-roll parameters. After the results on the running of the power spectra [76], second order results have been obtained using the Green's function method with the massless solution in a de Sitter space-time [75, 68]. Here we have employed the leading WKB approximation to obtain the scalar and tensor power spectra to second order in the slow-roll parameters. The key technical point is to use Eq. (6.21), which allows one to express the power spectra on large scales as a function of the quantities evaluated at the Hubble crossing, but with no explicit dependence on ΔN. As one of our main results, we find that the polynomial structure of the power spectra in the ϵ_i's obtained from the WKB method agrees with the one arising from the Green's function approach of Refs. [75, 68]. In Section 6.2.3 we employ the next-to-leading WKB approximation to second order in the ϵ_i's and, by requiring that the power spectra do not explicitly depend on ΔN (a property which instead was derived both in Sections 6.2.1 and 6.2.2), and using the expressions found in Section 6.2.2, we obtain unique expressions for the spectral indices and runnings. Our findings show that different ways of approximating cosmological perturbations show up at the leading order in the amplitude, but in the next-to-leading order in the derivatives of the power-spectra with respect to wave number k. The accuracy in the theoretical predictions on spectral indices to second order in the slow-roll parameters, evaluated at $k = k_*$, is now striking: the Green's function method yields a coefficient $C \simeq -0.7296$ which is replaced by $D_{\mathrm{WKB}*} \simeq -0.7302$ in the improved WKB method, leading to a precision of 1 part on 1000 in the predictions of the coefficients of $\mathcal{O}(\epsilon_i^2)$ terms in the spectral indexes.

In Section 6.2.3, starting from the general results (5.45a)-(5.45c), we have also computed the full analytic expressions for the inflationary power spectra to second slow-roll order in Eqs. (6.37a) and (6.37b) and found that the dependence on the horizon flow functions ϵ_i's is in agreement with that obtained by different schemes of approximation, such as the GFM [75] and the improved WKB approximation (see Sections 6.1 and 6.2). Moreover, the results obtained with the MCE do not contain undetermined coefficients, in contrast with the second slow-roll order results obtained with the WKB∗. Let us conclude by remarking that, just like the WKB approach, the MCE does not require any particular constraints on the functions ϵ_i's and therefore has a wider range of applicability than any method which assumes them to be small. As an example, we have discussed in some detail the accuracy of the MCE for the massive chaotic and arctan inflationary models. We have shown that the MCE leads to accurate predictions even for a model which violates the slow-roll approximation during inflation.

---

[6] Cosmological perturbations are amplified by inflation evolving from vacuum to highly squeezed states, which resemble classical states in the amplitude of fluctuations [80].

[7] The same limitation seems to affect the method used in Ref. [62].

In Appendix G we have also applied the Method of Comparison Equations to a different problem, namely the scalar field dynamics on the Schwarzschild background. We have considered modes with energy lower than the peak of the effective potential in the corresponding wave equation, so that there are two zeros (turning points). The comparison function has then been chosen of the Morse form with an argument which we have estimated analytically as well. This procedure was shown to be able to produced a fully analytical approximation of the wave-functions with good accuracy over the whole domain outside the Schwarzschild horizon.

Appendix A

First Order Fluctuations

We shall here summarise some technical aspects concerning the scalar, vector and tensor fluctuations of the geometry. As in the main text, we will assume a conformally flat (i.e., $\kappa = 0$) background metric of FRW type.

First off, the fluctuations of the Christoffel connections can be written to first order in the amplitude of the metric fluctuations as

$$\begin{aligned} \delta\,\Gamma^{\mu}_{\alpha\beta} &= \frac{1}{2}\,{}^{(0)}g^{\mu\nu}\,\left(\partial_{\beta}\,\delta\,g_{\nu\alpha} + \partial_{\alpha}\,\delta\,g_{\beta\nu} - \partial_{\nu}\,\delta\,g_{\alpha\beta}\right) \\ &\quad + \frac{1}{2}\,\delta\,g^{\mu\nu}\,\left(\partial_{\beta}\,{}^{(0)}g_{\nu\alpha} + \partial_{\alpha}\,{}^{(0)}g_{\beta\nu} - \partial_{\nu}\,{}^{(0)}g_{\alpha\beta}\right)\ , \end{aligned} \tag{A.1}$$

where ${}^{(0)}$ denotes quantities evaluated for the background geometry and the usual convention of summation over repeated indices is adopted. Analogously, the first-order fluctuation of the Ricci tensor is given by

$$\begin{aligned} \delta\,R_{\mu\nu} &= \partial_{\alpha}\,\delta\,\Gamma^{\alpha}_{\mu\nu} - \partial_{\nu}\,\delta\Gamma^{\beta}_{\mu\beta} \\ &\quad + \delta\,\Gamma^{\alpha}_{\mu\nu}\,{}^{(0)}\Gamma^{\beta}_{\alpha\beta} +^{(0)}\Gamma^{\alpha}_{\mu\nu}\,\delta\,\Gamma^{\beta}_{\alpha\beta} - \delta\,\Gamma^{\beta}_{\alpha\mu}\,{}^{(0)}\Gamma^{\alpha}_{\beta\nu} -^{(0)}\Gamma^{\beta}_{\alpha\mu}\,\delta\,\Gamma^{\alpha}_{\beta\nu}\ , \end{aligned} \tag{A.2}$$

which leads to

$$\delta\,R^{\nu}_{\mu} = \delta\,g^{\nu\alpha}\,{}^{(0)}R_{\alpha\mu} +^{(0)} g^{\nu\alpha}\,\delta R_{\alpha\mu} \tag{A.3}$$

$$\delta\,R = \delta\,g^{\alpha\beta}\,{}^{(0)}R_{\alpha\beta} +^{(0)} g^{\alpha\beta}\,\delta R_{\alpha\beta}\ . \tag{A.4}$$

Finally, the fluctuations of the Einstein tensor

$$\delta\,G^{\nu}_{\mu} = \delta\,R^{\nu}_{\mu} - \frac{1}{2}\,\delta^{\nu}_{\mu}\,\delta\,R\ , \tag{A.5}$$

can be easily obtained from Eqs. (A.3) and (A.4) and the perturbation of the covariant conservation equation is

$$\partial_{\mu}\,\delta T^{\mu\nu} +^{(0)}\Gamma^{\mu}_{\mu\alpha}\,\delta\,T^{\alpha\nu} + \delta\,\Gamma^{\mu}_{\mu\alpha}\,{}^{(0)}T^{\alpha\nu} +^{(0)}\Gamma^{\nu}_{\alpha\beta}\,\delta\,T^{\alpha\beta} + \delta\,\Gamma^{\nu}_{\alpha\beta}\,{}^{(0)}T^{\alpha\beta} = 0\ . \tag{A.6}$$

The Christoffel connections of the flat FRW background are explicitly given by

$$ {}^{(0)}\Gamma^0_{00} = \mathcal{H} \ , \quad {}^{(0)}\Gamma^0_{ij} = \mathcal{H}\,\delta_{ij} \ , \quad {}^{(0)}\Gamma^j_{0i} = \mathcal{H}\,\delta^j_i \tag{A.7} $$

while the components of the Ricci tensor and scalar are

$$ \begin{aligned} &{}^{(0)}R_{00} = -3\,\mathcal{H}' \ , && {}^{(0)}R^0_0 = -\frac{3}{a^2}\,\mathcal{H}' \\ &{}^{(0)}R_{ij} = \left(\mathcal{H}' + 2\,\mathcal{H}^2\right)\,\delta_{ij} \ , && {}^{(0)}R^j_i = -\frac{1}{a^2}\left(\mathcal{H}' + 2\,\mathcal{H}^2\right)\,\delta^j_i \\ &{}^{(0)}R = -\frac{6}{a^2}\left(\mathcal{H}^2 + \mathcal{H}'\right) \ . && \end{aligned} \tag{A.8} $$

A.1 Scalar modes

The scalar fluctuations of the geometry can be written to first-order as

$$ \begin{aligned} &\delta_{\rm s}\, g_{00} = 2\,a^2\,\phi \ , && \delta_{\rm s}\, g^{00} = -\frac{2}{a^2}\,\phi \\ &\delta_{\rm s}\, g_{ij} = 2\,a^2\,\left(\psi\,\delta_{ij} - \partial_i\,\partial_j\,E\right) \ , && \delta_{\rm s}\, g^{ij} = -\frac{2}{a^2}\,\left(\psi\,\delta^{ij} - \partial^i\,\partial^j\,E\right) \\ &\delta_{\rm s}\, g_{0i} = -a^2\,\partial_i\,B \ , && \delta_{\rm s}\, g^{0i} = -\frac{1}{a^2}\,\partial^i\,B \ . \end{aligned} \tag{A.9} $$

Inserting Eqs. (A.9) into Eq. (A.1), the first-order components of the (scalar) Christoffel fluctuations can now be easily computed

$$ \begin{aligned} &\delta_{\rm s}\,\Gamma^0_{00} = \phi' \\ &\delta_{\rm s}\,\Gamma^0_{ij} = -\left[\psi' + 2\,\mathcal{H}\,(\phi+\psi)\right]\,\delta_{ij} + \partial_i\,\partial_j\,\left(E' + 2\,\mathcal{H}\,E - B\right) \\ &\delta_{\rm s}\,\Gamma^0_{i0} = \delta_{\rm s}\,\Gamma^0_{0i} = \partial_i\,\left(\phi + \mathcal{H}\,B\right) \\ &\delta_{\rm s}\,\Gamma^i_{00} = \partial^i\,\left(\phi + B' + \mathcal{H}\,B\right) \\ &\delta_{\rm s}\,\Gamma^k_{ij} = \partial^k\,\psi\,\delta_{ij} - \partial_i\,\psi\,\delta^k_j - \partial_j\,\psi\,\delta^k_i + \partial_i\,\partial_j\,\partial^k\,E - \mathcal{H}\,\partial^k\,B\,\delta_{ij} \\ &\delta_{\rm s}\,\Gamma^j_{0i} = -\psi'\,\delta^j_i + \partial_i\,\partial^j\,E' \ . \end{aligned} \tag{A.10} $$

The first-order fluctuations of the Ricci tensors are

$$ \begin{aligned} \delta_{\rm s}\,R_{00} &= \nabla^2\,\left[\phi + (B-E')' + \mathcal{H}\,(B-E')\right] + 3\left[\psi'' + \mathcal{H}\,(\phi'+\psi')\right] \\ \delta_{\rm s}\,R_{0i} &= \partial_i\,\left[\left(\mathcal{H}' + 2\mathcal{H}^2\right)B + 2\left(\psi' + \mathcal{H}\,\phi\right)\right] \qquad\qquad (A.11) \\ \delta_{\rm s}\,R_{ij} &= -\delta_{ij}\,\left[\psi'' + 2\left(\mathcal{H}' + 2\,\mathcal{H}^2\right)\,(\psi+\phi) + \mathcal{H}\,(\phi' + 5\psi') - \nabla^2\,\psi\right. \\ &\qquad \left. + \mathcal{H}\,\nabla^2\,(B-E')\right] \\ &\quad +\partial_i\,\partial_j\,\left[(E'-B)' + 2\left(\mathcal{H}' + 2\,\mathcal{H}^2\right)\,E + 2\,\mathcal{H}\,(E'-B) + \psi - \phi\right] \ , \end{aligned} $$

while the first-order fluctuation of the Ricci scalar is

$$ \begin{aligned} \delta_{\rm s}\,R &= \frac{2}{a^2}\,\left\{3\,\psi'' + 6\,\left(\mathcal{H}' + \mathcal{H}^2\right)\,\phi + 3\,\mathcal{H}\,(\phi' + 3\,\psi')\right. \\ &\qquad \left. + \nabla^2\,\left[\phi - 2\psi + (B-E')' + 3\,\mathcal{H}\,(B-E')\right]\right\} \ . \end{aligned} \tag{A.12} $$

Using Eqs. (A.11) into Eqs. (A.3) and (A.4) the fluctuations of the Ricci tensor will be

$$\begin{aligned}
\delta_{\rm s}\, R_0^0 &= \frac{1}{a^2}\left\{\nabla^2\left[\phi + (B-E')' + \mathcal{H}\,(B-E')\right] + 3\left[\psi'' + \mathcal{H}\,(\phi' + \psi') + 2\,\mathcal{H}'\phi\right]\right\} \\
\delta_{\rm s}\, R_i^j &= \frac{\delta_i^j}{a^2}\,\left[\psi'' + 2\,\left(\mathcal{H}' + 2\,\mathcal{H}^2\right)\,\phi + \mathcal{H}\,(\phi' + 5\,\psi') - \nabla^2\,\psi + \mathcal{H}\,\nabla^2\,(B-E')\right] \\
&\quad - \frac{1}{a^2}\,\partial_i\,\partial^j\,\left[(E'-B)' + 2\,\mathcal{H}\,(E'-B) + \psi - \phi\right] \\
\delta_{\rm s}\, R_i^0 &= \frac{2}{a^2}\,\partial_i\,\left[\psi' + \mathcal{H}\,\phi\right] \\
\delta_{\rm s}\, R_0^i &= \frac{2}{a^2}\,\partial^i\,\left[-\left(\psi' + \mathcal{H}\,\phi\right) + \left(\mathcal{H}' - \mathcal{H}^2\right)\,B\right]\ .
\end{aligned} \tag{A.13}$$

Finally the fluctuations of the Einstein tensor are

$$\delta_{\rm s}\, G_0^0 = \frac{2}{a^2}\,\left\{\nabla^2\,\psi - \mathcal{H}\,\nabla^2\,(B-E') - 3\,\mathcal{H}\,(\psi' + \mathcal{H}\,\phi)\right\} \tag{A.14}$$

$$\begin{aligned}
\delta_{\rm s}\, G_i^j &= \frac{1}{a^2}\,\left\{-2\,\psi'' - 2\,\left(\mathcal{H}^2 + 2\,\mathcal{H}'\right)\,\phi - 2\,\mathcal{H}\,\phi' - 4\,\mathcal{H}\,\psi'\right. \\
&\quad \left. -\ \nabla^2\,\left[\phi - \psi + (B-E')' + 2\,\mathcal{H}\,(B-E')\right]\right\}\,\delta_i^j \\
&\quad - \frac{1}{a^2}\,\partial_i\,\partial^j\,\left[(E'-B)' + 2\,\mathcal{H}\,(E'-B) + \psi - \phi\right]
\end{aligned} \tag{A.15}$$

$$\delta_{\rm s}\, G_i^0 = \delta\, R_i^0\ . \tag{A.16}$$

A.2 Vector modes

The vector fluctuations of the geometry can be written as

$$\begin{aligned}
&\delta_{\rm v}\, g_{0i} = a^2\, S_i\ , &&\delta_{\rm v}\, g^{0i} = \frac{S^i}{a^2} \\
&\delta_{\rm v}\, g_{ij} = -a^2\,\left(\partial_i\, F_j + \partial_j\, F_i\right)\ , &&\delta_{\rm v}\, g^{ij} = \frac{1}{a^2}\,\left(\partial^i\, F^j + \partial^j\, F^i\right)
\end{aligned} \tag{A.17}$$

and the corresponding fluctuations of the Chrristoffel connections

$$\begin{aligned}
\delta_{\rm v}\,\Gamma_{i0}^0 &= -\mathcal{H}\, S_i \\
\delta_{\rm v}\,\Gamma_{ij}^0 &= \frac{1}{2}\,\left(\partial_i\, S_j + \partial_j, S_i\right) + \mathcal{H}\,\left(\partial_i\, F_j + \partial_j\, F_i\right) + \frac{1}{2}\,\left(\partial_i\, F_j' + \partial_j\, F_i'\right) \\
\delta_{\rm v}\,\Gamma_{00}^i &= -S^{i'} - \mathcal{H}\, S^i \\
\delta_{\rm v}\,\Gamma_{ij}^k &= \mathcal{H}\, S^k\,\delta_{ij} - \frac{1}{2}\,\partial^k\,\left(\partial_i\, F_j + \partial_j\, F_i\right) \\
&\quad + \frac{1}{2}\,\partial_j\,\left(\partial^k\, F_i + \partial_i\, F^k\right) + \frac{1}{2}\,\partial_i\,\left(\partial_j\, F^k + \partial^k\, F_j\right) \\
\delta_{\rm v}\,\Gamma_{i0}^j &= -\frac{1}{2}\,\left(\partial_i\, S^j - \partial^j\, S_i\right) + \frac{1}{2}\,\left(\partial^j\, F_i' + \partial_i\, F^{j'}\right)
\end{aligned} \tag{A.18}$$

where Eq. (2.11) for F_i and S_i has been used. The fluctuations of the Ricci tensor are

$$\begin{aligned}
\delta_{\rm v}\, R_{0i} &= - \left[\mathcal{H}' + 2\,\mathcal{H}^2\right]\, S_i + \frac{1}{2}\,\nabla^2\, S_i + \frac{1}{2}\,\nabla^2\, F_i' \\
\delta_{\rm v}\, R_{ij} &= \frac{1}{2}\, \left\{(\partial_i\, S_j + \partial_j\, S_i)' + 2\,\mathcal{H}\, (\partial_i\, S_j + \partial_j\, S_i)\right\} + \frac{1}{2}\, \left(\partial_i\, F_j'' + \partial_j\, F_i''\right) \\
&\quad + \mathcal{H}\, \left(\partial_i\, F_j' + \partial_j\, F_i'\right) + \frac{1}{2}\, (\partial_i\, F_j + \partial_j\, F_i)\, \left(2\,\mathcal{H}' + 4\,\mathcal{H}^2\right)\ ,
\end{aligned} \tag{A.19}$$

A.3 Tensor modes

Let us now considering the tensor modes of the geometry, that is the two polarisation of the graviton

$$\delta_{\rm t}\, g_{ij} = -a^2\, h_{ij}\ , \quad \delta_{\rm t}\, g^{ij} = \frac{h^{ij}}{a^2}\ . \tag{A.20}$$

From Eq. (A.1) the tensor contribution to the fluctuations of the connections can be expressed as

$$\begin{aligned}
\delta_{\rm t}\, \Gamma^0_{ij} &= \frac{1}{2}\, \left(h_{ij}' + 2\,\mathcal{H}\, h_{ij}\right) \\
\delta_{\rm t}\, \Gamma^j_{i0} &= \frac{1}{2}\, h_i^{j\,\prime} \\
\delta_{\rm t}\, \Gamma^k_{ij} &= \frac{1}{2}\, \left[\partial_j\, h_i^k + \partial_i\, h_j^k - \partial^k\, h_{ij}\right]\ ,
\end{aligned} \tag{A.21}$$

and the Ricci tensor becomes

$$\delta_{\rm t}\, R_{ij} = \frac{1}{2}\, \left[h_{ij}'' + 2\,\mathcal{H}\, h_{ij} + 2\, \left(\mathcal{H}' + 2\,\mathcal{H}^2\right)\, h_{ij} - \nabla^2\, h_{ij}\right] \tag{A.22}$$

$$\delta_{\rm t}\, R_i^j = -\frac{1}{2a^2}\, \left[h_i^{i\,\prime\prime} + 2\,\mathcal{H}\, h_i^{j\,\prime} - \nabla^2\, h_i^j\right]\ . \tag{A.23}$$

A.4 Energy-Momentum Tensor

The background energy-momentum tensor of a perfect fluid is

$$T_{\mu\nu} = (p + \rho)\, u_\mu\, u_\nu - p\, g_{\mu\nu}\ . \tag{A.24}$$

From the normalisation condition

$$g_{\mu\nu}\, u^\mu\, u^\nu = 1\ , \tag{A.25}$$

one finds that $u_0 = a$ and $\delta\, u^0 = -\phi/a$. Hence, the scalar perturbations become

$$\delta_{\rm s}\, T^0_0 = \delta\, \rho\ , \quad \delta_{\rm s}\, T^{00} = \frac{1}{a^2}\, (\delta\, \rho - 2\, \rho\, \phi) \tag{A.26}$$

and

$$\begin{aligned}
\delta_{\rm s}\, T^j_i &= -\delta\, p\, \delta^j_i && \text{(A.27)}\\
\delta_{\rm s}\, T^{ij} &= \frac{1}{a^2}\, \left[\delta\, p\, \delta^{ij} + 2\, p\, \left(\psi\, \delta^{ij} - \partial^i\, \partial^j\, E\right)\right] && \text{(A.28)}\\
\delta_{\rm s}\, T^i_0 &= (p+\rho)\; v^i && \text{(A.29)}\\
\delta_{\rm s}\, T^{0i} &= \frac{1}{a^2}\, \left[(p+\rho)\; v^i + \partial^i\, B\right]\; . && \text{(A.30)}
\end{aligned}$$

where we have defined $\delta\, u^i \equiv v^i/a$. The velocity field can be split into divergenceless and divergencefull parts

$$v^i = \partial^i\, v + \mathcal{V}^i\;, \quad \partial_i\, \mathcal{V}^i = 0 \tag{A.31}$$

For collisionless matter, the anisotropic stress must be considered both in the Einstein equations and in the covariant conservation equations. The anisotropic stress is then introduced as

$$\delta_s\, T^j_i = -\delta\, p\, \delta^j_i + \Pi^j_i\;, \tag{A.32}$$

where $\Pi^j_i \equiv T^j_i - \delta^j_i\, T^k_k/3$. For the scalar fluctuations we adopt the notation

$$\partial_j\, \partial^i\, \Pi^j_i \equiv -\,(p+\rho)\; \nabla^2\, \sigma\;. \tag{A.33}$$

The perturbed velocity field can be defined in two ways,

$$\delta_{\rm s}\, T^i_0 = (p+\rho)\; u_0\, \delta\, u^i \equiv (p+\rho)\; v^i \equiv (p+\rho)\; \partial^i\, v \tag{A.34}$$

or

$$\delta_{\rm s}\, T^0_i = (p+\rho)\; u^0\, \delta\, u_i = (p+\rho)\; \overline{v}_i \equiv (p+\rho)\; \partial_i\, \overline{v}\;, \tag{A.35}$$

where, from the normalization condition (A.25), $u_0 = a$ and $u^0 = 1/a$. The velocity fields $\overline{v}$ and v defined in Eqs. (A.34) and (A.35) are not equivalent. In fact $\delta u_i = a\, \overline{v}_i$ and $\delta u^i = v^i/a$. Using

$$\begin{aligned}
\delta\, u^i &= \delta\, \left(g^{i\alpha}\, u_\alpha\right) \equiv \delta\, g^{i0}\, u_0 + g^{ik}\, \delta\, u_k && \text{(A.36)}\\
\delta\, g^{i0} &= -\partial^i B/a^2\;, && \text{(A.37)}
\end{aligned}$$

and inserting the definitions of δu^i and δu_k in terms of v^i and $\overline{v}_k$ we have

$$v_i = -\overline{v}_i - \partial_i\, B\;. \tag{A.38}$$

The gauge transformations for v_i and $\overline{v}_i$ are correspondingly different,

$$\begin{aligned}
&v_i \to \tilde{v}_i = v_i + \partial_i\, \epsilon'\\
&\overline{v}_i \to \tilde{\overline{v}}_i = \overline{v}_i - \partial_i\, \epsilon_0\;. && \text{(A.39)}
\end{aligned}$$

In this thesis we use the velocity field as defined in Eq. (A.34).

Let us now consider the energy-momentum tensor of a scalar field φ characterized by a potential $V(\varphi)$,

$$T_{\mu\nu} = \partial_\mu \varphi \, \partial_\nu \varphi - g_{\mu\nu} \left[\frac{1}{2} g^{\alpha\beta} \, \partial_\alpha \varphi \, \partial_\beta \varphi - V(\varphi) \right] \; . \tag{A.40}$$

Denoting with χ the first-order fluctuation of the scalar field φ, we have

$$\begin{aligned} \delta_{\rm s} T_{\mu\nu} = {} & \partial_\mu \chi \, \partial_\nu \varphi + \partial_\mu \varphi \, \partial_\nu \chi - \delta_{\rm s} g_{\mu\nu} \left[\frac{1}{2} g^{\alpha\beta} \, \partial_\alpha \varphi \, \partial_\beta \varphi - V \right] \\ & - g_{\mu\nu} \left[\frac{1}{2} \delta_{\rm s} g^{\alpha\beta} \, \partial_\alpha \varphi \, \partial_\beta \varphi + g^{\alpha\beta} \, \partial_\alpha \chi \, \partial_\beta \varphi - \frac{\partial V}{\partial \varphi} \chi \right] \; , \end{aligned} \tag{A.41}$$

or, explicitly,

$$\begin{aligned} \delta_{\rm s} T_{00} &= \chi' \varphi' + 2 a^2 \phi V + a^2 \frac{\partial V}{\partial \varphi} \chi \\ \delta_{\rm s} T_{0i} &= \varphi' \partial_i \chi + a^2 \partial_i B \left[\frac{\varphi'^2}{2 a^2} - V \right] \\ \delta_{\rm s} T_{ij} &= \delta_{ij} \left[\varphi' \chi' - \frac{\partial V}{\partial \varphi} \chi a^2 - (\phi + \psi) \varphi'^2 + 2 a^2 V \psi \right] \\ & \quad +2 a^2 \left[\frac{\varphi'^2}{2 a^2} - V \right] \partial_i \partial_j E \; . \end{aligned} \tag{A.42}$$

On using

$$^{(0)}T_{00} = \frac{\varphi'^2}{2} + a^2 V \; , \quad ^{(0)}T_{ij} = \left[\frac{\varphi'^2}{2} - a^2 V \right] \delta_{ij} \tag{A.43}$$

the perturbed components of the energy-momentum tensor can then be written as

$$\delta_{\rm s} T^\nu_\mu = \delta_{\rm s} T_{\alpha\mu} \, {}^{(0)}g^{\alpha\nu} +^{(0)} T_{\alpha\mu} \, \delta_{\rm s} g^{\alpha\nu} \; , \tag{A.44}$$

that is

$$\delta_{\rm s} T^0_0 = \frac{1}{a^2} \left(-\phi \varphi'^2 + \frac{\partial V}{\partial \varphi} a^2 \chi + \chi' \varphi' \right) \tag{A.45}$$

$$\delta_{\rm s} T^j_i = \frac{1}{a^2} \left(\phi \varphi'^2 + \frac{\partial V}{\partial \varphi} a^2 \chi - \chi' \varphi' \right) \delta^j_i \tag{A.46}$$

$$\delta_{\rm s} T^i_0 = -\frac{1}{a^2} \varphi' \partial^i \chi - \frac{\varphi'^2}{a^2} \partial^i B \; . \tag{A.47}$$

The covariant conservation of the energy-momentum tensor implies the validity of the Klein-Gordon equation which can be written as

$$g^{\alpha\beta} \nabla_\alpha \nabla_\beta \varphi + \frac{\partial V}{\partial \varphi} a^2 = 0 \; . \tag{A.48}$$

From Eq. (A.48) the perturbed Klein-Gordon equation is

$$\begin{aligned}&\delta_{\mathrm{s}}\, g^{\alpha\beta}\,\left[\partial_\alpha\,\partial_\beta\,\varphi - {}^{(0)}\,\Gamma^\sigma_{\alpha\beta}\,\partial_\sigma\,\varphi\right]\\ &+{}^{(0)}g^{\alpha\beta}\,\left[\partial_\alpha\,\partial_\beta\,\chi - \delta_{\mathrm{s}}\,\Gamma^\sigma_{\alpha\beta}\,\partial_\sigma\,\varphi - {}^{(0)}\,\Gamma^\sigma_{\alpha\beta}\,\partial_\sigma\,\chi\right] + \frac{\partial^2 V}{\partial\varphi^2} = 0\ ,\end{aligned} \tag{A.49}$$

or, more explicitly,

$$\begin{aligned}&\chi'' + 2\,\mathcal{H}\,\chi' - \nabla^2\,\chi + \frac{\partial^2\,V}{\partial\,\varphi^2}\,a^2\,\chi\\ &+2\,\phi\,\frac{\partial\,V}{\partial\,\varphi}\,a^2 - \varphi'\,\left(\phi' + 3\,\psi'\right) + \varphi'\,\nabla^2\,\left(E' - B\right) = 0\ .\end{aligned} \tag{A.50}$$

A.5 Gauge invariant scalar perturbations

We show here the generalised evolution equations for scalar fluctuations obtained without fixing a particular gauge. From Eqs. (A.14), (A.26), (A.16) and (A.29) the Hamiltonian and momentum constraints become

$$\nabla^2\,\psi - \mathcal{H}\,\nabla^2\,\left(B - E'\right) - 3\,\mathcal{H}\,\left(\psi' + \mathcal{H}\,\phi\right) = 4\,\pi\,G\,a^2\,\delta\,\rho \tag{A.51}$$

$$\partial^i\,\left[\left(\psi' + \mathcal{H}\,\phi\right) + \left(\mathcal{H}^2 - \mathcal{H}'\right)\,B\right] = -4\,\pi\,G\,a^2\,\left(p + \rho\right)\,v^i\ , \tag{A.52}$$

From Eqs. (A.15) and (A.28) we obtain the spatial components of the perturbed equations,

$$\begin{aligned}4\,\pi\,G\,a^2\,\left[\delta\,p\,\delta^j_i - \Pi^j_i\right] = &\left[\psi'' + \left(\mathcal{H}^2 + 2\,\mathcal{H}'\right)\,\phi + \mathcal{H}\,\left(\phi' + 2\,\psi'\right)\right]\,\delta^j_i\\ &+\frac{1}{2}\,\delta^j_i\,\nabla^2\,\left[\phi - \psi + \left(B - E'\right)' + 2\,\mathcal{H}\,\left(B - E'\right)\right]\\ &-\frac{1}{2}\,\partial_i\,\partial^j\,\left[\phi - \psi + \left(B - E'\right)' + 2\,\mathcal{H}\,\left(B - E'\right)\right]\ .\end{aligned} \tag{A.53}$$

From Eq. (A.53) we can separate the traceless part as

$$\begin{aligned}4\,\pi\,G\,a^2\,\delta\,p &= \psi'' + \mathcal{H}\,\left(\phi' + 2\,\psi'\right) + \left(\mathcal{H}^2 + 2\,\mathcal{H}'\right)\,\phi\\ &\quad+\frac{1}{3}\,\nabla^2\,\left[\phi - \psi + \left(B - E'\right)' + 2\,\mathcal{H}\,\left(B - E'\right)\right]\\ 12\,\pi\,G\,a^2\,\left(p + \rho\right)\,\sigma &= \nabla^2\,\left[\phi - \psi + \left(B - E'\right)' + 2\,\mathcal{H}\,\left(B - E'\right)\right]\ .\end{aligned} \tag{A.54}$$

The (0) and (i) components of Eq. (A.6) can be written

$$\begin{aligned}0 = &\,\partial_0\,\delta_{\mathrm{s}}\,T^{00} + \partial_j\,\delta_{\mathrm{s}}\,T^{j0} + \left(2\,\delta_{\mathrm{s}}\,\Gamma^0_{00} + \delta_{\mathrm{s}}\,\Gamma^k_{k0}\right)\,{}^{(0)}T^{00}\\ &+\left(2\,{}^{(0)}\Gamma^0_{00} + {}^{(0)}\,\Gamma^k_{k0}\right)\,\delta_{\mathrm{s}}\,T^{00} + {}^{(0)}\,\Gamma^0_{ij}\,\delta_{\mathrm{s}}\,T^{ij} + \delta_{\mathrm{s}}\,\Gamma^0_{ij}\,{}^{(0)}T^{ij}\end{aligned} \tag{A.55}$$

$$\begin{aligned}0 = &\,\partial_0\,\delta_{\mathrm{s}}\,T^{0j} + \partial_k\,\delta_{\mathrm{s}}\,T^{kj} + \left(\delta_{\mathrm{s}}\,\Gamma^0_{0k} + \delta_{\mathrm{s}}\,\Gamma^m_{mk}\right)\,{}^{(0)}T^{kj}\\ &+\left({}^{(0)}\Gamma^0_{00} + {}^{(0)}\,\Gamma^k_{k0}\right)\,\delta_{\mathrm{s}}\,T^{0j} + \delta_{\mathrm{s}}\,\Gamma^j_{00}\,{}^{(0)}T^{00} + \delta_{\mathrm{s}}\,\Gamma^j_{km}\,{}^{(0)}T^{km} + 2\,{}^{(0)}\Gamma^j_{0k}\,\delta_{\mathrm{s}}\,T^{0k}\ .\end{aligned} \tag{A.56}$$

Inserting the perturbed connections (A.10) into Eqs. (A.55) and (A.56) we have

$$\begin{aligned} 0 &= \delta\,\rho' - 3\,\psi'\,(p+\rho) + (p+\rho)\,\theta + 3\,\mathcal{H}\,(\delta\,\rho + \delta\,p) + (p+\rho)\,\nabla^2 E' \qquad (A.57) \\ 0 &= (p+\rho)\,\theta' + \theta\,[p' + \rho' + 4\,\mathcal{H}\,(p+\rho)] + (p+\rho)\,\nabla^2 B' \\ &\quad + [p' + \mathcal{H}\,(p+\rho)]\,\nabla^2 B + \nabla^2\,\delta\,p + (p+\rho)\,\nabla^2\,\phi\,, \qquad (A.58) \end{aligned}$$

where the divergence of the velocity field $\theta \equiv \partial_i\,v^i = \partial_i\,\partial^i\,v$ has been introduced.

Appendix B

Slow-Roll *vs* Horizon Flow

In this Appendix, we compare the HFF we used in the text with some other (equivalent) hierarchies.

In Table B.1, we give the relations between the slow-roll parameters defined by some other authors and the HFF defined in Eq. (3.65).

J. Martin *et al.* [69]† S. Habib *et al.* [73]	E.D. Stewart *et al.* [67, 75]* S. Habib *et al.* [62, 74]
$\epsilon = \epsilon_1$	$\epsilon = \epsilon_1$
$\delta = \epsilon_1 - \frac{1}{2}\,\epsilon_2$	$\delta_1 = \frac{1}{2}\,\epsilon_2 - \epsilon_1$
$\xi_2 = \frac{1}{2}\,\epsilon_2\,\epsilon_3$	$\delta_2 = -\frac{5}{2}\,\epsilon_1\,\epsilon_2 + 2\,\epsilon_1^2 + \frac{1}{4}\,\epsilon_2^2 + \frac{1}{2}\,\epsilon_2\,\epsilon_3$

Table B.1: Relation between (some) slow-roll parameters and the HFF used here and in Ref. [58]. *In Ref. [67] ϵ_1, δ, and $\dddot{\phi}\,\delta/H\,\ddot{\phi}$ are used instead of ϵ, δ_1 and δ_2 respectively. †In Ref. [69] ξ is used instead of ξ_2.

We also compare the Hubble-slow-roll (HSR) and the potential-slow-roll (PSR) parameters (see Ref. [81, 82]) with the HFF. We recall that some authors redefine ξ_V and ξ_H as ξ_V^2 and ξ_H^2 and write only ϵ, η and ξ, which can be confusing. The relations between the ϵ_i's and HSR parameters are

$$\begin{aligned} \epsilon_H &= \epsilon_1\ , \quad \eta_H = \epsilon_1 - \frac{1}{2}\,\epsilon_2 \\ \xi_H^2 &= \epsilon_1^2 - \frac{3}{2}\,\epsilon_1\,\epsilon_2 + \frac{1}{2}\,\epsilon_2\,\epsilon_3\ , \end{aligned} \tag{B.1}$$

and for the PSR parameters we have

$$
\begin{aligned}
\epsilon_V &= \epsilon_1 \left[1 + \frac{\epsilon_2}{2\,(3-\epsilon_1)}\right]^2 \sim \epsilon_1 \\
\eta_V &= \frac{6\,\epsilon_1 - \frac{3}{2}\,\epsilon_2 - 2\,\epsilon_1^2 + \frac{5}{2}\,\epsilon_1\,\epsilon_2 - \frac{1}{4}\,\epsilon_2^2 - \frac{1}{2}\,\epsilon_2\,\epsilon_3}{3-\epsilon_1} \sim 2\,\epsilon_1 - \frac{1}{2}\,\epsilon_2 \\
\xi_V^2 &= \frac{(2\,\epsilon_1 - 6 - \epsilon_2)\,[8\,\epsilon_1^3 - 6\,\epsilon_1^2\,(4+3\,\epsilon_2) + \epsilon_1\,\epsilon_2\,(18 + 6\,\epsilon_2 + 7\,\epsilon_3) - \epsilon_2\,\epsilon_3\,(3 + \epsilon_2 + \epsilon_3 + \epsilon_4)]}{4\,(3-\,\epsilon_1)^2} \\
&\sim 4\,\epsilon_1^2 - 3\,\epsilon_1\,\epsilon_2 + \frac{1}{2}\,\epsilon_2\,\epsilon_3 \;, \qquad \text{(B.2)}
\end{aligned}
$$

where we have shown both the exact formulas and approximate relations to the order of interest.

We complete this review with the first three exact connection formulae between the PSR and HSR parameters [81, 82]

$$
\begin{gathered}
\frac{\epsilon_V}{\epsilon_H} = \frac{(3-\eta_H)^2}{(3-\epsilon_H)^2}\;, \quad \eta_V = \frac{3\,(\epsilon_H + \eta_H) - \eta_H^2 - \xi_H^2}{3-\epsilon_H} \\
\xi_V^2 = \frac{9\;(3\epsilon_H\eta_H + \xi_H^2 - \epsilon_H\eta_H^2) - 3\,(4\eta_H\xi_H^2 - \eta_H^2\xi_H^2 + \sigma_H^3) + \eta_H\sigma_H^3}{(3-\epsilon_H)^2}\;,
\end{gathered} \qquad \text{(B.3)}
$$

and so on with σ_H the next HSR parameter.

Appendix C

An application of MCE

Here we use the Method of Comparison Equations to solve the differential equation (4.32) with the frequency $\omega^2(x) = e^x - 1 + a\,\sin(x)$, which does not admit an exact solution. In fact we shall solve in a semi-analytical way the equation

$$\frac{d^2\chi(x)}{dx^2} = \frac{1}{\varepsilon}\left[e^x - 1 + a\,\sin(x)\right]\chi(x)\ . \tag{C.1}$$

We shall give the semi-analytical results to leading and next-to-leading order of our approximation, correspondingly to 0^{th} and 1^{st}-order in ϵ. To build the semi-analytical solution we need the first two terms of the asymptotic expansion (4.38), i.e.

$$y(x) = y_0(x) + \epsilon\, y_1(x)\ , \tag{C.2}$$

and also the function

$$\sigma(x) = \sigma_0 + \int_0^x \frac{dx'}{y^2(x')}\ . \tag{C.3}$$

The function $y(x)$ appears in Eq. (4.34) as a prefactor (See Eq. (4.36)), while $\sigma(x)$ emerges in the argument of the analytical part of the solution (4.34), i.e. in $U\left[\sigma(x)\right]$. The above quatities will be estimated numerically taking $\epsilon = 1$ and $a = 1/10$ [1]. The initial conditions are $u(-20) = 1$ and $\dot{u}(-20) = 0$, while the range of the plots is $-20 \leq x \leq 4$. We recall that the quantity σ_0 changes from first to the second order of approximation, as we have shown in section 4.4.1 for the linear case. We shall use $\sigma_0 = 0$ for the leading order, while at the next-to-leading order we shall recalculate its value utilising the previous order. Finally, the analytical part will be a general solution of Eq. (4.33).

In the following we shall consider two comparison functions; a linear one, i.e. $\Theta^2(\sigma) = \sigma$, and a more complicated one, i.e. $\Theta^2(\sigma) = \mathrm{e}^{\sigma} - 1$

C.0.1 Linear comparison function

For the linear (i.e. Langer) case $y_0(x)$ and $y_1(x)$ are given by Eqs. (4.51) and (4.55a), respectively. In Fig. C.1 we show the function $y_1(x)$, while in Fig. C.2 we plot the function

---

[1] We use a “small” value for a in order to avoid other turning points in the oscillating region.

$y(x)$ at 0^{th} and 1^{st}-order in ϵ. The function $\sigma(x)$ at 0^{th} and 1^{st}-order in ϵ, calculated

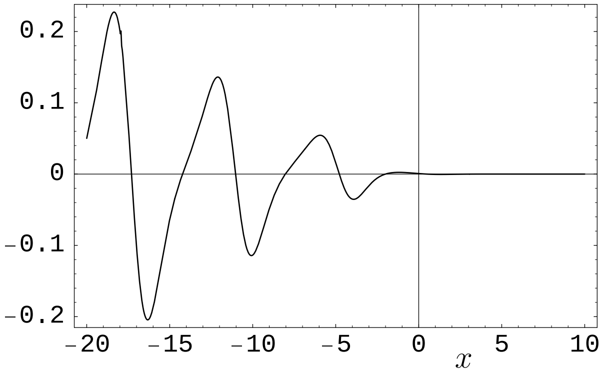

Figure C.1: Function $y_1(x)$ for a linear comparison equation.

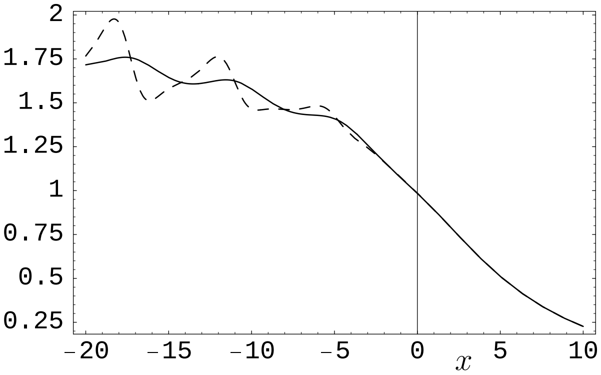

Figure C.2: Function $y_0(x)$ (solid line) and $y(x) = y_0(x) + \epsilon\, y_1(x)$ (dashed line) for a linear comparison equation.

from Eq. (C.3), is shown in Fig. C.3.

The analytical part of the solution follows from

$$\frac{d^2U(\sigma)}{d\sigma^2} = \frac{1}{\varepsilon}\sigma U(\sigma) \ , \tag{C.4}$$

and is a linear combination of Airy functions Ai and Bi

$$U\left[\sigma(x)\right] = A \cdot \mathrm{Ai}\left[\epsilon^{-1/3}\sigma(x)\right] + B \cdot \mathrm{Bi}\left[\epsilon^{-1/3}\sigma(x)\right] \ . \tag{C.5}$$

Finally the complete solution becomes

$$\chi(x) \quad = \quad y(x)\ \left\{A \cdot \mathrm{Ai}\left[\epsilon^{-1/3}\sigma(x)\right] + B \cdot \mathrm{Bi}\left[\epsilon^{-1/3}\sigma(x)\right]\right\} \ . \tag{C.6}$$

In Fig. C.4 we exhibit the exact numerical solution and the first and second order solutions in our approximation scheme.

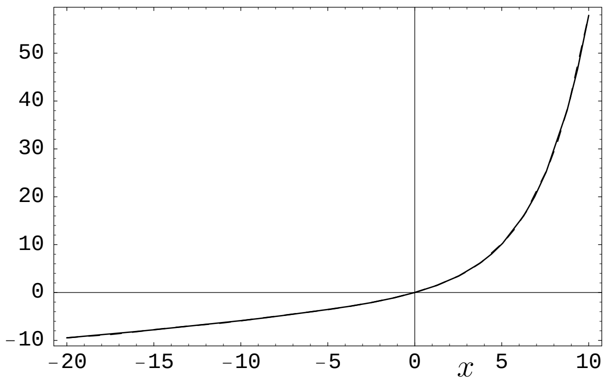

Figure C.3: Function $\sigma(x)$, for a linear comparison equation, to 0^{th} and 1^{st}-order in ϵ (solid and dashed line respectively). One can not distinguish the two curves.

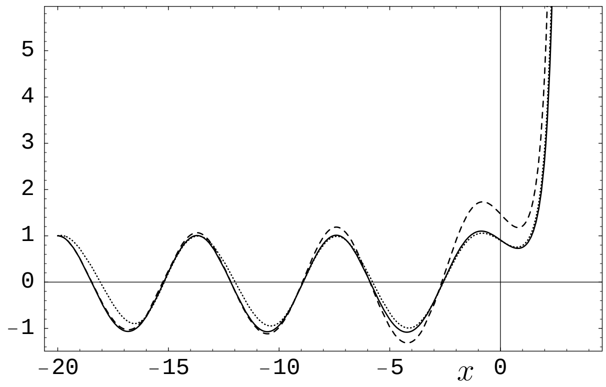

Figure C.4: Solution $\chi(x)$ of Eq. (C.1) for a linear comparison equation; the solid line is the full numerical solution, while the dashed and dotted ones are the 0^{th} and 1^{st}-order in ϵ respectively.

C.0.2 A more complicated comparison function

For the comparison function $\Theta^2(\sigma) = \mathrm{e}^{\sigma} - 1$ the quantities $y_0(x)$ is implicitly given by Eq. (4.75), while $y_1(x)$ is given by Eq. (4.79) on using Eqs. (4.80a) and (4.78). In Fig. C.5 we show the function $y_1(x)$ while in Fig. C.6 we plot the function $y(x)$ at 0^{th} and 1^{st}-orders in ϵ. In Fig. C.7 we exhibit the function $G(x)$ from Eq. (4.78). The function $\sigma(x)$ at 0^{th} and 1^{st}-orders in ϵ, calculated from Eq. (C.3), is shown in Fig. C.8.

The analytical part of the solution follows from

$$\frac{d^2U(\sigma)}{d\sigma^2} = \frac{1}{\varepsilon}\left(\mathrm{e}^{\sigma} - 1\right)U(\sigma)\ , \tag{C.7}$$

and it is a linear combination of Bessel functions I

$$U\left[\sigma(x)\right] = A \cdot I_{-\frac{2i}{\sqrt{\epsilon}}}\left[\frac{2\sqrt{\sigma(x)}}{\sqrt{\epsilon}}\right] + B \cdot I_{\frac{2i}{\sqrt{\epsilon}}}\left[\frac{2\sqrt{\sigma(x)}}{\sqrt{\epsilon}}\right]\ . \tag{C.8}$$

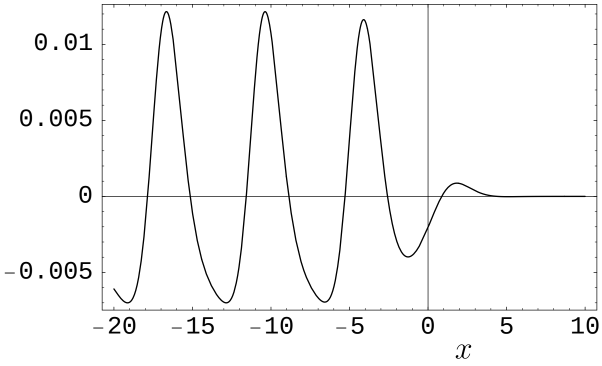

Figure C.5: The function $y_1(x)$ for a more complicated comparison function.

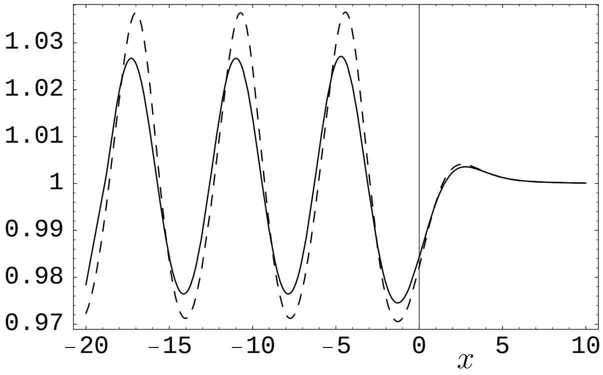

Figure C.6: The functions $y_0(x)$ (solid line) and $y(x) = y_0(x) + \epsilon\, y_1(x)$ (dashed line) for a more complicated comparison function.

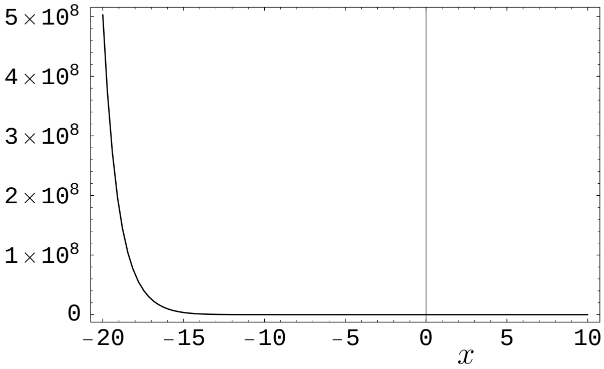

Figure C.7: Function $G(x)$.

Finally the complete solution becomes

$$\chi(x) \;=\; y(x)\left\{A\cdot I_{-\frac{2i}{\sqrt{\epsilon}}}\left[\frac{2\sqrt{\sigma(x)}}{\sqrt{\epsilon}}\right] + B\cdot I_{\frac{2i}{\sqrt{\epsilon}}}\left[\frac{2\sqrt{\sigma(x)}}{\sqrt{\epsilon}}\right]\right\}\;. \tag{C.9}$$

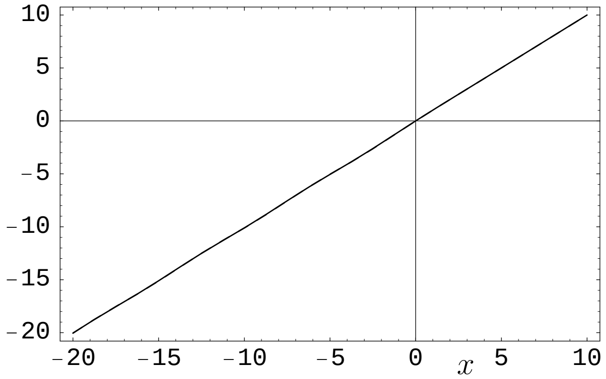

Figure C.8: The function $\sigma(x)$, for a more complicated comparison function, to 0^{th} and 1^{st}-orders in ϵ, solid and dashed lines respectively. As in the linear case one can not distinguish the two curves.

In Fig. C.9 we exhibit the exact numerical solution, the first and second order solutions in our approximation scheme.

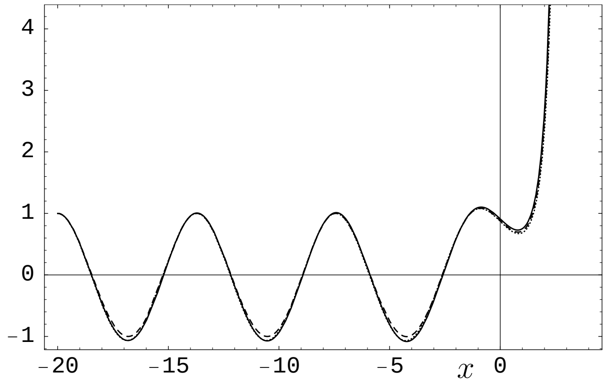

Figure C.9: Solution $\chi(x)$ of Eq. (C.1) for a more complicated comparison function; the solid line is the full numerical solution, while the dashed and dotted lines are respectively the 0^{th} and 1^{st}-orders in ϵ.

In Fig. C.4 we can note that the leading solution calculated with a linear comparison function is close to the true solution in the oscillating region, while the next-to-leading solution is better in the exponential region. It is quite natural because an iterative scheme is more stable in regions where a function under consideration has a monotonic behaviour. From Fig. C.4 and Fig. C.9 we can see that the more complicated comparison function leads to better solutions than the linear one. This feature is true because the more complicated comparison function remains close to the original frequency in the whole range of interest, in contrast with the linear case.

Appendix D

Other results in the literature

We use Table B.1 and Eqs. (B.1), to compare the results for spectral indices - and for PS and runnings when available - in terms of the HFF in Tables D.1 and D.2.

In Table D.1 we summarize the results for scalar and tensor perturbations given in Ref. [68], as calculated with the method proposed in Ref. [75]. We also refer to some other papers which give the same results, although expressed in different hierarchies.

Let us then compare with the results obtained by the uniform approximation [73, 62, 74]. The integrand in Eq. (9) of Ref. [73] can be obtained from our Eq. (5.1) by the change of variables $x = \ln(-k\,\eta)$, $u = \mathrm{e}^{-x/2}\,\mu$, which of course differs from our Eq. (5.9). Therefore, the integrands in our Eq. (4.14b) and Eq. (9) of Ref. [73] differ by $\mathcal{O}(\epsilon_i^4)$ terms, once both are expressed in conformal time. We also note that in Refs. [73, 62, 74], the authors just give expressions for the spectral indices which depend on k (i.e. without referring to a pivot scale $k = k_*$). Further, it is not easy to see that they obtain the correct scaling in $\ln(k/k_*)$, which yields the α-runnings, and the ϵ_i's are evaluated at the classical turning points for the frequencies.

In Tables D.2, we display the results for scalar and tensor perturbations given in Ref. [74]. As it was properly stated in Ref. [74], the results for scalar and tensor spectral indices given in Ref. [73, 62] were not fully expanded to second order in the slow-roll parameters.

Table D.1: Results obtained with the Green's function method [68] suggested in Ref. [75]; $C \equiv \ln 2 + \gamma_E - 2 \simeq -0.7296$ with γ_E the Euler-Mascheroni constant. We display the original results for spectral indices, α-runnings and tensor-to-scalar ratio evaluated at the pivot scale k_*.

E.D. Stewart *et al.* [67], E.D. Stewart *et al.* [75], S.M. Leach *et al.* [68], A.R. Liddle *et al.* [81, 82].
$\mathcal{P}_\zeta = \frac{H^2}{\pi \epsilon_1 m_{\mathrm{Pl}}^2} \Big\{ 1 - 2(C+1)\,\epsilon_1 - C\,\epsilon_2 + \left(2\,C^2 + 2\,C + \frac{\pi^2}{2} - 5\right)\epsilon_1^2 + \left(C^2 - C + \frac{7\pi^2}{12} - 7\right)\epsilon_1\,\epsilon_2 + \left(\frac{1}{2}\,C^2 + \frac{\pi^2}{8} - 1\right)\epsilon_2^2 + \left(-\frac{1}{2}\,C^2 + \frac{\pi^2}{24}\right)\epsilon_2\,\epsilon_3 + \left[-2\,\epsilon_1 - \epsilon_2 + 2\,(2\,C+1)\,\epsilon_1^2 + (2\,C-1)\,\epsilon_1\,\epsilon_2 + C\,\epsilon_2^2 - C\,\epsilon_2\,\epsilon_3\right] \ln\left(\frac{k}{k_*}\right) + \frac{1}{2}\left(4\,\epsilon_1^2 + 2\,\epsilon_1\,\epsilon_2 + \epsilon_2^2 - \epsilon_2\,\epsilon_3\right) \ln^2\left(\frac{k}{k_*}\right) \Big\}$
$\mathcal{P}_h = \frac{16\,H^2}{\pi\, m_{\mathrm{Pl}}^2} \Big\{ 1 - 2\,(C+1)\,\epsilon_1 + \left(2\,C^2 + 2\,C + \frac{\pi^2}{2} - 5\right)\epsilon_1^2 + \left(-C^2 - 2\,C + \frac{\pi^2}{12} - 2\right)\epsilon_1\,\epsilon_2 + \left[-2\,\epsilon_1 + 2\,(2\,C+1)\,\epsilon_1^2 - 2\,(C+1)\,\epsilon_1\,\epsilon_2\right] \ln\left(\frac{k}{k_*}\right) + \frac{1}{2}\left(4\,\epsilon_1^2 - 2\,\epsilon_1\,\epsilon_2\right) \ln^2\left(\frac{k}{k_*}\right) \Big\}$
$n_{\mathrm{S}} - 1 = -2\,\epsilon_1 - \epsilon_2 - 2\,\epsilon_1^2 - (2\,C+3)\,\epsilon_1\,\epsilon_2 - C\,\epsilon_2\,\epsilon_3 \quad , \quad n_{\mathrm{T}} = -2\,\epsilon_1 - 2\,\epsilon_1^2 - 2\,(C+1)\,\epsilon_1\,\epsilon_2$
$\alpha_{\mathrm{S}} = -2\,\epsilon_1\,\epsilon_2 - \epsilon_2\,\epsilon_3 \quad , \quad \alpha_{\mathrm{T}} = -2\,\epsilon_1\,\epsilon_2$
$R = 16\,\epsilon_1 \left[1 + C\,\epsilon_2 + \left(C - \frac{\pi^2}{2} + 5\right)\epsilon_1\,\epsilon_2 + \left(\frac{1}{2}\,C^2 - \frac{\pi^2}{8} + 1\right)\epsilon_2^2 + \left(\frac{1}{2}\,C^2 - \frac{\pi^2}{24}\right)\epsilon_2\,\epsilon_3\right]$

Table D.2: Results obtained with the uniform approximation.

S. Habib *et al.* [74]
$n_{\mathrm{S}} - 1 = -2\,\epsilon_1 - \epsilon_2 - 2\,\epsilon_1^2 - \left(\frac{20}{3} - 2\,\pi\right)\epsilon_1\,\epsilon_2 - \left(\frac{11}{6} - \pi\right)\epsilon_2\,\epsilon_3$
$n_{\mathrm{T}} = -2\,\epsilon_1 - 2\,\epsilon_1^2 - \left(\frac{14}{3} - \frac{3}{2}\pi\right)\epsilon_1\,\epsilon_2$

Appendix E

Undetermined parameters in the WKB*

To clarify the impact of the undetermined parameters $b_{\rm S}$, $b_{\rm T}$, and $d_{\rm S} = 2$ on the results to second order in the HFF, the percentage differences between the numerical coefficients of some second order terms in the power spectra are displayed in Table E.1 and of some of those in the scalar-to-tensor ratio in Table E.2. All the entries are for $b_{\rm S} = b_{\rm T} = d_{\rm S} = 2$, as is used in the main text, since other choices would give larger differences, as we explicitly show in Fig. E.1 for the numerical coefficient in front of $\epsilon_1\,\epsilon_2$ in P_h (since the behaviour is the same for all coefficients, we do not display other plots).

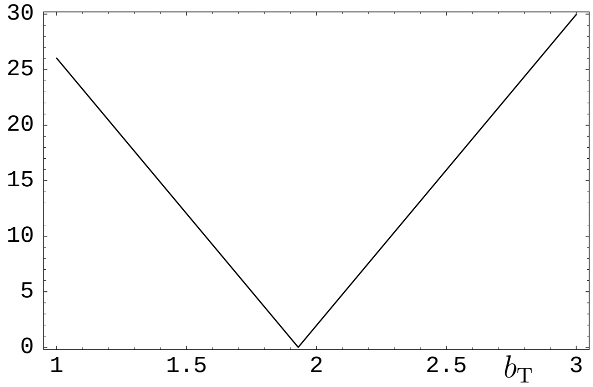

Figure E.1: Percentage difference between the numerical coefficients of $\epsilon_1\,\epsilon_2$ in P_h from WKB$*$ and GFM as a function of $b_{\rm T}$. The difference vanishes for $b_{\rm T} \simeq 1.93$ ($\simeq 2$, the value used in the main text).

	ϵ_1^2; P_ζ, P_h	ϵ_2^2; P_ζ	$\epsilon_1\,\epsilon_2$; $P_\zeta(b_{\rm S}=2)$	$\epsilon_1\,\epsilon_2$; $P_h(b_{\rm T}=2)$
WKB	2.3%	3.0%	353.3%	37.2%
WKB$*$	0.03%	0.06%	29.1%	2.0%

Table E.1: Percentage differences between the numerical coefficients of some second order terms in the power spectra given by WKB and WKB$*$ with respect to those obtained by the GFM.

	$\epsilon_2\,\epsilon_3$; $(d_{\rm S}=2)$	$\epsilon_1\,\epsilon_2$; $(b_{\rm S}-b_{\rm T}=0)$	ϵ_2^2
WKB	56.7%	1.5%	117.3%
WKB$*$	1.3%	0.03%	1.5%

Table E.2: Percentage differences between the numerical coefficients of some second order terms in the scalar-to-tensor ratio given by WKB and WKB$*$ with respect to those obtained from GFM. Note that the numerical coefficient of $\epsilon_2\,\epsilon_3$ in R is the same as that in P_ζ. Further, the coefficient of $\epsilon_1\,\epsilon_2$ does not depend on any undetermined parameters if $b_{\rm S}=b_{\rm T}$.

Appendix F

Perturbative approximations

In this Appendix we present a possible method of obtaining the complete result to second order in the HFF. We start by noting that any given function $f = f(x) = f(\epsilon, x)$ can be written as the power series

$$f(\epsilon, x) = \sum_{n=0}^{\infty} \frac{x^n}{n!} \left(-\sum_i \frac{\hat{\epsilon}_i \, \hat{\epsilon}_{i+1}}{1 - \hat{\epsilon}_1} \frac{\partial}{\partial \hat{\epsilon}_i} \right)^n f(\hat{\epsilon}_i, x) \equiv \sum_{n=0}^{\infty} \frac{x^n}{n!} f_n(x) \ , \tag{F.1}$$

where $\hat{\epsilon}_i = \epsilon_i(x_*)$ are the HFF evaluated at the horizon crossing (i.e. at $x = x_*$) and $f(\hat{\epsilon}_i, x) = f(\epsilon_i = \hat{\epsilon}_i, x)$. On using Eqs. (F.1) to express both ω^2 and χ in Eq. (4.6), we obtain

$$\chi_0(x) \sum_{n=1}^{\infty} \frac{x^n}{n!} \omega_n^2(x) + \left[\frac{\mathrm{d}^2}{\mathrm{d}x^2} + \sum_{m=0}^{\infty} \frac{x^m}{m!} \omega_m^2(x) \right] \sum_{n=1}^{\infty} \frac{x^n}{n!} \chi_n(x) = 0 \ , \tag{F.2}$$

where we have used

$$\left[\frac{\mathrm{d}^2}{\mathrm{d}x^2} + \omega_0^2(x) \right] \chi_0(x) = 0 \ , \tag{F.3}$$

with $\omega_0^2(x) = \omega^2(\epsilon_i = \hat{\epsilon}_i; x)$ and $\chi_0(x)$ is a linear combination (i.e. the MCE leading order solution) of Eq. (5.42) for $\Theta^2(x) = \omega_0^2(x)$ and $\sigma \to x$ in the argument of the Bessel functions. One may solve Eq. (F.2) for higher orders by introducing

$$\frac{x^n}{n!} \chi_n(x) \equiv g_n(x) \, \chi_0(x) \ , \tag{F.4}$$

and using the standard formulae for second order differential equations with a source term, so that

$$g_n(x) = -\int_{\infty}^{x} \frac{\mathrm{d}y}{\chi_0^2(y)} \int_{\infty}^{y} \mathrm{d}z \, \chi_0^2(z) \left[\frac{z^n}{n!} \omega_n^2(z) + \sum_{m=1}^{n-1} g_m(z) \frac{z^{n-m}}{n-m} \omega_{n-m}^2(z) \right] \ . \tag{F.5}$$

The problem has therefore been reduced to computing $2\,n$ integrals.

The above formalism can be modified in order to provide an alternative way for calculating the power spectra, spectral indices and runnings to second order in the HFF. We start from Eq. (5.1) using the exact relations

$$\begin{aligned} \frac{z_{\mathrm{T}}''}{z_{\mathrm{T}}} &= a^2\,H^2\,(2-\epsilon_1) \\ \frac{z_{\mathrm{S}}''}{z_{\mathrm{S}}} &= a^2\,H^2\left(2-\epsilon_1+\frac{3}{2}\,\epsilon_2-\frac{1}{2}\,\epsilon_1\,\epsilon_2+\frac{1}{4}\,\epsilon_2^2+\frac{1}{2}\,\epsilon_2\,\epsilon_3\right)\ . \end{aligned} \tag{F.6}$$

With a redefinitions of the wave-function and variable

$$\psi = \mathrm{e}^{-x/2}\,\mu\ , \qquad \tilde{x} = \ln\left(-k\,\eta\right) \tag{F.7}$$

we obtain

$$\left[\frac{\mathrm{d}^2}{\mathrm{d}\tilde{x}^2}+\tilde{\omega}^2(\tilde{x})\right]\,\psi(\tilde{x}) = 0\ , \tag{F.8}$$

where

$$\begin{aligned} \tilde{\omega}_{\mathrm{T}}^2 &= \mathrm{e}^{2\,\tilde{x}}-\frac{1}{4}-\eta^2 a^2 H^2\,(2-\epsilon_1) \\ \tilde{\omega}_{\mathrm{S}}^2 &= \mathrm{e}^{2\,\tilde{x}}-\frac{1}{4}-\eta^2 a^2 H^2\left(2-\epsilon_1+\frac{3}{2}\,\epsilon_2-\frac{1}{2}\,\epsilon_1\,\epsilon_2+\frac{1}{4}\,\epsilon_2^2+\frac{1}{2}\,\epsilon_2\,\epsilon_3\right)\ . \end{aligned} \tag{F.9}$$

On now using the approximate relation

$$\eta \simeq -\frac{1}{a\,H}\,\left(1+\epsilon_1+\epsilon_1^2+\epsilon_1\,\epsilon_2\right)\ , \tag{F.10}$$

the frequencies become

$$\begin{aligned} \tilde{\omega}_{\mathrm{T}}^2 &\simeq \mathrm{e}^{2\,\tilde{x}}-\left(\frac{9}{4}+3\,\epsilon_1+4\,\epsilon_1^2+4\,\epsilon_1\epsilon_2\right) \\ \tilde{\omega}_{\mathrm{S}}^2 &\simeq \mathrm{e}^{2\,\tilde{x}}-\left(\frac{9}{4}+3\,\epsilon_1+\frac{3}{2}\,\epsilon_2+4\,\epsilon_1^2+\frac{13}{2}\,\epsilon_1\epsilon_2+\frac{1}{4}\,\epsilon_2^2+\frac{1}{2}\,\epsilon_2\epsilon_3\right)\ , \end{aligned} \tag{F.11}$$

where we only keep the second order terms in the (still $\tilde{x}$-dependent) HFF. We can now expand linearly each HFF around the horizon crossing to obtain

$$\begin{aligned} &\frac{\mathrm{d}^2\,\psi_{\mathrm{T}}}{\mathrm{d}\,\tilde{x}^2}+\left[\mathrm{e}^{2\,\tilde{x}}-\left(\frac{9}{4}+3\,\hat{\epsilon}_1+4\,\hat{\epsilon}_1^2+4\,\hat{\epsilon}_1\hat{\epsilon}_2\right)\right]\psi_{\mathrm{T}} = -3\,\hat{\epsilon}_1\,\hat{\epsilon}_2\,\tilde{x}\,\psi_{\mathrm{T}} \\ &\frac{\mathrm{d}^2\,\psi_{\mathrm{S}}}{\mathrm{d}\,\tilde{x}^2}+\left[\mathrm{e}^{2\,\tilde{x}}-\left(\frac{9}{4}+3\,\hat{\epsilon}_1+\frac{3}{2}\,\hat{\epsilon}_2+4\,\hat{\epsilon}_1^2+\frac{13}{2}\,\hat{\epsilon}_1\hat{\epsilon}_2+\frac{1}{4}\,\hat{\epsilon}_2^2+\frac{1}{2}\,\hat{\epsilon}_2\hat{\epsilon}_3\right)\right]\psi_{\mathrm{S}} \\ &\qquad = -3\left(\hat{\epsilon}_1\,\hat{\epsilon}_2+\frac{1}{2}\,\hat{\epsilon}_2\,\hat{\epsilon}_3\right)\tilde{x}\,\psi_{\mathrm{S}}\ , \end{aligned} \tag{F.12}$$

which, beside the use of $\tilde{x}$ instead of x and the appearance of $\tilde{\omega}$ instead of ω, is equivalent to the expansion in Eq. (F.1) for $f = \tilde{\omega}^2$ and can be solved by means of a standard perturbative approach (such as in Ref. [75]). The method is close to GFM and gives the same results of Eq. (41) in Ref. [75] and Eq. (29) in Ref. [68] for the scalar and tensor power spectra, respectively.

Let us finally note that, for the GFM, the scalar spectral index and its running are calculated by taking the derivative of Eq. (41) in Ref. [75], i.e. the power spectra evaluated at $k = a\,H$, in terms of $\ln k$, while in our MCE (but also in the WKB approximation [70, 71]) the dependences in $\ln(k/k_*)$ are obtained explicitly (see, for example, Eqs. (6.37a) and (6.37b)).

Appendix G

MCE and Black Holes

In this Appendix we employ the Method of Comparison Equations to study the propagation of a massless minimally coupled scalar field on the Schwarzschild background as an example of a potential with two turning point in the wave equation. In particular, we show that this method allows us to obtain explicit approximate expressions for the radial modes with energy below the peak of the effective potential which are fairly accurate over the whole region outside the horizon. This case can be of particular interesting, for example, for the problem of black hole evaporation.

Wave equations on black hole backgrounds cannot be solved exactly in terms of known simple functions (for a review, see, *e.g.*, Ref. [83]). Although it is usually fairly easy to find asymptotic expressions near the (outer) horizon or at spatial infinity, numerical analysis is what one eventually employs to obtain a detailed profile of the wave-functions. However, our understanding of the field dynamics on curved backgrounds would still benefit of analytical approximations to the exact modes, for example in the study of the (renormalized) energy-momentum tensor of quantum fields [33] and, in particular, of the Hawking radiation [84, 85], or of quasi-normal modes [86].

By making use of the black hole symmetry, one can usually separate the wave-functions and reduce the problem to the one task of solving a second order differential equation for the radial part. The latter takes the form of the one-dimensional Schrödinger equation for the transmission through a potential barrier [83]

$$\left[\frac{\mathrm{d}^2}{\mathrm{d}x^2} + Q_s(x)\right]\psi = 0 \ , \tag{G.1}$$

and, for the general case of a Kerr-Newman black hole, is known as the Teukolsky master equation for waves of spin-weight $s = 0$, 1 and 2 [87, 83].

In the next Section, we shall briefly review the equation of motion for massless scalar fields on a spherically symmetric black hole background. This includes the simplest case of linear perturbations of a Schwarzschild black hole which will be used to show the application of our method in all details (including the use of a convenient radial coordinate and rescaling of the wave-function). In Section G.2, we shall then apply the MCE and obtain approximate expressions for scalar wave-modes with energy below the peak of the potential. This case is of particular interest, for example, for evaluating the grey-body factors involved in the Hawking effect [84, 85]. It also presents a major complication with respect to the typical case of Cosmological Pertubations, namely the presence of two zeros of the potential ("turning points"). We shall use units with $c = G = 1$. The last three Sections will give some tecnical results which complete this Appendix.

G.1 Scalar field on Schwarzschild background

Let us begin by recalling that the metric in a static and spherically symmetric vacuum space-time can be written in general as

$$\mathrm{d}s^2 = h(r)\,\mathrm{d}t^2 - \frac{\mathrm{d}r^2}{h(r)} - r^2\,\mathrm{d}\Omega^2 \ , \tag{G.2}$$

where $\mathrm{d}\Omega$ is the area element on the unit two-sphere. The propagation of massless, minimally coupled scalar particles in this background is governed by the Klein-Gordon equation $\Phi^{;\mu}{}_{;\mu} = 0$. Due to the symmetry of the background, the field Φ can be decomposed into eigenmodes of normal frequency $\bar{\omega}$ and angular momentum numbers ℓ, m as [83]

$$\Phi(t, r, \Omega) = \mathrm{e}^{-i\,\bar{\omega}\,t}\,Y_\ell^m(\Omega)\,R(r) \ , \tag{G.3}$$

where Y_ℓ^m are spherical harmonics. The Klein-Gordon equation then separates and the dynamics is described by the function R which satisfies the radial equation

$$\frac{\mathrm{d}}{\mathrm{d}r}\left[r^2\,h(r)\,\frac{\mathrm{d}R(r)}{\mathrm{d}r}\right] + \left[\frac{\bar{\omega}^2\,r^2}{h(r)} - \ell\,(\ell+1)\right] R(r) = 0 \ , \tag{G.4}$$

where $\ell\,(\ell+1)$ is the separation constant. No exact solution of the above equation is known even for as simple a background as the four-dimensional Schwarzschild space-time with

$$h(r) = 1 - \tilde{r}^{-1} \ , \tag{G.5}$$

where we have introduced the dimensionless radial coordinate $\tilde{r} = r/r_{\mathrm{H}}$ and r_{H} is the Schwarzschild radius.

It is now convenient to introduce the "tortoise-like" coordinate [1]

$$\mathrm{d}\,x = \frac{\mathrm{d}\,\tilde{r}}{\tilde{r}\,h(\tilde{r})} \ , \tag{G.6a}$$

and the new radial function

$$R\left[\tilde{r}(x)\right] = \exp\left[-\frac{1}{2}\int^{x} h(x')\,\mathrm{d}\,x'\right]\chi\left[\tilde{r}(x)\right] \ , \tag{G.6b}$$

---

[1] A similar coordinate was already used in Ref. [88].

so that the radial equation takes the Schrödinger form

$$\frac{\mathrm{d}^2\,\chi(x)}{\mathrm{d}x^2}+\left\{\tilde{\omega}^2\,\tilde{r}^2(x)-\ell\,(\ell+1)\,h[\tilde{r}(x)]-\frac{1}{4}\,h^2[\tilde{r}(x)]-\frac{1}{2}\,\frac{\mathrm{d}h[\tilde{r}(x)]}{\mathrm{d}x}\right\}\chi(x)=0\ . \tag{G.7}$$

where we also defined the dimensionless energy $\tilde{\omega}\equiv\bar{\omega}\,r_{\mathrm{H}}$. For the four-dimensional Schwarzschild case we have

$$x(\tilde{r})=\ln(\tilde{r}-1)\ , \tag{G.8}$$

so that the new variable x ranges from $x(\tilde{r}_{\mathrm{H}}=1)=-\infty$ to $x(\tilde{r}=+\infty)=+\infty$ and x and $\chi(x)$ are of Langer's form [37]. The Klein-Gordon equation finally becomes

$$\left[\frac{\mathrm{d}^2}{\mathrm{d}x^2}+\omega^2(x)\right]\,\chi(x)=0\ , \tag{G.9}$$

where the "frequency"

$$\omega^2(x)=\tilde{\omega}^2\,(1+\mathrm{e}^x)^2-\frac{\ell\,(\ell+1)\,\mathrm{e}^x}{1+\mathrm{e}^x}-\frac{\mathrm{e}^x\,(2+\mathrm{e}^x)}{4\,(1+\mathrm{e}^x)^2}\ , \tag{G.10}$$

is not necessarily a positive quantity. In fact, the above expression shows two qualitatively different behaviors depending on the values of $\tilde{\omega}$ and ℓ. In particular, for a given angular momentum ℓ, there exists a critical value

$$\tilde{\omega}_{\mathrm{c}}=\tilde{\omega}_{\mathrm{c}}(\ell)\ , \tag{G.11}$$

such that if the energy $\tilde{\omega}>\tilde{\omega}_{\mathrm{c}}$ there are no turning points, otherwise there are two, say $\omega(x_1)=\omega(x_2)=0$ with $x_1<x_2$. The latter case is the one we want to analyze in detail (see Sec. G.2.1 for more details and the solid line in Fig. G.1 for an example).

G.2 MCE solutions

Referring to Section 4.4 for the basic formulae characterising the MCE, we can find the approximate solution of Eq. (G.9),

$$\chi_{\mathrm{MCE}}(x)=\left(\frac{\mathrm{d}\sigma}{\mathrm{d}x}\right)^{-1/2}U(\sigma)\ , \tag{G.12}$$

which is valid in the whole range of x and including the turning points.

We are now dealing with a problem of the form (G.9) with two turning points, $x_1<x_2$. In order to implement the MCE, we need a "comparison frequency" with the same behavior. We shall use the Morse potential [89]

$$\Theta^2(\sigma)=A\,\mathrm{e}^{2\,\sigma}-B\,\mathrm{e}^{\sigma}+D\ . \tag{G.13}$$

The coefficients A and B are then fixed by imposing that the turning points of the comparison function are the same as those of the exact frequency, that is

$$\Theta(\sigma_1 = x_1) = \Theta(\sigma_2 = x_2) = 0 \ , \tag{G.14a}$$

and the coefficient D will then follow form the relation

$$\xi \equiv \int_{x_1}^{x_2} \sqrt{-\,\omega^2(y)}\,\mathrm{d}\,y = \int_{x_1}^{x_2} \sqrt{-\,\Theta^2(\rho)}\,\mathrm{d}\,\rho \ . \tag{G.14b}$$

The system of non-linear equations (G.14a) and (G.14b) thus yields

$$A = \frac{4\,\xi^2}{\pi^2\left(w_1 + w_2 - 2\sqrt{w_1\,w_2}\right)^2} \tag{G.15a}$$

$$B = (w_1 + w_2)\,A \tag{G.15b}$$

$$D = w_1\,w_2\,A \ , \tag{G.15c}$$

where the exact expression for ξ is given in Sec. G.2.2. A sample plot of both the exact frequency and the comparison function thus obtained is given in Fig. G.1.

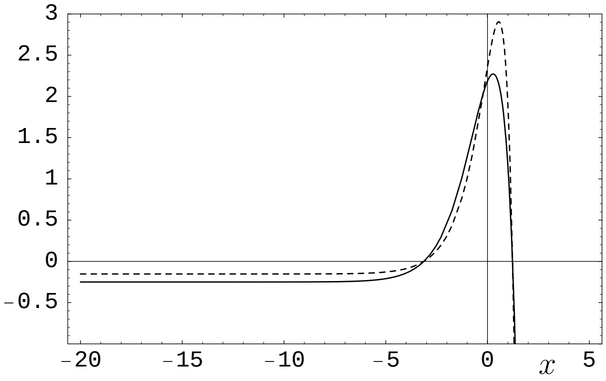

Figure G.1: Comparison between the exact potential $-\omega^2(x)$ (solid line) and the approximate Morse potential $-\Theta^2[\sigma(x)]$ obtained after solving Eqs. (G.14a) and (G.14b) (dotted line) for $\tilde{\omega} = 1/2$ and $\ell = 2$. The two turning points are $x_1 \approx -3.13$ and $x_2 \approx 1.23$.

The "comparison solution" is a linear combination of confluent hypergeometric functions [39] of the type ${}_1\mathrm{F}_1$ (for more details, see Ref. [89]),

$$\begin{aligned} U(\sigma) &= C_+\,\mathrm{e}^{i\left(\sqrt{A}\,\mathrm{e}^{\sigma}+\sqrt{D}\,\sigma\right)}\,{}_1\mathrm{F}_1\left(\frac{1}{2} + i\sqrt{D} + i\,\frac{B}{2\sqrt{A}}, 1 + 2\,i\sqrt{D}, -2\,i\sqrt{A}\,\mathrm{e}^{\sigma}\right) \\ &+C_-\,\mathrm{e}^{i\left(\sqrt{A}\,\mathrm{e}^{\sigma}-\sqrt{D}\,\sigma\right)}\,{}_1\mathrm{F}_1\left(\frac{1}{2} - i\sqrt{D} + i\,\frac{B}{2\sqrt{A}}, 1 - 2\,i\sqrt{D}, -2\,i\sqrt{A}\,\mathrm{e}^{\sigma}\right) \ , \end{aligned} \tag{G.16}$$

and $\sigma(x)$ is given implicitly by Eq. (4.31) with

$$\begin{aligned} &\int_{x_1}^{\sigma} \sqrt{\Theta^2(\rho)}\,\mathrm{d}\,\rho = \sqrt{\Theta^2(\sigma)} \\ &-\ln\left[\left(2\,A\,\mathrm{e}^{\sigma} - B + 2\sqrt{A\,\Theta^2(\sigma)}\right)^{\frac{B}{2\sqrt{A}}}\left(2\,D\,\mathrm{e}^{-\sigma} - B + 2\,\mathrm{e}^{-\sigma}\sqrt{D\,\Theta^2(\sigma)}\right)^{\sqrt{D}}\right] \ . \end{aligned} \tag{G.17}$$

The above expression is rather complex. Hence, we just consider the asymptotic relation between σ and x to the left of the smaller turning point (that is, for $x \ll x_1$)

$$\sigma(x) \simeq \frac{\tilde{\omega}}{\sqrt{D}}\, x \tag{G.18a}$$

and to the right of the larger one ($x \gg x_2$)

$$\sqrt{A}\, \mathrm{e}^{\sigma(x)} - \frac{B}{2\sqrt{A}}\, \sigma(x) \simeq \tilde{\omega}\, (\mathrm{e}^x + x) \ . \tag{G.18b}$$

As an approximate expression for $\sigma(x)$ for $x < \kappa_1 x_1$ (with $\kappa_1 \gtrsim 1$) we shall then use Eq. (G.18a) and the condition that $\sigma(x_1) = x_1$. Analogously, for $x > \kappa_2 x_2$ (with $\kappa_2 \gtrsim 1$) we shall use the approximate solution of Eq. (G.18b) to next-to-leading order for large x. Moreover, in the region between $\kappa_1 x_1$ and $\kappa_2 x_2$ we shall use an interpolating cubic function. The reason for introducing two new parameters κ_1 and $\kappa_2 \gtrsim 1$ is that the asymptotic forms in Eqs. (G.18a) and (G.18b) may differ significantly from the correct $\sigma(x)$ around the turning points x_1 and x_2 and suitable values of κ_1 and κ_2 usually improve the final result. To summarize, we have

$$\sigma = \begin{cases} \dfrac{\tilde{\omega}}{\sqrt{D}}\, x + x_1 \left(1 - \dfrac{\tilde{\omega}}{\sqrt{D}}\right) \ , & x_0 < x < \kappa_1 x_1 \\[2ex] C_0 + C_1\, x + C_2\, x^2 + C_3\, x^3, & \kappa_1 x_1 < x < \kappa_2 x_2 \\[2ex] x + \ln\left(\dfrac{\tilde{\omega}}{\sqrt{A}}\right) \ , & x > \kappa_2 x_2 \ , \end{cases} \tag{G.19}$$

with κ_1 and $\kappa_2 \gtrsim 1$ and $x_0 < \kappa_1 x_1$ is the value of x at which we wish to impose the initial conditions for $\chi(x)$ and its derivative [2]. The explicit expressions for the coefficients C_0, C_1, C_2 and C_3 are rather cumbersome and will be given in Sec. G.2.3.

In the upper left panel of Fig. G.2, we plot $\sigma(x)$ for the same values of $\tilde{\omega}$ and ℓ used in Fig. G.1. The solid line represents the numerical solution of Eq. (4.31) and the dashed line the approximate expression (G.19) with $\kappa_1 = 1$ and $\kappa_2 = 3$. It is clear that these values of κ_1 and κ_2 already lead to a very good approximation for σ around the turning points x_1 and x_2 and that larger values of κ_1 or κ_2 would not improve significantly the final result. In the upper right panel of Fig. G.2, we compare an MCE approximate wave-function with the exact solution (solid line) obtained numerically for the same case. The MCE solution shown by a dashed line is given by the expression (G.12) with $U(\sigma)$ as in Eq. (G.16) and $\sigma(x)$ determined by solving Eq. (4.31) numerically. The coefficients $C_\pm$ are fixed by imposing that the MCE mode and its derivative equal the corresponding values of the chosen numerical solution at $x = -20$. Since the two curves coincide almost

---

[2] Of course, if we are interested in setting the initial conditions at $x_0 \gg x_2$ the expressions must be adjusted correspondingly.

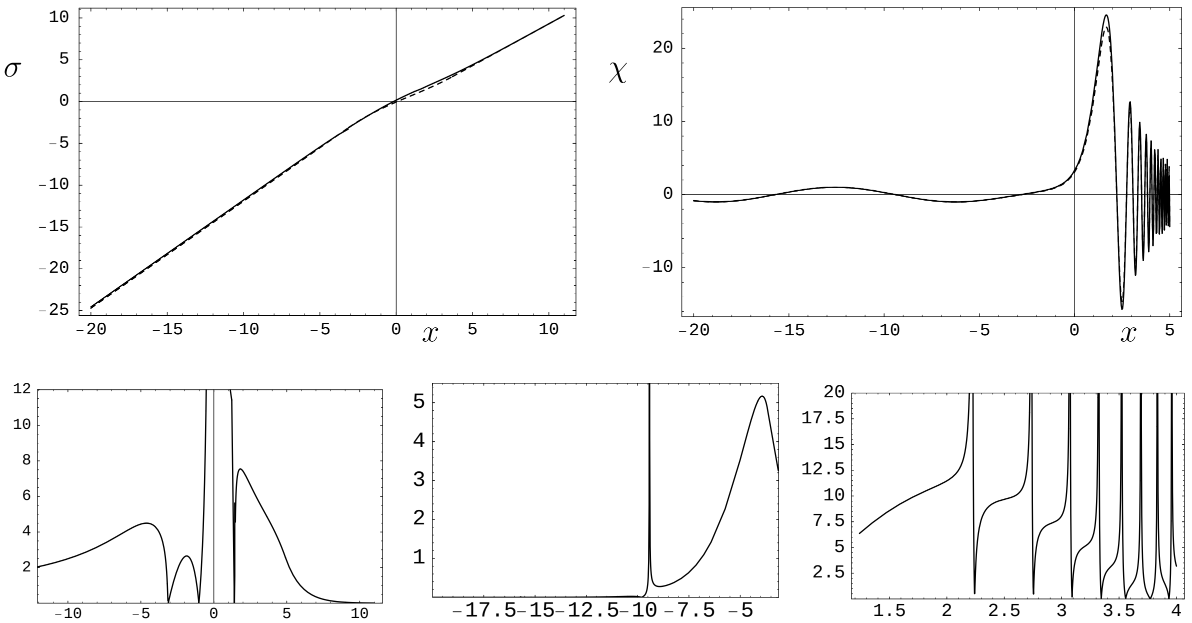

(a) (b) (c)

Figure G.2: Upper left graph: The function $\sigma = \sigma(x)$ obtained by integrating Eq. (4.31) numerically (solid line) and its approximate expression (G.19) with $\kappa_1 = 1$ and $\kappa_2 = 3$ (dashed line). Upper right graph: Comparison between the exact solution (solid line) and the approximate MCE solution (G.12) with $\sigma(x)$ evaluated numerically (dashed line) for $C_+ \approx 0.517 - 0.228\,i$ and $C_- \approx 0.517 + 0.228\,i$. Panel (a) shows the percentage error for the same approximate function σ given in the upper left graph. Panel (b) shows the percentage error for the approximate χ in the upper right graph for $x < x_1$ and panel (c) for $x_2 < x$. All plots are for $\tilde{\omega} = 1/2$, $\ell = 2$ as in Fig. G.1.

everywhere, it is clear that solving the approximate equation (4.31) for $\sigma(x)$ is, to all practical extents, equivalent to solving the original equation (G.9).

In order to further clarify this point, in panel (a) of Fig. G.2, we plot the relative difference (in percent) between the approximate expression (G.19) and the exact numerical solution of Eq. (4.31). We can see that the error is less than 10% almost everywhere, except near the zero of $\sigma(x)$. In the same figure, we also show the percentage error for the approximate solution shown in Fig. G.2 on the left of x_1 and on the right of x_2. The latter error remains small, too, except around the zeros of χ due to the slight difference in phases.

Finally, in Fig. G.3, the dashed lines represent the same MCE solution with $\sigma(x)$ given by its analytical approximation in Eq. (G.19) with $\kappa_1 = 1$ and $\kappa_2 = 3$. This is the fully analytical expression obtained from the application of the MCE and is still remarkably good, with a more significant error around the larger turning point ($x_2 \approx 1.23$). From the three graphs in Fig. G.3 and the upper left panel in Fig. G.2, it clearly appears that such an error develops in the region between the two turning points, where the discrepancy between the exact $\sigma(x)$ and the approximate expression (G.19) is indeed larger. In this

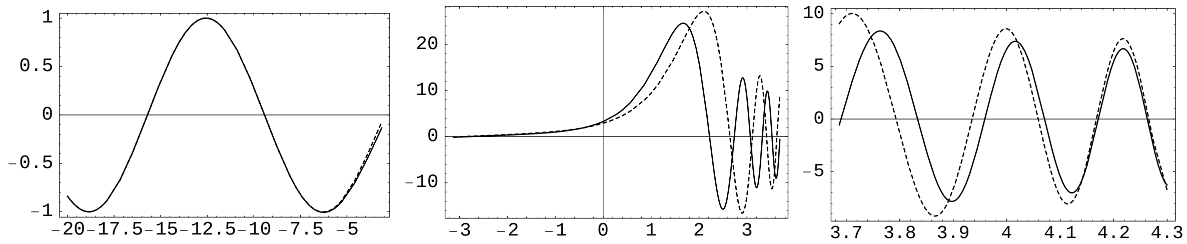

(a) (b) (c)

Figure G.3: Comparison between the exact solution (solid line) and the approximate MCE solution (G.12) with $\sigma(x)$ given in Eq. (G.19) with $\kappa_1 = 1$ and $\kappa_2 = 3$ (dashed line) for $\tilde{\omega} = 1/2$ and $\ell = 2$ (same as in Figs. G.1 and G.2). Panel (a) shows the result for $x < \kappa_1 x_1$, panel (b) for $\kappa_1 x_1 < x < \kappa_2 x_2$ and panel (c) for $x > \kappa_2 x_2$.

respect, let us note that, had we imposed initial conditions at $x \gg x_2$, the larger error would have occurred around the smaller turning point ($x_1 \approx -3.13$). Moreover, when we used a linear (or quadratic) interpolating function for $\kappa_1 x_1 < x < \kappa_2 x_2$, the accuracy was (expectedly) worse. Should one need better accuracy, a higher order polynomial interpolation between $\kappa_1 x_1$ and $\kappa_2 x_2$ could therefore be used instead.

Let us now make a few remarks. Firstly, the application of the MCE is not as straightforward as the standard WKB approximation. In fact, the MCE usually requires solving some technical tasks specific to the problem at hand in order to obtain the argument $\sigma = \sigma(x)$ of the known function $U = U(\sigma)$. In the present case, with two turning points, all expressions become more involved. The best approximation for $\sigma(x)$ we found convenient to display in Eq. (G.19) makes use of a cubic interpolation over the region containing the two turning points and is given in terms of two arbitrary parameters κ_1 and κ_2 which can be fixed in order to minimize the error. Of course, one could employ higher order interpolating functions and further improve the result at the price of complexity if better accuracy is needed. Our aim for the work presented in this Appendix was mainly to test the effectiveness of the MCE to produce approximate wave modes on black hole backgrounds.

In the next three technical Sections we give explicit expressions for the turning points, the calculation of the quantity ξ and some details of the cubic interpolation used to obtain $\sigma(x)$.

G.2.1 Turning Points

If we define $w = \mathrm{e}^x$, we see that $\omega^2(x) = 0$ for the exact frequency in Eq. (G.10) becomes the quartic polynomial equation

$$w^4 + 4\,w^3 + b\,w^2 + c\,w + 1 = 0 \ , \tag{G.20a}$$

with

$$\begin{aligned} b &= 6 - \frac{1}{4\,\tilde{\omega}^2} - \frac{\ell\,(\ell+1)}{\tilde{\omega}^2} && \text{(G.20b)} \\ c &= 4 - \frac{1}{2\,\tilde{\omega}^2} - \frac{\ell\,(\ell+1)}{\tilde{\omega}^2}\ . && \text{(G.20c)} \end{aligned}$$

Its four roots can be written as

$$w_i = -1 + \frac{\epsilon_i}{2}\sqrt{4 - \frac{2}{3}\,b + \frac{\gamma}{3}} - \frac{\theta_i}{2}\sqrt{8 - \frac{4}{3}\,b + \epsilon_i \frac{4\,b - 16 - 2\,c}{\sqrt{4 - \frac{2}{3}\,b + \frac{\gamma}{3}}} - \frac{\gamma}{3}}\ , \qquad \text{(G.21a)}$$

where $i = 1, \ldots, 4$ and

$$\begin{aligned} \alpha &= 12 + b^2 - 12\,c && \text{(G.21b)} \\ \beta &= 2\,b^3 - 36\,b\,c + 27\,c^2 + 432 - 72\,b && \text{(G.21c)} \\ \gamma &= \frac{2^{\frac{1}{3}}\,\alpha}{\left(\beta + \sqrt{\beta^2 - 4\,\alpha^3}\right)^{\frac{1}{3}}} + \frac{\left(\beta + \sqrt{\beta^2 - 4\,\alpha^3}\right)^{\frac{1}{3}}}{2^{\frac{1}{3}}}\ . && \text{(G.21d)} \end{aligned}$$

The coefficients $\epsilon_1 = \epsilon_2 = -\epsilon_3 = -\epsilon_4 = \theta_1 = -\theta_2 = \theta_3 = -\theta_4 = 1$, and the values of $\tilde{\omega}$ and ℓ determine the signs of the roots. There can be at most two positive roots, in which case, say, $w_3 \le w_4 \le 0 \le w_1 = \mathrm{e}^{x_1} \le w_2 = \mathrm{e}^{x_2}$, and only x_1 and x_2 can be valid turning points. The critical value of $\tilde{\omega}$ in Eq. (G.11) is then determined by the condition $0 \le w_1 = w_2$.

G.2.2 Evaluation of ξ

In order to evaluate the integral in Eq. (G.14b), we start from the general relation (again with $w = \mathrm{e}^x$)

$$\begin{aligned} \frac{1}{\tilde{\omega}}\int_{x_1}^{\ln(w)} \sqrt{-\,\omega^2(y)}\,\mathrm{d}\,y = {} & \sqrt{\frac{(w-w_3)(w-w_1)(w-w_2)}{w-w_4}} + \frac{1}{\sqrt{(w_1-w_3)(w_4-w_2)}} \\ & \times \Big\{ (w_3-w_1)(w_4-w_2)\,\mathrm{E}(z;W) - (w_4-w_1)(w_4-w_2)\,\mathrm{F}(z;W) \\ & \quad + (w_4-w_1)(w_3+w_4+w_1+w_2+2)\,\Pi\left[\frac{w_1-w_2}{w_4-w_2}; z; W\right] \\ & \quad - 2\,(w_4-w_1)(w_3+1)(w_2+1)\,\Pi\left[\frac{(w_4+1)(w_1-w_2)}{(w_1+1)(w_4-w_2)}; z; W\right] \\ & \quad + 2\,(w_4-w_1)w_3\,w_2\,\Pi\left[\frac{w_4\,(w_1-w_2)}{w_1\,(w_4-w_2)}; z; W\right] \Big\}\ , \qquad \text{(G.22)} \end{aligned}$$

where E, F and Π are elliptic functions [39],

$$z = \mathrm{ArcSin}\left[\sqrt{\frac{(w-w_1)(w_4-w_2)}{(w-w_4)(w_1-w_2)}}\right] \ , \tag{G.23}$$

$$W = \frac{(w_3-w_4)(w_1-w_2)}{(w_3-w_1)(w_4-w_2)} \ , \tag{G.24}$$

and $w_i = \mathrm{e}^{x_i}$ are the roots of $\omega^2(x)$ as given in the previous Section. The above expression evaluated at $w = w_2$ yields

$$\begin{aligned}
\xi = \ & \frac{\tilde{\omega}}{\sqrt{(w_1-w_3)(w_4-w_2)}} \left\{ (w_3-w_1)(w_4-w_3)\,\mathrm{E}(W) + (w_4-w_1)\,(w_2-w_4)\,\mathrm{K}(W) \right. \\
& +(w_4-w_1)\,(w_3+w_4+w_1+w_2+2)\,\Pi\left[\frac{w_1-w_2}{w_4-w_2};W\right] \\
& -2(w_3+1)(w_2+1)(w_4-w_1)\,\Pi\left[\frac{(w_4+1)(w_1-w_2)}{(w_1+1)(w_4-w_2)};W\right] \\
& \left. \quad +2\,w_3\,w_2\,(w_4-w_1)\,\Pi\left[\frac{w_4\,(w_1-w_2)}{w_1\,(w_4-w_2)};W\right]\right\} \ ,
\end{aligned} \tag{G.25}$$

in which we used $\mathrm{E}(\pi/2;q) = \mathrm{E}(q)$, $\mathrm{F}(\pi/2;q) = \mathrm{K}(q)$ and $\Pi(p;\pi/2;q) = \Pi(p,q)$ [39].

G.2.3 Cubic interpolation

In Section G.2, we use the analytic approximation for $\sigma(x)$ in Eq. (G.19) which involves the cubic interpolation

$$\sigma = C_0 + C_1\,x + C_2\,x^2 + C_3\,x^3 \ , \tag{G.26}$$

for $\kappa_1\,x_1 < x < \kappa_2\,x_2$. The above coefficients C_i, with $i = 0,\ldots,3$, can be easily expressed in terms of the parameters A, B and D for the Morse potential (G.13) as

$$\begin{aligned}
C_0 &= \kappa_1\,x_1\,\frac{\left(2\sqrt{D}-1\right)\,{\kappa_2}^2\,{x_2}^2\,\left(\kappa_2\,x_2-\kappa_1\,x_1\right) - 2\sqrt{D}\,\ln\left(2\sqrt{A}\right)\kappa_1\,x_1\,(3\,\kappa_2\,x_2-\kappa_1\,x_1)}{2\sqrt{D}\,(\kappa_2\,x_2-\kappa_1\,x_1)^3} \\
C_1 &= \frac{(\kappa_2\,x_2-\kappa_1\,x_1)\left[\kappa_2\,x_2\,\left(2\,\kappa_1\,x_1+\kappa_2\,x_2\right) - 2\sqrt{D}\,\kappa_1\,x_1\,\left(4\,\kappa_2\,x_2-\kappa_1\,x_1\right)\right]}{2\sqrt{D}\,(\kappa_2\,x_2-\kappa_1\,x_1)^3} \\
&\quad + \frac{12\sqrt{D}\,\ln\left(2\sqrt{A}\right)\,\kappa_1\,\kappa_2\,x_1\,x_2}{2\sqrt{D}\,(\kappa_2\,x_2-\kappa_1\,x_1)^3} \\
C_2 &= \frac{6\sqrt{D}\,\ln\left(2\sqrt{A}\right)(\kappa_1\,x_1+\kappa_2\,x_2) + \left(2\sqrt{D}-1\right)\left({\kappa_1}^2\,{x_1}^2+\kappa_1\,\kappa_2\,x_1\,x_2-2\,{\kappa_2}^2\,{x_2}^2\right)}{2\sqrt{D}(\kappa_1\,x_1-\kappa_2\,x_2)^3} \\
C_3 &= \frac{4\sqrt{D}\,\ln\left(2\sqrt{A}\right) - \left(2\sqrt{D}-1\right)\,\left(\kappa_2\,x_2-\kappa_1\,x_1\right)}{2\sqrt{D}\,(\kappa_2\,x_2-\kappa_1\,x_1)^3} \ .
\end{aligned} \tag{G.27}$$

Finally, one can express everything in terms of the original parameters $\tilde{\omega}$ and ℓ by making use of Eqs. (G.15a)-(G.15c).

Bibliography

[1] A. H. Guth. *Phys. Rev. D*, 23:347, 1981.

[2] S. Weinberg. *Gravitation and Cosmology.* John Wiley & Sons, New York, US, 1972.

[3] E. W. Kolb and M. S. Turner. *The Early Universe.* Addison-Wesley, US, 1990.

[4] H. Kodama and M. Sasaki. *Prog. Theor. Phys. Suppl.*, 78:1, 1984.

[5] V. F. Mukhanov, H. A. Feldman and R. H. Brandenberger. *Phys. Rep.*, 215:203, 1992.

[6] R. K. Sachs and A. M. Wolfe. *Astrophys. J.*, 147:73, 1967.

[7] J. Silk. *Nature*, 215:1155, 1967.

[8] J. Silk. *Astrophys. J.*, 151:459, 1968.

[9] P. J. E. Peebles and J. T. Yu. *Astrophys. J.*, 162:815, 1970.

[10] A. G. Doroshkevich, Ya. B. Zeldovich, and R. A. Sunyaev. *Sov. Astron.*, 22:523, 1978.

[11] M. L. Wilson and J. Silk. *Astrophys. J.*, 243:14, 1981.

[12] A. D. Sakharov. *Sov. Phys. JETP*, 22:241, 1965.

[13] C. L. Bennet *et al. Astrophys. J. Lett.*, 464:L1, 1996.

[14] M. Tegmark. *Astrophys. J. Lett.*, 464:L35, 1996.

[15] P. de Bernardis *et al. Astrophys. J.*, 564:559, 2002.

[16] C. B. Netterfield *et al. Astrophys. J.*, 571:604, 2002.

[17] A. T. Lee *et al. Astrophys. J.*, 561:L1, 2001.

[18] N. W. Halverson *et al. Astrophys. J.*, 568:38, 2002.

[19] A. Benoît *et al. Astron. Astrophys.*, 399:L19, 2003.

[20] C. Dickinson *et al. Mon. Not. Roy. Astron. Soc.*, 353:732, 2004.

[21] B. S. Mason *et al. Astrophys. J.*, 591:540, 2003.

[22] T. J. Pearson *et al. Astrophys. J.*, 591:556, 2003.

[23] C. L. Kuo *et al. Astrophys. J.*, 600:32, 2004.

[24] L. Page *et al. Astrophys. J. Suppl.*, 148:223, 2003.

[25] C. L. Bennett *et al. Astrophys. J. Suppl.*, 148:1, 2003.

[26] M. Tegmark *et al. Astrophys. J.*, 606:702, 2004.

[27] N. Bachall *et al. Astrophys. J.*, 585:182, 2003.

[28] B. Fields and S. Sarkar. *Phys. Lett. B*, 592:202, 2004.

[29] J. M. Bardeen. *Phys. Rev. D*, 22:1882, 1980.

[30] V. F. Mukhanov. *Sov. Phys. JETP Lett.*, 41:493, 1985.

[31] V. F. Mukhanov. *Sov. Phys. JETP Lett.*, 67:1297, 1988.

[32] C. M. Bender and S. A. Orszag. *Advanced mathematical methods for scientists and engineers.* McGraw-Hill Book Company, 1978.

[33] N. D. Birrel and P. C. W. Davies. *Quantum Fields in Curved Space.* Cambridge University Press, Cambridge, England, 1982.

[34] H. Jeffreys. *Proc. Lon. Math. Soc. (2)*, 23:428, 1923.

[35] R. E. Langer. *Bull. Am. Math. Soc.*, 40:545, 1934.

[36] P. Hunt and S. Sarkar. *Phys. Rev. D*, 70:103518, 2004.

[37] R. E. Langer. *Phys. Rev.*, 51:669, 1937.

[38] L. I. Schiff. *Quantum Mechanics.* McGraw-Hill Book Company, 1952.

[39] M. Abramowitz and I. Stegun. *Handbook of mathematical functions with formulas, graphs, and mathematical table.* Dover Publishing, 1965.

[40] R. E. Langer. *Trans. Am. Math. Soc.*, 67:461, 1949.

[41] S. C. Miller and R. H. Good. *Phys. Rev.*, 91:174, 1953.

[42] R. B. Dingle. *Appl. Sci. Res. B*, 5:345, 1956.

[43] M. V. Berry and K. E. Mount. *Rep. Prog. Phys.*, 35:315, 1972.

[44] C. E. Hecht and J. E. Mayer. *Phys. Rev.*, 106:1156, 1957.

[45] H. Moriguchi. *J. Phys. Soc. Japan*, 14:1771, 1959.

[46] P. Pechukas. *J. Chem. Phys.*, 54:3864, 1971.

[47] A. Kamenshchik, M. Luzzi and G. Venturi. Remarks on the method of comparison equations (generalized wkb method) and the generalized ermakov-pinney equation. *arXiv:math-ph/0506017*, 2005.

[48] V. P. Ermakov. *Univ. Izv. Kiev, series III*, 9:1, 1880.

[49] E. Pinney. *Proc. Amer. Math. Soc.*, 1:681, 1950.

[50] I. S. Gradstein and I. M. Ryzhik. *Tables of integrals, series and products.* Academic Press, New York, 1980.

[51] H. R. Lewis. *J. Math. Phys.*, 9:1976, 1968.

[52] W. E. Milne. *Phys. Rev.*, 35:863, 1930.

[53] P. Espinosa. *Ermakov-Lewis dynamic invariants with some applications.* MS Thesis, Instituto de Física - Universidad de Guanajuato, Leòn, 2000.

[54] U. Fano and A. R. P. Rau. *Atomic Collisions and Spectra.* Academic Press, Orlando, 1986.

[55] C. J. Eliezer and A. Gray. *SIAM J. Appl. Math.*, 30:46, 1976.

[56] M. V. Ioffe and H. J. Korsch. *Phys. Lett. A*, 311:200, 2003.

[57] J. R. Ray and J. L. Reid. *Phys. Lett. A*, 71:317, 1979.

[58] J. Martin and D. J. Schwarz. *Phys. Rev. D*, 67:083512, 2003.

[59] R. Casadio, F. Finelli, M. Luzzi and G. Venturi. *Phys. Rev. D*, 71:043517, 2005.

[60] R. Casadio, F. Finelli, A. Kamenshchik, M. Luzzi and G. Venturi. *JCAP*, 04:011, 2006.

[61] L. Wang, V. F. Mukhanov and P. J. Steinhardt. *Phys. Lett. B*, 414:18, 1997.

[62] S. Habib, A. Heinen, K. Heitmann, G. Jungman and C. Molina-París. *Phys. Rev. D*, 70:083507, 2004.

[63] F. W. J. Olver. *Asymptotics and special functions.* AKP Classics, Wellesley, MA, 1997.

[64] D. H. Lyth and E. D. Stewart. *Phys. Lett. B*, 274:168, 1992.

[65] L. F. Abbott and M. B. Wise. *Nucl. Phys. B*, 244:541, 1984.

[66] J. Martin and D. J. Schwarz. *Phys. Rev. D*, 57:3302, 1998.

[67] E. D. Stewart and D. H. Lyth. *Phys. Lett. B*, 302:171, 1993.

[68] S. M. Leach, A. R. Liddle, J. Martin and D. J. Schwarz. *Phys. Rev. D*, 66:023515, 2002.

[69] J. Martin and D. J. Schwarz. *Phys. Rev. D*, 62:103520, 2000.

[70] R. Casadio, F. Finelli, M. Luzzi and G. Venturi. *Phys. Lett. B*, 625:1, 2005.

[71] R. Casadio, F. Finelli, M. Luzzi and G. Venturi. *Phys. Rev. D*, 72:103516, 2005.

[72] L. Lewin. *Dilogarithms and associated functions.* Macdonald, 1958.

[73] S. Habib, K. Heitmann, G. Jungman and C. Molina-París. *Phys. Rev. Lett.*, 89:281301, 2002.

[74] S. Habib, A. Heinen, K. Heitmann and G. Jungman. *Phys. Rev. D*, 71:043518, 2005.

[75] E. D. Stewart and J. O. Gong. *Phys. Lett. B*, 510:1, 2001.

[76] A. Kosowsky and M. S. Turner. *Phys. Rev. D*, 52:1739, 1995.

[77] A. D. Linde. *Phys. Lett. B*, 129:177, 1983.

[78] C. Bertoni, F. Finelli and G. Venturi. *Phys. Lett. A*, 237:331, 1998.

[79] F. Finelli, G. Marozzi, G. P. Vacca, and G.Venturi. *Phys. Rev. D*, 65:103521, 2002.

[80] D. Polarski and A. A. Starobinsky. *Class. Quant. Grav.*, 13:377, 1996.

[81] A. R. Liddle, P. Parsons and J. D. Barrow. *Phys. Rev. D*, 50:7222, 1994.

[82] J. E. Lidsey, A. R. Liddle, E. W. Kolb, E. J. Copeland, T. Barreiro and M. Abney. *Rev. Mod. Phys.*, 69:373, 1997.

[83] S. Chandrasekhar. *The mathematical theory of black holes.* Oxford University Press, Oxford, 1992.

[84] S. W. Hawking. *Nature*, 248:30, 1974.

[85] S. W. Hawking. *Comm. Math. Phys.*, 43:199, 1975.

[86] H. P. Nollert. *Class. Quantum Grav.*, 16:R159, 1999.

[87] S. A. Teukolsky. *Astrophys. J.*, 185:635, 1973.

[88] P. Kanti and J. March-Russell. *Phys. Rev. D*, 66:024023, 2002.

[89] G. Rawitscher, C. Merow, M. Nguyen and I. Simbotin. *Am. J. Phys.*, 70:935, 2002.